PROTON SPIN RELAXATION IN PURE CH_4 AND IN MIXTURES OF CH_4 WITH OTHER GASES

A Thesis Submitted
In Partial Fulfilment of the Requirements
for the Degree of
DOCTOR OF PHILOSOPHY

By
S. RAJAN

to the

DEPARTMENT OF PHYSICS
INDIAN INSTITUTE OF TECHNOLOGY KANPUR
JANUARY, 1975

If a man will begin with certainties, he shall end in doubts; but if he will be content to begin with doubts, he shall end in certainties.

'Advancement of Learning, 1'

-Francis Bacon

CERTIFICATE

Certified that the work described in this thesis is the original work of Mr. S. Rajan performed under my supervision, and has not been submitted elsewhere for a degree.

January 6 , 1975

K Lalita

(K. Lalita)
Assistant Professor of Physics
Indian Institute of Technology
Kanpur, (U.P.), India

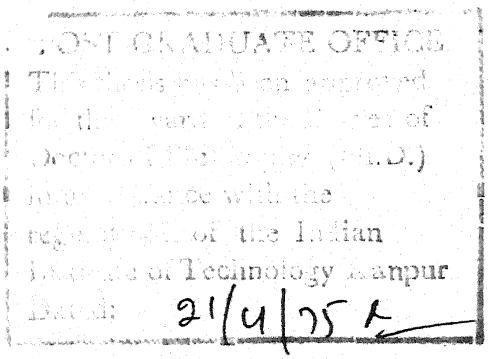

ACKNOWLEDGEMENTS

I express my sincere gratitude to Dr. K. Lalita for her able guidance and active participation throughout the course of this work. Her unassuming, informal nature made this work an interesting experience.

I am deeply indebted to Professor V. Subba Rao of Chemical Engineering for his kind interest and the many facilities he provided for the successful completion of this work.

I am grateful to Professors T.M. Srinivasan and R.K. Ray of the Low Temperature Division for providing the Varian magnet facility.

I remember the several useful hours which Mr. K.M.S. Prasad of Chemical Engineering spent with me during instrumentation and with pleasure I acknowledge his help.

My association with Dr. S.V. Babu of Chemical Engineering during the later part of my work proved quite fruitful and it is with appreciation that I thank him. The warm friendship and the many conversations I had with Dr. Y.V.C. Rao need particular mention.

Numerous friends have helped me in many ways; thanks are due to my dear I.V., for his constant help and encouragement; to Prasanna for many discussions and whose unhesitant co-operation enabled me to have a smooth schedule for running the experiments; to Hariharan for his able assistance in computer programming;

to S. Aravamudhan for his interest and appreciation; to L. Pandey for taking care of some of the experimental runs.

The companionship and the support received from the various students of Energy Transfer Laboratory are gratefully acknowledged.

To conclude, it is my pleasure to record my thanks to Mr. J.S. Virdi of Chemical Engineering Workshop for the commendable job in making the pressure vessel, to Mr. B.S. Pandey for the neat and accurate typing and Mr. D.S. Panesar for the tracings.

Financial assistance from the Department of Atomic Energy India, and later a Research Assistantship from the Department of Physics, IIT-Kanpur are acknowledged.

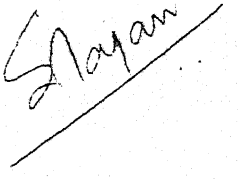

TABLE OF CONTENTS

* * *

LIST OF FIGURES

* * *

LIST OF TABLES

* * *

SYNOPSIS

This thesis presents a study of proton spin-lattice relaxation in pure methane and in mixtures of CH_4-N_2, CH_4-CO_2 and CH_4-Inert gas atom (He, Ne and Ar) using spin-echo technique. The measurements were made as a function of density ($\simeq 1 < \rho < 12$) amagats) and composition in the temperature range 300-600°K. A spin-echo spectrometer operating at 30 MHz was fabricated for this purpose. The temperature dependences of the spin-lattice relaxation time per unit density., T_1/ρ , in case of pure CH_4 and the extrapolated values of (T_1/ρ) to 100% N_2, CO_2 or Inert gas atom in case of mixtures along with the data of Armstrong and Tward[18] in CF_4 and SiF_4 have been interpreted to obtain information about the intermolecular potentials, especially the anisotropic potential in these systems. The analysis is made assuming that the average lifetime of a molecule in a J state can be approximated by the correlation time of spin-rotation interaction, the dominant mechanism of relaxation in the systems under consideration. The average lifetime of a molecule in a J state is calculated following the theory of Bloom and Oppenheim for a given anisotropic intermolecular potential using "weak collision approximation". The molecular quantities such as the hyperpolarizability of CH_4, the octopole moments of CH_4, CF_4 and SiF_4 have been determined from the experimental data and the results are discussed.

The first chapter of the thesis introduces the importance of gas phase nuclear spin relaxation studies in providing valuable information on the anisotropy of intermolecular interactions. The chapter includes an outline of the basic principles of nuclear magnetic resonance. Finally the inter and intra molecular contributions to the relaxation rate are discussed.

Chapter II deals with the description of the spin-echo apparatus fabricated for this work. A brief description of the spin-echo technique is given. The essential features of the pulsed spectrometer are that the operating frequency is at 30 MHz and phase coherent detection is incorporated. Tektronix waveform and pulsewidth generators in combination with a pulse sequencer, a pulsewidth generator of the phantastron type and a pulse amplifier produce the necessary sequence of d.c. pulses. These d.c. pulses are used to gate a continuous wave crystal controlled oscillator at 10 MHz. The gated output is amplified, tripled and again power amplified to produce rf pulses at 30 MHz. The transmitter is capable of delivering about 1.8 KW of pulsed power output. The receiver system consists of a pre-amplifier, an integrated rf amplifier and a high gain L.E.L. amplifier. The overall recovery time of the receiver system is less than 50 μ secs. Boxcar integrator is used to sample the detected output from the receiver system. Electronic scanning of the pulses enables one, to record the recovery of magnetization

automatically on a strip chart recorder as a function of time. The sample holder used in the experiments is made of Be-Cu alloy. The pressure seals are satisfactory upto 3000 psi at room temperature. CH_4, He, Ne, N_2 and CO_2 gases used were of research grade and were obtained from Matheson Gas Co., Ar was obtained from Indian Oxygen Co., and was of 99.97% purity.

The theory used in the analysis of the experimental results of this work is described in Chapter III. Following the treatment given by Bloom et al[19] expression relating T_1 to intramolecular dipolar interaction and spin-rotation interaction have been arrived at, and considering the relative contributions of these two interactions to the relaxation rate, it is shown that in CH_4, spin-rotation interaction is the dominant mechanism of relaxation.

A general procedure to evaluate the average lifetime of a molecule in a J state is outlined for a given anisotropic potential. First order perturbation theory is used to calculate the transition rates. The attractive part of the anisotropic intermolecular potential in case of the pure gases CH_4, CF_4 and SiF_4 is written in the most general form of multipole interaction following Gray[47] and is given by an octopole-octopole interaction, the isotropic potential being either a hard-sphere potential or a Lennard-Jones potential.

In polyatomic mixtures CH_4-N_2 and CH_4-CO_2, the attractive part of the anisotropic potential is given by the interaction

between the electric octopole moment of CH_4 and the quadrupole moment of N_2 or CO_2. In CH_4-Inert gas atom the attractive anisotropic potential has a term proportional to r^{-7} as derived by Buckingham[50] for the interaction between a spherical and a tetrahedral molecule. The isotropic potential is considered to be adequately described only by a Lennard-Jones potential in all the mixtures. The repulsive part of the anisotropic potential is assumed to vary as r^{-12} having the same angle dependence as that of the attractive part in all the systems studied.

Chapter IV presents the experimental data of proton spin-lattice relaxation in pure CH_4. The temperature dependence of T_1/ρ can be fitted with a power law of the form $T_1/\rho \propto T^{-n}$ where $n = 1.47 \pm 0.03$. This is in good agreement with the earlier work done in CH_4. The data reported in CF_4 and SiF_4 by Armstrong and Tward also follow a 3/2 law and are presented. An analysis of the experimental data in these three systems yield the anisotropic potential parameters for the model intermolecular potentials considered and also the scalar values of the octopole moments of CH_4, CF_4 and SiF_4. The octopole moments of CH_4 and CF_4 are compared with the values obtained by other experiments and the results are discussed.

Chapter V is a continuation on Experimental Results and Discussions. This describes proton spin-lattice relaxation in

CH_4-N_2, CH_4-CO_2 and CH_4-Inert gas atom systems. The extrapolated values of (T_1/ρ) to 100% N_2, CO_2 or Inert gas atom, $(T_1/\rho)_{CH_4\text{-}X}$ where X could be either N_2 or CO_2 or inert gas atom give the contribution to (T_1/ρ) due to CH_4-X collisions only and are tabulated. The temperature dependence of $(T_1/\rho)_{CH_4\text{-}X}$ can be fitted with a power law of the form $(T_1/\rho)_{CH_4\text{-}X} \propto T^{-n}$, where $n = 0.28 \pm 0.08$ for CH_4-He, 1.1 ± 0.1 for CH_4-Ne and 1.25 ± 0.09 for CH_4-Ar, and $n = 0.67 \pm 0.14$ for CH_4-N_2 and 0.91 ± 0.1 for CH_4-CO_2. An analysis of the data in CH_4-N_2 and CH_4-CO_2 using the theory described in Chapter III, knowing the scalar values of the quadrupole moments of N_2 and CO_2, gives the scalar value of the octopole moment of CH_4. The octopole moment obtained from CH_4-N_2 data is in reasonable agreement with the values reported from other experiments and also with the value obtained from pure CH_4 data presented in Chapter IV. The octopole moment of CH_4 obtained from CH_4-CO_2 system is, however, smaller by a factor of two. The anisotropic potential parameters and the octopole moments of CH_4 obtained are tabulated and the results have been discussed. An analysis of the data on CH_4-Inert gas atom yields the anisotropic potential parameters and the hyperpolarizability of CH_4. The hyperpolarizability of CH_4 obtained from the experimental data is comparable to the theoretical estimates.

Chapter VI summarizes the significant results obtained in this work.

This thesis contains two appendices. Appendix A contains a collection of circuit diagrams used in the spin-echo set up. Appendix B contains a Fortran IV program written for the numerical evaluation of integrals of type

$$I(p,n,n') = \int_0^{\infty} dy \left[\left(\int_0^{\infty} dx \left[g(x) \right]^{\frac{1}{2}} J_{p+\frac{1}{2}}(xy)\, x^{3/2-n} \right) \times \left(\int_0^{\infty} dx \left[g(x) \right]^{\frac{1}{2}} J_{p+\frac{1}{2}}(xy)\, x^{3/2-n'} \right) \right]$$

where $g(x) = \exp[-\beta V_o(x)]$ for the classical dilute gas,

$\beta = 1/KT$ and $V_o(x)$ = Hard sphere potential or L-J Potential

$J_{p+\frac{1}{2}}(xy)$ = Bessel function of order p; x and y are dimensionless variables of integration.

* * *

CHAPTER I

INTRODUCTION

I.1 Intermolecular Potentials from NMR Data

The study of intermolecular forces has received considerable attention as an active field of research over many years in chemical physics. Significant progress has been made in the understanding of central forces between molecules,[1,2] such as are conventionally represented by Lennard-Jones type potentials. Generally much less is known about the anisotropic intermolecular potentials which depend on the molecular reorientation and shape. There are, of course, quite a few experimental techniques such as sound absorption in gases,[3] spectral line broadening[4] and nuclear magnetic resonance in gases[5-8] which have proved useful in providing valuable information about the anisotropy of intermolecular interactions. These techniques have the advantage that they are sensitive to the anisotropic intermolecular forces and relatively insensitive to the much investigated isotropic forces.

Thus nuclear spin relaxation studies in gases provide one of the important methods to probe the details of the anisotropic intermolecular potential which causes transitions between the molecular rotational states. The spin-lattice relaxation time (T_1), which is the rate at which the nuclear spins approach

thermal equilibrium with their surroundings, can be measured experimentally. The nuclear spin transitions which bring the system to equilibrium are caused by the local fields set up at the nuclear sites. These fields are rendered time dependent by the random reorientations of the molecule caused by collisions. Therefore, nuclear spin-lattice relaxation times provide detailed information on the process of molecular re-orientation which in turn give information about the anisotropic interactions between the molecules. There have been several previous experimental investigations of T_1 in H_2[5,9-11] and in mixtures of hydrogen with other gases,[12-15] where an analysis of the proton T_1 of the ortho-H_2 molecules as a function of density, temperature and concentration of H_2 in binary gas mixtures, yielded detailed information on the anisotropic part of the intermolecular potential.

A useful step forward in the direction of understanding the intermolecular forces would be the extension of these studies to polyatomic molecules and their mixtures. The temperature dependence of the proton spin relaxation time T_1 has been reported in many spherical[16-19] and symmetric top[19-23] molecules and also for CH_4 infinitely diluted with He.[24] In many pure gases where spin rotation interaction is the dominant mechanism of relaxation it was found that $T_1/\rho \propto T^{-3/2}$, where ρ is the density and T is temperature. This result was explained by a model in which the collisions are 'weak' and the isotropic part of the intermolecular potential is given by a hard sphere potential. So far

no detailed analysis has been done to obtain information on the anisotropic intermolecular potentials in polyatomic molecules and their mixtures.

This thesis covers a study of proton spin relaxation in pure CH_4 and in mixtures of CH_4-N_2, CH_4-CO_2 and CH_4-Inert gas atom as a function of density ($1 < \rho < 12$ amagats), composition and temperature; the aim is to extract possible information on the intermolecular potentials of these systems, especially the anisotropic potentials; the data of fluorine spin relaxation in pure CF_4 and SiF_4 reported by Armstrong et.al[18] would also be considered to obtain similar information on intermolecular potentials.

I.2 Outline of the Principles of NMR:

The principles of magnetic resonance will be briefly discussed here and a more complete treatment can be found in Abragam.[25] An external magnetic field H_o along the Z axis applied to a nucleus with spin angular momentum $\bar{I}$ and magnetic moment $\bar{\mu} = \gamma \hbar \bar{I}$ produces an interaction Hamiltonian given by

$$H = -\bar{\mu} \cdot \bar{H}_o = \gamma H_o \hbar I_z \qquad (1.1)$$

where γ is the gyromagnetic ratio. The allowed energies are

$$E_m = -\gamma \hbar H_o m \qquad (1.2)$$

where $m = -I, -I+1, \ldots\ldots +I$.

The fractional populations of these energy levels at equilibrium are given by

$$P_m = \frac{\exp(-E_m/KT)}{\sum_m \exp(-E_m/KT)} \qquad (1.3)$$

where K is the Boltzmann constant and T is the absolute temperature of the gas. The equilibrium magnetization for a system of N weakly interacting spins is given by

$$M_o = N \sum_m P_m \gamma \hbar m$$

$$= N \gamma^2 \hbar^2 I(I+1)/3KT \qquad (1.4)$$

where the high temperature approximation $\gamma h H_o/KT \ll 1$ is used.

The approach to equilibrium of the magnetization after being disturbed is often describable by the phenomenological Bloch equations,

$$\frac{d\bar{M}}{dt} = \gamma \bar{M} \times \bar{H} - \frac{M_x \bar{i} + M_y \bar{j}}{T_2} + \frac{M_o - M_z}{T_1} \bar{k} \qquad (1.5)$$

where T_1 and T_2 are longitudinal and transverse relaxation times. If relaxation effects are neglected, the equation of motion for $\bar{M}$ in a reference frame rotating with angular frequency ω may be written,

$$\frac{\partial \bar{M}}{\partial t} = \gamma \bar{M} \times (\bar{H} + \bar{\omega}/\gamma) \qquad (1.6)$$

$\bar{M}$ is stationary in the rotating frame for $\bar{H} = H_o \bar{k}$ if $\bar{\omega} = -\gamma H_o \bar{k}$. The angular frequency $\omega_o = -\gamma H_o$ is called the 'Larmor frequency'. If $\bar{H}$ consists of a static magnetic field $H_o \bar{k}$ and a time varying field $\bar{H}_1(t)$ where

$$\bar{H}_1(t) = H_1 [\bar{i} \cos\omega t + \bar{j} \sin\omega t] \qquad (1.7)$$

represents the applied radio-frequency magnetic field, the equation of motion for $\bar{M}$ in the rotating frame with the X-axis along $\bar{H}_1(t)$ is,

$$\begin{aligned} \frac{\partial}{\partial t}\bar{M} &= \gamma \bar{M} \times [(H_o + \omega/\gamma)\bar{k} + H_1 \bar{i}] \\ &= \gamma \bar{M} \times \bar{H}_{eff} \end{aligned} \qquad (1.8)$$

where

$$\bar{H}_{eff} = (H_o + \omega/\gamma)\bar{k} + H_1 \bar{i} \qquad (1.9)$$

It can be seen from equation 1.8 that $\bar{M}$ precesses about $\bar{H}_{eff}$ with an angular frequency $-\gamma \bar{H}_{eff}$. When $\omega = \omega_o$, $\bar{H}_{eff} = H_1 \bar{i}$ and the magnetization therefore precesses about $\bar{H}_1$. This phenomenon is nuclear magnetic resonance.

If the time varying field is applied for a time t_w, then $\bar{M}$ will precess at resonance about $\bar{H}_1$ through an angle $\theta = \gamma H_1 t_w$. H_1 and the pulse width t_w can be chosen so that $\theta = 180°$ or $90°$.

After the application of a 90°($\pi/2$) pulse, $\bar{M}$ precesses in the x-y plane about H_o and induces an e.m.f. in the coil which is referred to as a free induction decay. If a π pulse is applied at a time $t = \tau$ after the $\pi/2$ pulse, the spins tend to rephase in the x-y plane at a time $t=2\tau$ resulting in a free induction signal known as a spin echo.

When relaxation effects are considered, the solutions to eq. 1.5 for

$$\bar{H} = \bar{k}\, H_o + \bar{i}\, 2 H_1 \cos\omega t,\ H_1 \ll H_o \qquad (1.10)$$

are found to be

$$M_x(t) = M_{xy}(0)\,[\cos(\omega t + \phi)]\,\exp(-t/T_2) \qquad (1.11)$$

$$M_y(t) = M_{xy}(0)\,[\sin\omega t + \phi)]\,\exp(-t/T_2) \qquad (1.12)$$

$$M_z(t) = M_o + [M_z(0) - M_o]\,\exp(-t/T_1) \qquad (1.13)$$

where

$$M_{xy} = \sqrt{M_x^2 + M_y^2}$$

Hence T_1 and T_2 can be determined experimentally, by observing $M_z(t)$ and $M_x(t)$ (or $M_y(t)$) respectively as a function of time. This thesis is concerned only with measurement of T_1 and its interpretation.

I.3 A Note on Relaxation Mechanisms:

In most molecular fluids, T_1 may be written

$$\frac{1}{T_1} = R_A + R_B + R_C \qquad (1.14)$$

where R_A is the relaxation rate due to intra-molecular dipolar and quadrapolar (for $I > 1/2$ only) interactions, i.e., those interactions which transform as $Y_{2m}(\Omega)$ under rotations of the molecule. where Ω denotes the orientation of a vector fixed to the molecule, R_B is the relaxation rate due to inter-molecular dipolar interactions and R_C is the relaxation rate due to spin-rotation interactions, whose dominant term transforms as $\bar{J}$, the rotational angular momentum. In molecular gases which are not too dense, R_B is negligible. The intra molecular dipolar and spin-rotation interactions are modulated in time through fluctuations in $Y_{2m}(\Omega(t))$ and $\bar{J}(t)$ due to molecular collisions which cause transitions between molecular states having different quantum numbers, denoted by J, K and M for spherical top molecules.

The mechanism by which the spins relax was first proposed by Schwinger[26] and then extended by Needler and Opechowski[27] and Johnson and Waugh[6]. In case of H_2, they have obtained expressions relating spin-lattice relaxation times to the correlati times of intra-molecular interactions. Bloom and Oppenheim have treated the dynamics of the system with 'Constant Acceleration Approximation' (CAA) and obtained expressions for the correlation

times of the intramolecular interactions in terms of the intermolecular interactions. Scattering calculations have been carried out by Kinsey et.al[28] and Foster and Rugheimer.[13]

I.4 Scope of the Present Work:

The theory required to interpret the experimental data in order to obtain information about the intermolecular forces is presented in Chapter III. The apparatus and experimental techniques that were used in obtaining the data are presented in Chapter II. Chapter IV describes the study of proton spin relaxation in pure CH_4; along with pure CH_4, the data on CF_4 and $Si^{18}F_4$ are also interpreted to obtain anisotropic intermolecular potential parameters and the respective octopole moments. Chapter V deals with the experimental results and interpretations on polyatomic gas mixtures. The analysis yields potential parameters and molecular quantities such as octopole moment and hyperpolarizability of CH_4. Chapter VI summarizes the various results and the conclusions. Appendix A contains circuit details of the pulsed spectrometer. Appendix B contains a Fortran IV program written for the numerical evaluation of integrals of type

$$I(p,n,n') = \int_0^\infty dy \left\{ \left[\left(\int_0^\infty dx\, J_{p+\frac{1}{2}}(xy)\, x^{1.5-n} \left[g(x) \right]^{\frac{1}{2}} \right) x \right.\right.$$
$$\left.\left. \left(\int_0^\infty dx\, J_{p+\frac{1}{2}}(xy)\, x^{1.5-n'} \left[g(x) \right]^{\frac{1}{2}} \right] \right\} \qquad (1.15)$$

where $J_{p+\frac{1}{2}}(xy)$ is a Bessel function of order p; $g(x)$ = radial distribution function given by $\exp(-\beta V_o(x))$, $\beta = 1/KT$ and $V_o(x)$ is given by either a Lennard-Jones potential or a hard sphere potential.

Gaussian quadrature technique is used for the evaluation of these integrals.

* * *

CHAPTER II

EXPERIMENTAL TECHNIQUES AND APPARATUS

II.1 The Method of Spin-Echoes:

Spin-Echoes originally developed by Hahn[29] is a very useful technique to measure nuclear magnetic resonance phenomena, especially relaxation times, in a simple and direct way.

When a bulk sample containing a large number of nuclear spin moments is placed in a static magnetic field $\bar{H}_o$ along the Z axis say, a state of thermodynamic equilibrium is attained with a net macroscopic magnetization $\bar{M}_o$ along $\bar{H}_o$. The equilibrium magnetization $\bar{M}_o$ can be rotated from the Z axis through any desired angle θ by applying a radio frequency field $\bar{H}_1$ perpendicular to $\bar{H}_o$ at the Larmor frequency of the spins. An intense rf pulse is used to tip the magnetization $\bar{M}_o$ through an angle θ in a time much shorter than T_1 or T_2 so that the relaxation effects, while $\bar{H}_1$ is on can be neglected. The angle θ through which the magnetization $\bar{M}_o$ is rotated by the rf pulse is determined from the relation,

$$\theta = \gamma H_1 t_w \qquad (2.1)$$

where γ is the gyromagnetic ratio, H_1 is the magnitude of the rf field and t_w is the duration for which the rf pulse has been applied. In a static field $\bar{H}_o$ along the Z axis, the

magnetization $\bar{M}_o$ precesses around the Z axis at the 'Larmor frequency' characteristic of the nuclei. Consider the situation when a $\pi/2$ pulse is applied along the positive X' axis in the 'frame rotating' at the rf. Following the pulse, $\bar{M}_o$ lies entirely along the Y' axis (Fig. 1a)[30]. The magnetization precessing in the XY plane after the application of a $\pi/2$ pulse induces an emf in the coil which can be detected and observed and this is referred to as "Free Induction Decay" (FID). As transverse relaxation occurs, the signal decays. In a perfectly homogeneous field the time constant of the decay in the XY plane would be T_2. But the applied static field will have an inhomogeneity ΔH_o. The total magnetization $\bar{M}_o$ can be thought of as the vector sum of the individual macroscopic magnetizations $\bar{m}_i$ arising from nuclei in different parts of the sample and hence experiencing slightly different values of the applied field due to field inhomogeneity. Thus there is a range of precession frequencies centered about the Larmor frequency ω_o which we have taken as the 'rotation frequency' of the rotating frame. Hence the macroscopic magnetizations $\bar{m}_i$, known as "isochromats" begin to fan out, as some nuclei precess faster and some slower than the frame (Fig.1b). Thus because of the presence of the field inhomogeneity, the magnetization in the XY plane decays in a time of the order of $1/\gamma\Delta H_o$). The phase differences following the $\pi/2$ pulse can be reversed by the application of a π pulse at time τ ($\ll T_1$ or T_2)

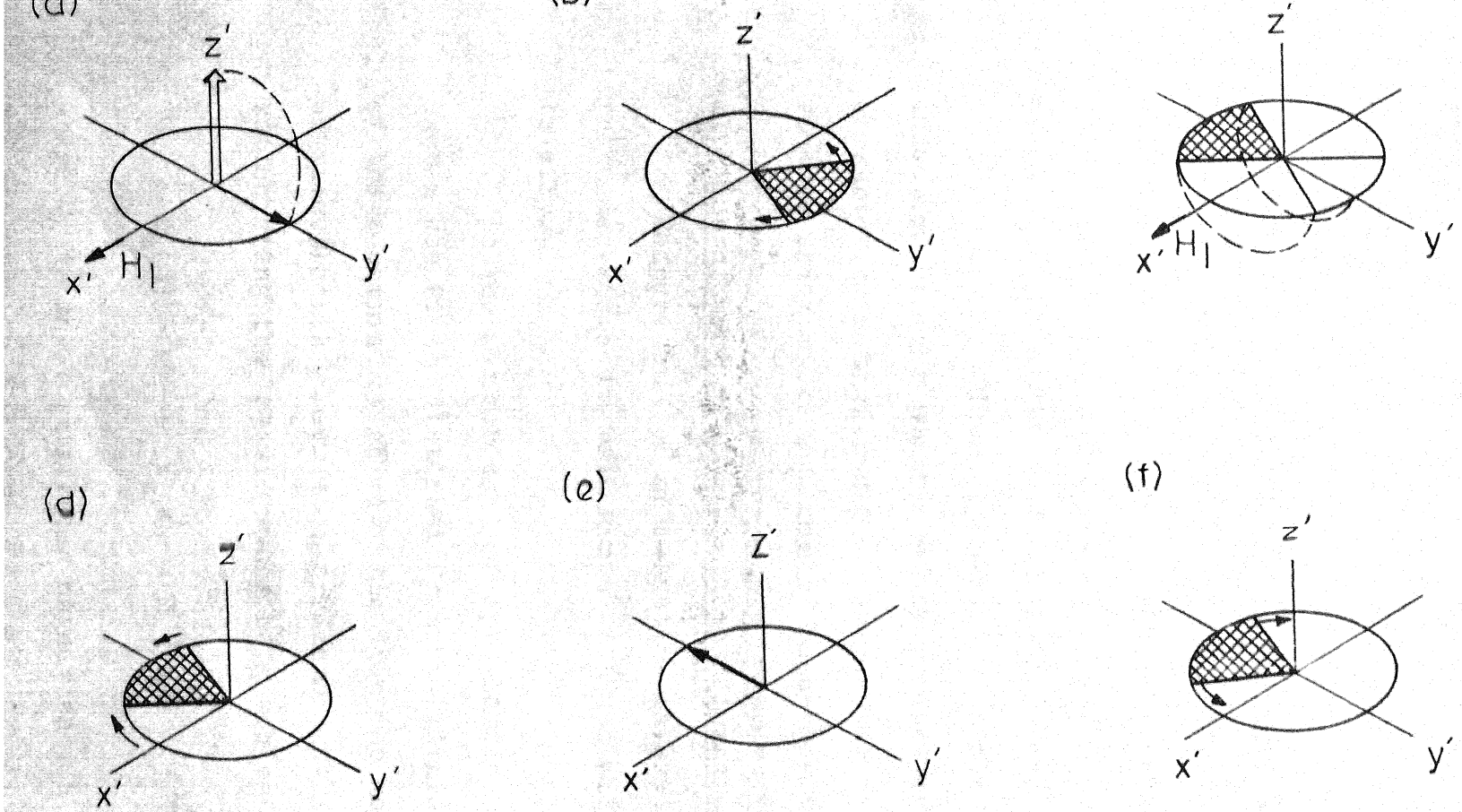

Fig. 1 - Echo formation following a $\pi/2 - \tau - \pi$ sequence.

after the $\pi/2$ pulse (Fig. 1c). The "isochromats" continue to precess in the same direction as they were before the application of a π pulse (Fig. 1d). This leads to a reclustering of the macroscopic magnetizations $\bar{m}_i$ (Fig. 1e), at a time $t = 2\tau$ after the $\pi/2$ pulse. The continuing movement of the $\bar{m}_i$ causes them again to lose phase coherence giving rise to an echo (Fig. 1f). Thus "spin-Echoes" refer to spontaneous nuclear induction signals which are observed to appear due to the constructive interference of precessing macroscopic moment vectors after more than one rf pulse has been applied.

II.2 Measurement of Spin-Lattice Relaxation Time T_1:

Measurement of spin-lattice relaxation time T_1 by the pulse technique is well known[25,29] and will be described here briefly.

In the measurement of spin-lattice relaxation time, the system was first disturbed from equilibrium and then the growth of the z-component of magnetization was monitored as a function of time. Bloch's[31] equation predicts that the growth of magnetization along the z-axis would be given as

$$M_z(t) = M_o + [M_z(0) - M_o] \exp(-t/T_1) \qquad (2.2)$$

where M_o is the equilibrium magnetization. Experimentally T_1 was measured as follows:

First the application of a π pulse tipped the magnetization M_z to the negative Z direction and its growth along the Z axis was monitored by the application of a $\pi/2 - \tau' - \pi$ sequence. If τ' was kept constant throughout the experiment, the magnitude of the echo would be proportional to the value of M_z preceeding the $\pi/2$ pulse.

The pulse sequence $\pi - \tau - \pi/2 - \tau' - \pi$ (τ was continuously varied whereas τ' was kept constant throughout the experiment) was repeated after every time interval $t \geq 10\ T_1$, so that the spins relax and attain equilibrium in between the sequences. A Boxcar integrator model no. CW 160, of Princeton Applied Research was used to sample the detected output from the L.E.L. amplifier. The use of Boxcar integrator improves the S/N ratio. In order to avoid any possible integration distortion effects of Boxcar integrator while measuring relaxation times, the integration time constant RC was chosen to satisfy the relation[32]

$$\frac{T}{t_s} RC \ll \alpha T_1 \qquad (2.3)$$

where T is the repetition rate, t_s is the sampling gate width, α is the inverse of the rate at which the pulse separation was varied and T_1 is the spin-lattice relaxation time. The Boxcar was triggered by the $\pi/2$ pulse and the sampling gate of the Boxcar was adjusted to sample the echo height. The magnitude

of the echo and hence the recovery of M_z was plotted on a Bausch and Lamb recorder Model VOM 6. The time t between the first π pulse and $\pi/2$ pulse was measured with a Hewlett-Packard 524-C electronic counter and the time was printed out automatically by a Hewlett-Packard 526-B digital recorder. An event marker on the Bausch and Lamb strip chart recorder made a mark whenever the time was printed out by the digital recorder. The M_z at various times could then be identified. Typical plots of T_1 recovery are shown in Figs. 2a and 2b.

A plot of log $(M_o - M_z(t))$ versus t gives (Refer eq. 2.2) at a straight line with a negative slope equal to $1/T_1$.

II.3 The Spin-Echo Apparatus:

i) General: In this section the description of a complete pulsed nuclear resonance spectrometer is given. Standard techniques as described by Hahn[29] and Clark[33] were used in building the spectrometer. The essential features of the spectrometer are a) the operating frequency is 30 MHz b) The use of phase coherent detection c) the construction of a sample holder and d) the use of Boxcar integrator to measure relaxation times to a better accuracy. Circuit details are presented in Appendix A. A block diagram of the spectrometer is shown in Fig. 3. All the major items will be described briefly.

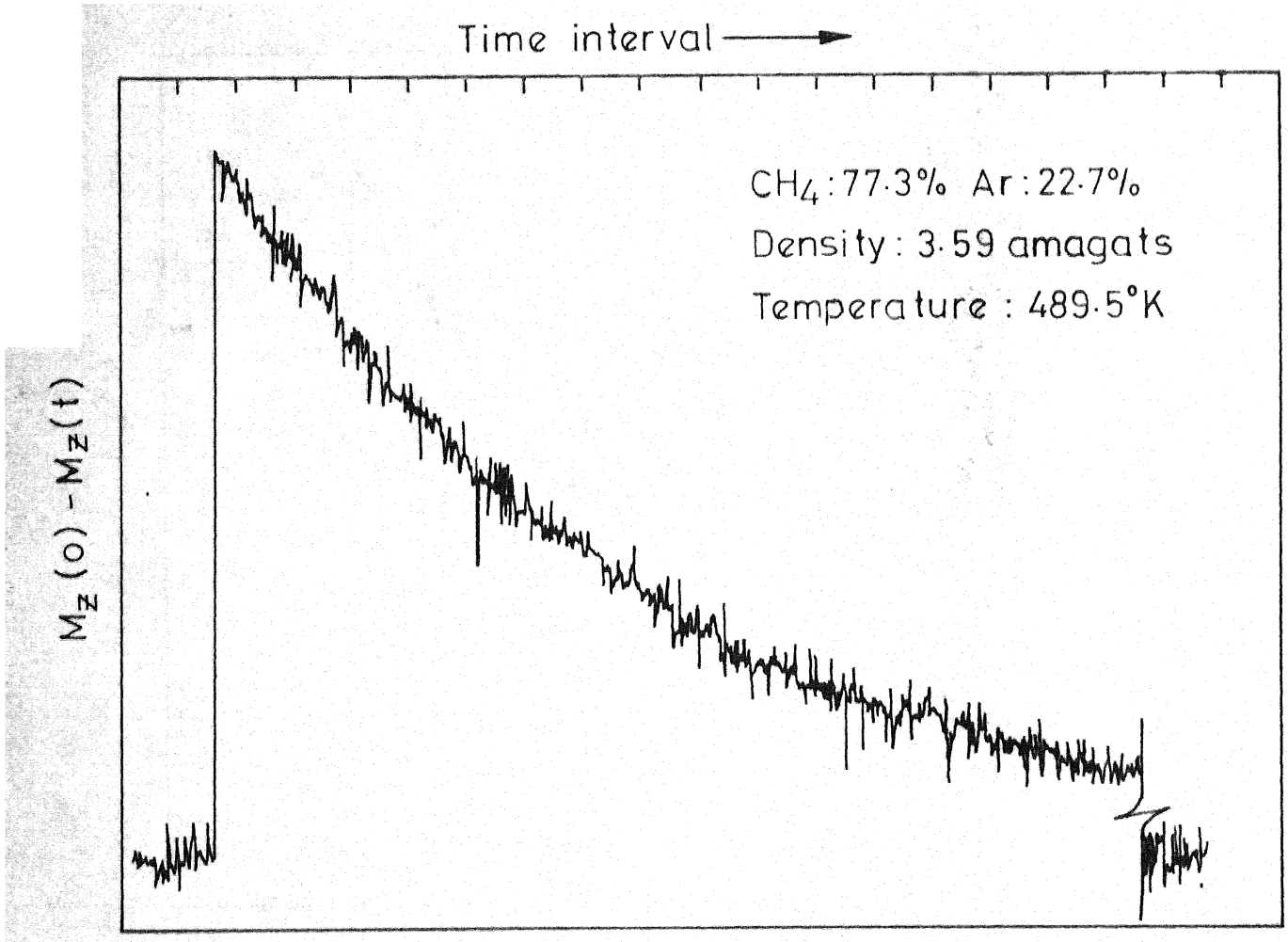

Fig. 2a - A Typical T_1 recovery.
($\pi - \tau - \pi/2 - \tau' - \pi$ sequence)

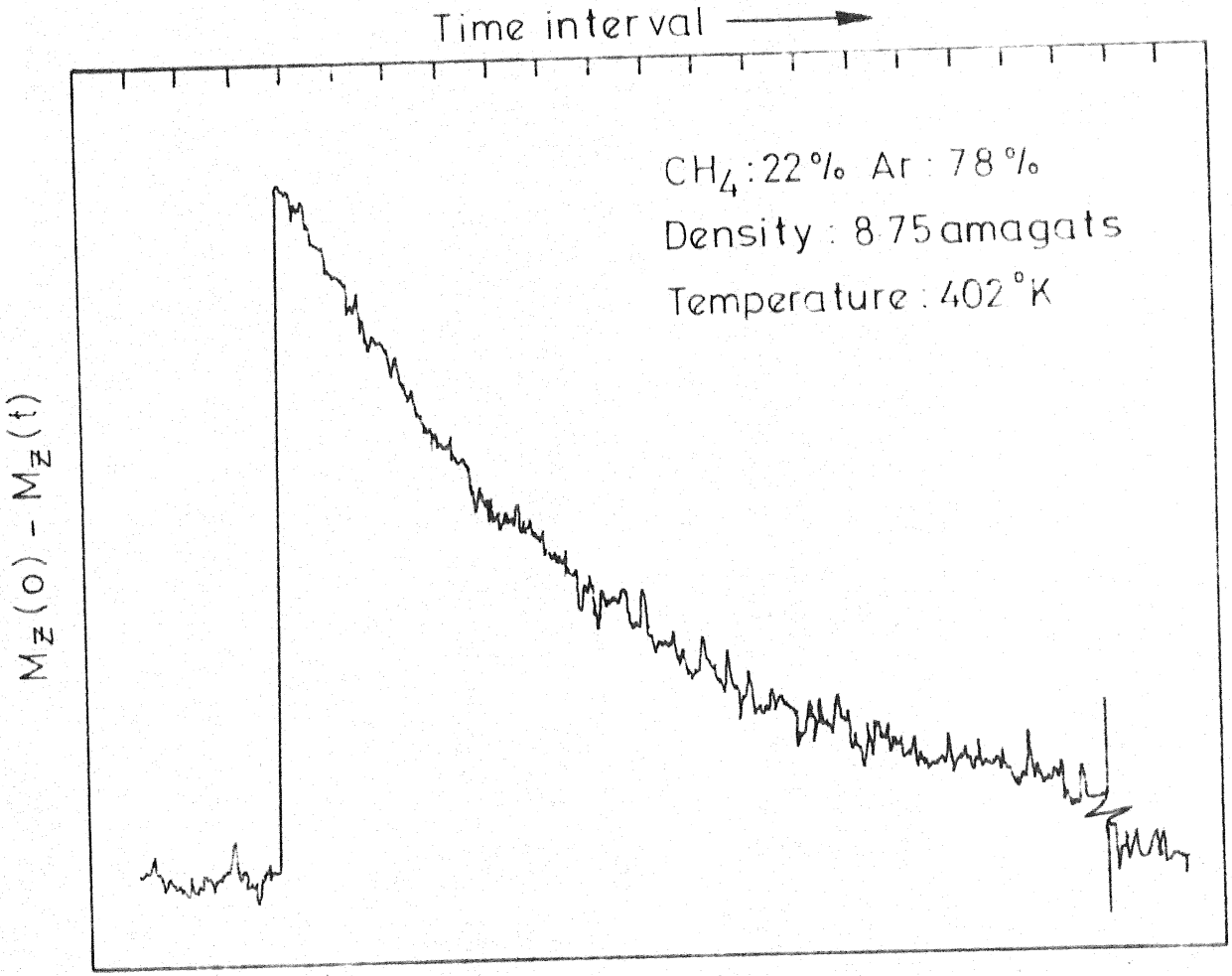

Fig. 2b - A Typical M_z recovery.
($\pi - \tau - \pi/2 - \tau' - \pi$ sequence)

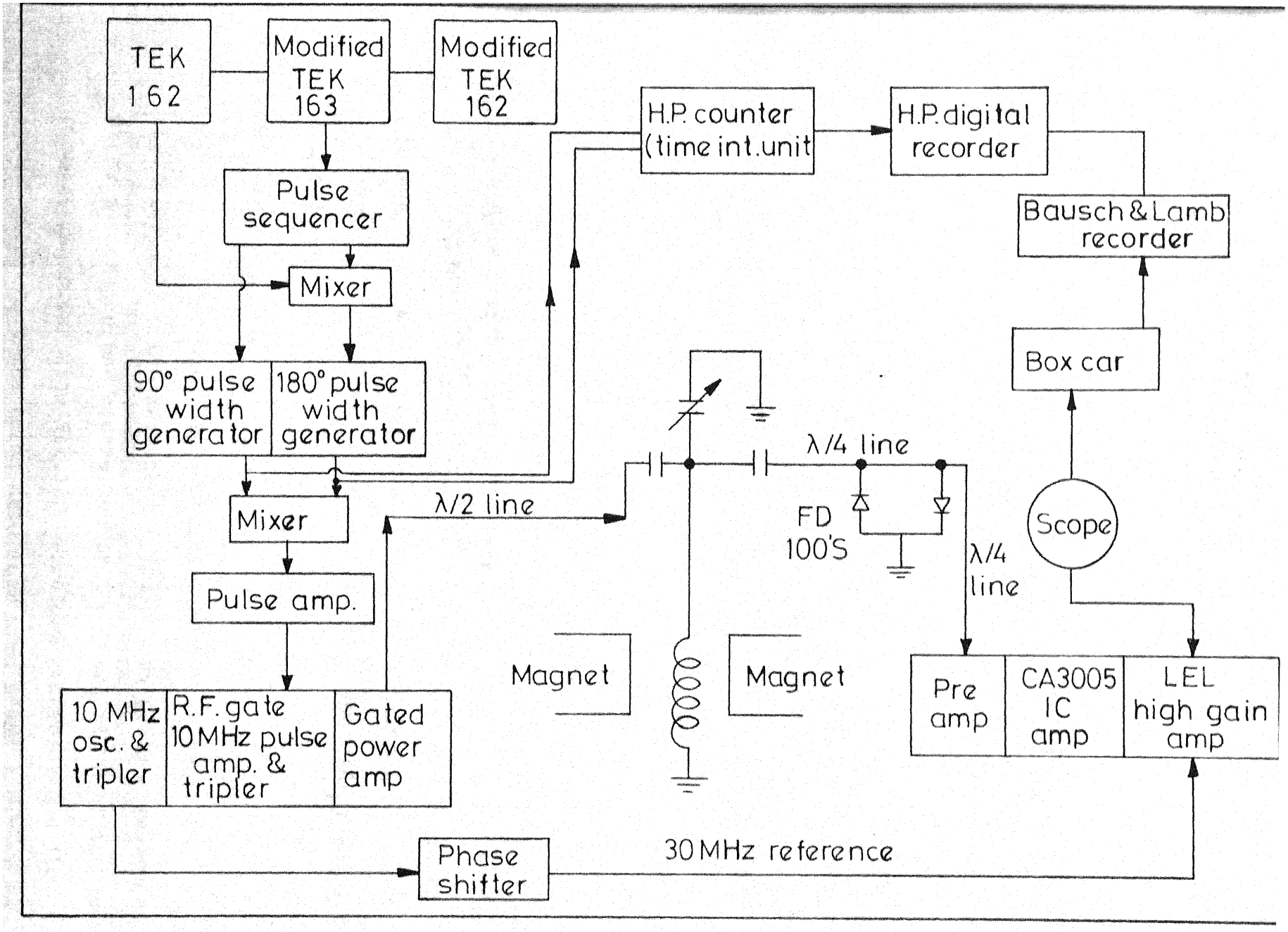
TEK 162
Modified TEK 163
Modified TEK 162
H.P. counter (time int.unit
H.P. digital recorder
Bausch & Lamb recorder
Pulse sequencer
Mixer
90° pulse width generator
180° pulse width generator
Box car
λ/4 line
λ/2 line
Mixer
FD 100'S
λ/4 line
Scope
Pulse amp.
Magnet
Magnet
Pre amp
CA3005 IC amp
LEL high gain amp
10 MHz osc. & tripler
R.F. gate 10 MHz pulse amp. & tripler
Gated power amp
Phase shifter
30 MHz reference

ii) Spin-Echo Spectrometer:

a) Timing Circuit:

The timing circuit consists of a collection of Tektronix wave form and pulse generator units. The Tektronix type 162 wave form generator was designed primarily as an interval timer and repetition rate generator. It was used in recurrent mode to provide the first π pulse. The saw-tooth from the same generator started running down at the same time and was fed to a modified ultra-slow Tektronix type 162 wave form generator.[34] The modified ultra-slow Tek.162 was particularly useful in producing the required slowly varying delay of the $\pi/2 - \pi$ pulse sequence with respect to the first π pulse while sampling the recovery of the magnetization. Provision was made so that the d.c. level from which the run down of the ultra-slow starts could be varied, instead always from +120 volts to +20 volts (Fig. A1). A reset mechanism was incorporated in the modified Tektronix type 162 waveform generator to enable one to stop and start the run down at any time instead of waiting for the run down to be completed of its own.

b) Pulse Sequencer:

The pulse from the modified Tek.163 pulse-generator was taken to a pulse sequencer (Fig. A2) to produce two pulses whose separation was controlled by the pulse width of the input pulse. The pulse from Tek.162 waveform generator and the second pulse from the pulse sequencer were added together in a

mixer circuit. These two pulses were taken to the 180° channel of the pulse width generator whereas the first pulse from the pulse sequencer went to the 90° channel of the pulse width generator.

c) Pulse-Width Generator and Pulse Amplifier:

The circuit diagram of the pulse width generator is given in Fig. A3. The two channels of the pulse width generator were identical and were designed using Phantastron[35] circuits. The screen and the suppressor voltages of 5725 were obtained from a divider arrangement R_1-R_2-R_3. These resistors were chosen such that in the quiescent state the suppressor grid was sufficiently negative so that no plate current flew, all the space current going to the screen. Triggering was done with negative pulses applied to the plate and hence fed to the grid through the capacitor C. A negative trigger so applied, reduced the cathode current and consequently raised the screen voltage. The rise of screen voltage was transmitted to the suppressor to bring the suppressor above the point of plate current cut off. The trigger size was large enough to start the regenerative action but not so large as to cut off the tube current. When the tube is driven below cut off, the grid voltage will rise initially with a time constant RC into the conducting region, and there will be a delay between the application of the trigger and the start of the sweep. The pulse-width was controlled by adjusting

the voltage V_R. A cathode follower was interposed between the plate of the amplifier and the capacitor C in order to have shorter fall times for the pulses. The last stage was a mixer stage, the output of which was taken to a pulse amplifier for further amplification. The range of the pulse width could be varied from 0-35 μ sec continuously. It is possible to increase the range of the pulse width still further by changing RC appropriately. The circuit of the pulse amplifier is shown in Fig. A4. The amplifier stage was driven from cut off to saturation. The output stage was a cathode follower. A beam power tube was used so that the loaded pulse amplitude does not fall below 110 volts.

d) Radiofrequency Transmitter:

The schematic diagram of the 30 MHz transmitter is shown in Fig. 4. The 30MHz transmitter was designed to deliver high pulsed power output, and short rf rise and fall times. To meet the power requirements class C operation was preferred in certain stages following the rf gate. A crystal controlled oscillator (Fig. A5) at 10 MHz was housed in a rf leak tight copper can. In the master oscillator design[36] which is of modified colpitts type, it is noted that the capacitance connected from base to emitter is several times more than that connected from emitter to ground, thus effecting an impedance transformation.

The ceramic triode 7077 was used in the grounded grid configuration for gating the 10 MHz rf from the source follower.

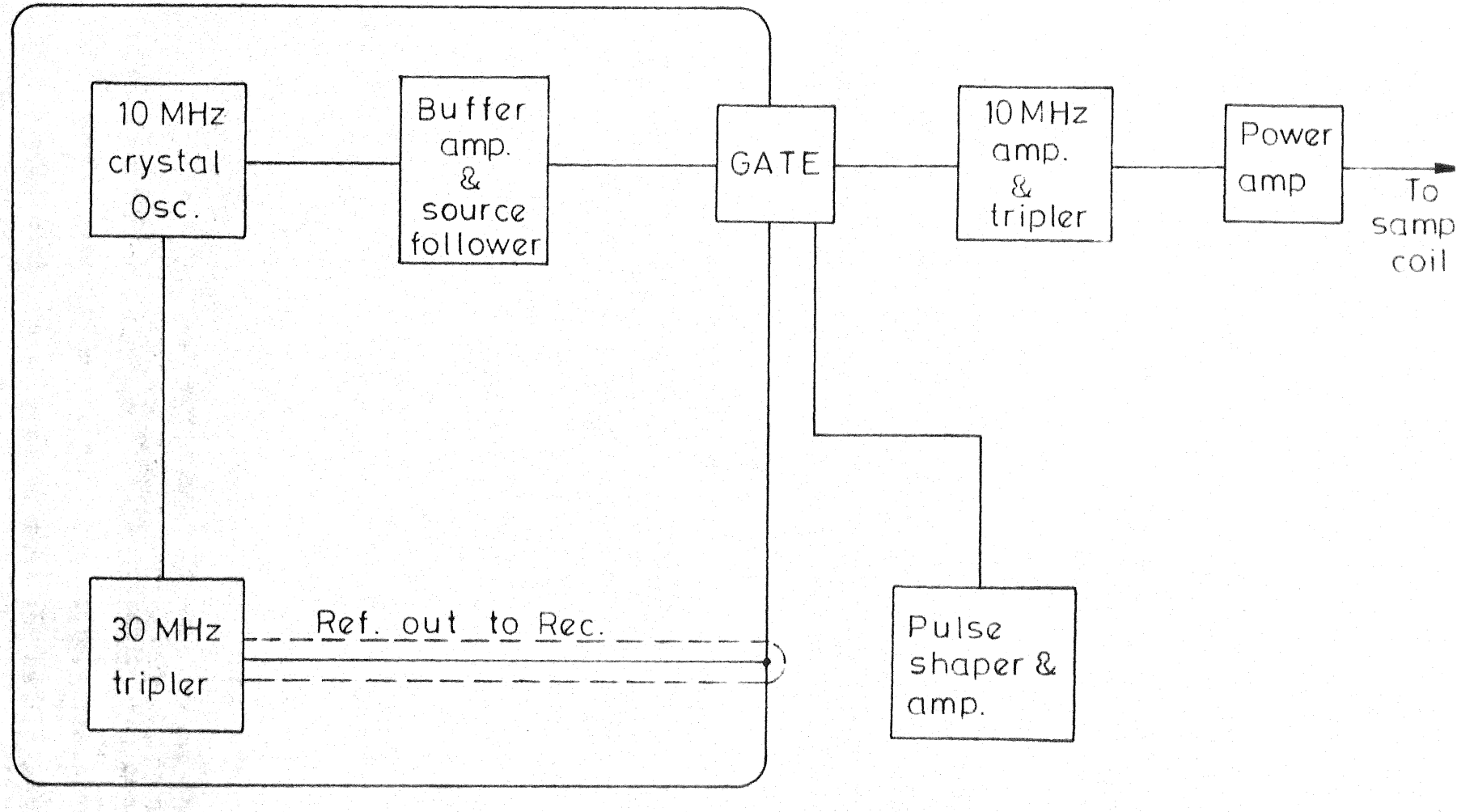

Fig. 4 - Block diagram : 30 MHz transmitter.

The rectangular pulses from the pulse amplifier were used to turn the triode 7077 on, for the duration of the pulse widths. The gated 10 MHz output was taken to a 10 MHz amplifier through a cathode follower; then it was tripled and amplified by a push-pull stage. The output from the push-pull stage was taken to a final power amplifier stage at 30 MHz. The power amplifier produced about 1.8 KW of pulsed power output (Figs. A6, A7 and A8).

The output from the master oscillator went through a phase-shifter to a tripler (Fig. A9). A commercial delay line Ad-Yu Type 559m was used as a phase-shifter which provided a delay of 0°-180°. The reference voltage obtained from the tripler output was coupled to the last stage of the high gain amplifier (L.E.L. Receiver) for phase sensitive detection.

e) Sample Coil:

A single coil which allows optimization in the transmitting and receiving modes was used as a sample coil. It was made of approximately 12 to 15 turns of 20 SWG wire and was about 1½" long. The insulation on the wire was completely stripped off and the wire was cleaned thoroughly before use. A thin-walled glass tube was fitted tightly inside the pressure vessel to insulate the coil from the vessel. The sample coil was wound to fit exactly inside the glass tube. The space outside the sample coil was plugged so that the entire gas sample was

confined to the coil. In the transmitting mode the sample coil was required to have low Q in order to avoid ringing of rf pulses after their application. While picking up the nuclear induction decay it was required to have high Q. A loose coupling scheme was adapted and the schematic is shown in Fig. 5.

f) Pre-Amplifier:

The circuit diagram of the pre-amplifier is shown in the Fig. A10. It is similar to the design by Clark.[33] The pre-amplifier was required to have high sensitivity and recover quickly from large overload signals. Use of the tube 7722 at the input stage provided low input noise as the g_m was high. A tuned circuit at the input enabled maximum input to the pre-amplifier when the signal was picked up. The crossed diodes at the plate of the first stage prevented loading of the subsequent stage. The output stage was a cathode follower, with an output impedence of about 80 ohms. The voltage gain of the pre-amplifier was about 10.

g) Integrated rf Amplifier:

The RCA 3005 integrated rf amplifier was used following the pre-amplifier to further increase the voltage level of the signal before it was fed to the high gain amplifier. The input and output impedances of CA 3005 were matched for 50 ohms. The design of CA 3005 amplifier was taken from the RCA application

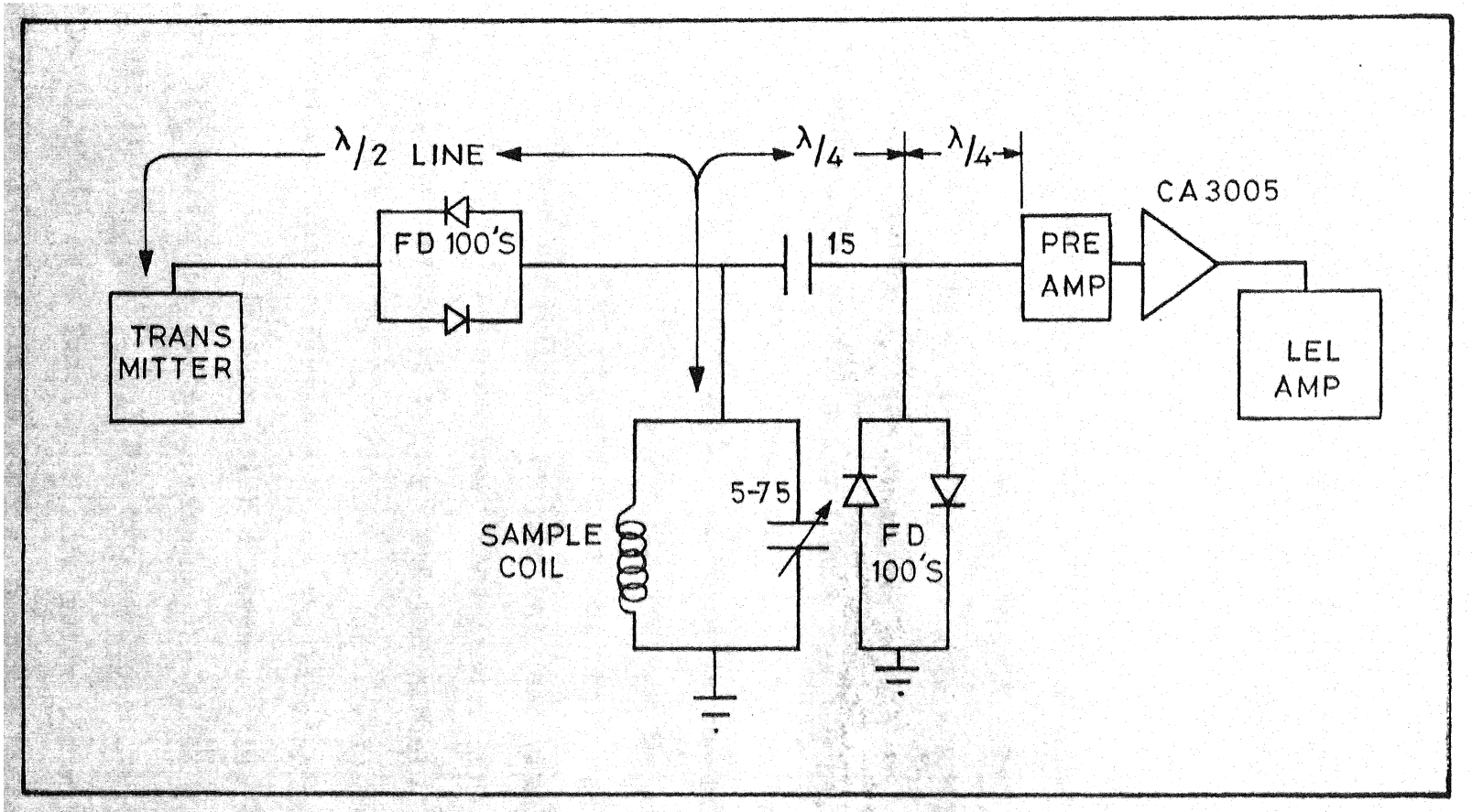

Fig. 5 - Schematic: coupling of RF head.

note ICAN-5022 and the circuit elements used are shown in Fig. A11. The integrated amplifier had a power gain of about 25 db.

h) High-Gain Receiver:

The rf receiver was a L.E.L. amplifier of the varian associates, model No. 1MN2-30-15-50. The centre frequency was at 30 MHz. The 3 db band width was 10 MHz. Two outputs were provided, the one after detection has a gain of 90 db maximum and the other after a video stage has a gain 115 db minimum at 0 volt bias. The quoted noise figure was 1.8 db. The input impedance was 50 ohms.

A 1N295A diode detector was used in the L.E.L. amplifier. Ordinary diode detection is not linear over the entire region and the non-linearity becomes important while dealing with small signals. Phase sensitive detection was used which allowed operation in the linear region of the diode. The diode detects the sum of the reference voltage and the signal. The signal was kept below 1/10 of the reference voltage to avoid distortion. An experiment was performed to find the biasing voltage of the diode for linear detection. For a given setting of the spectrometer, the reference voltage, biasing the diode detector was varied and the output signal level was recorded each time. The NMR signal strength as a function of the reference voltage is shown in the Fig. 6. It is obvious that for linear detection,

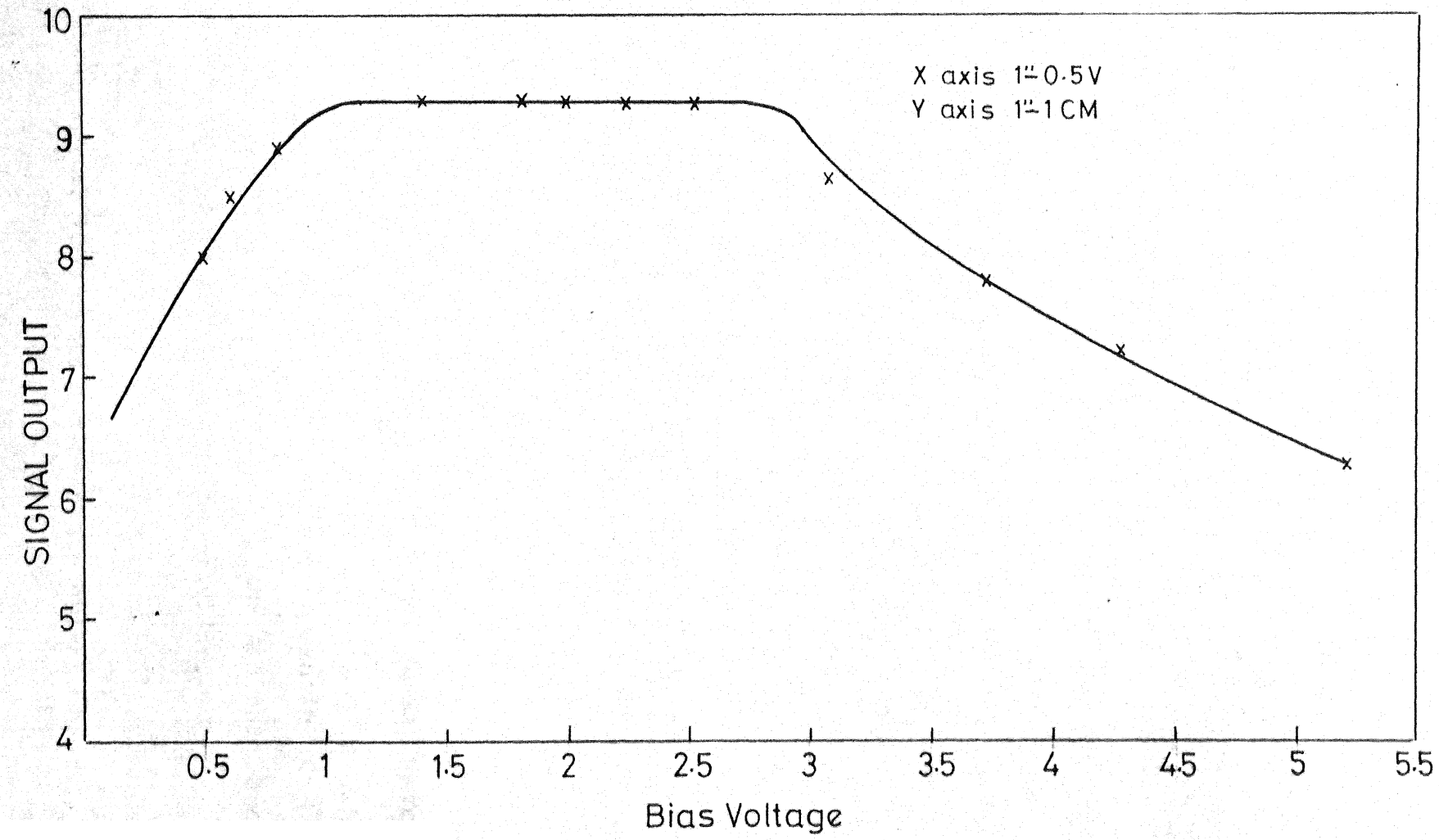

Fig. 6 - Diode detector response.

the reference voltage biasing the diode detector must be kept between 1.8 and 2.8 volts negative.

i) Sample Holder and Gas Handling System:

The high pressure sample holder (Fig. 7) consists of a thick walled Be-Cu vessel (o.d. 2.7 cm and i.d. 1 cm) and Be-Cu plugs A and B. The standard high pressure sealing technique was adapted in all pressure sealings (AE cone fitting). The seats were machined to have a taper of 60° while the plugs A and B have a taper of 59°. The return lead of the sample coil was fastened to the plug B by means of a screw. The plug A was first tightened to make the seal and then the plug B was sealed in its position by tightening the nut E. The rf head was sealed against pressure at room temperature with a teflon washer. The pressure seals were satisfactory upto about 3,000 psi at room temperature.

The pressures were measured using Bourdon pressure gauges which were calibrated using a dead weight gauge of Ruska Instrument Corporation, Texas.

The gas handling system is shown in the schematic of Fig. 8. All high pressure connectors used in the gas handling system were purchased from Autoclave Engineering Inc.

j) Heater:

A commercial 1000 watts non-magnetic spiral, heater

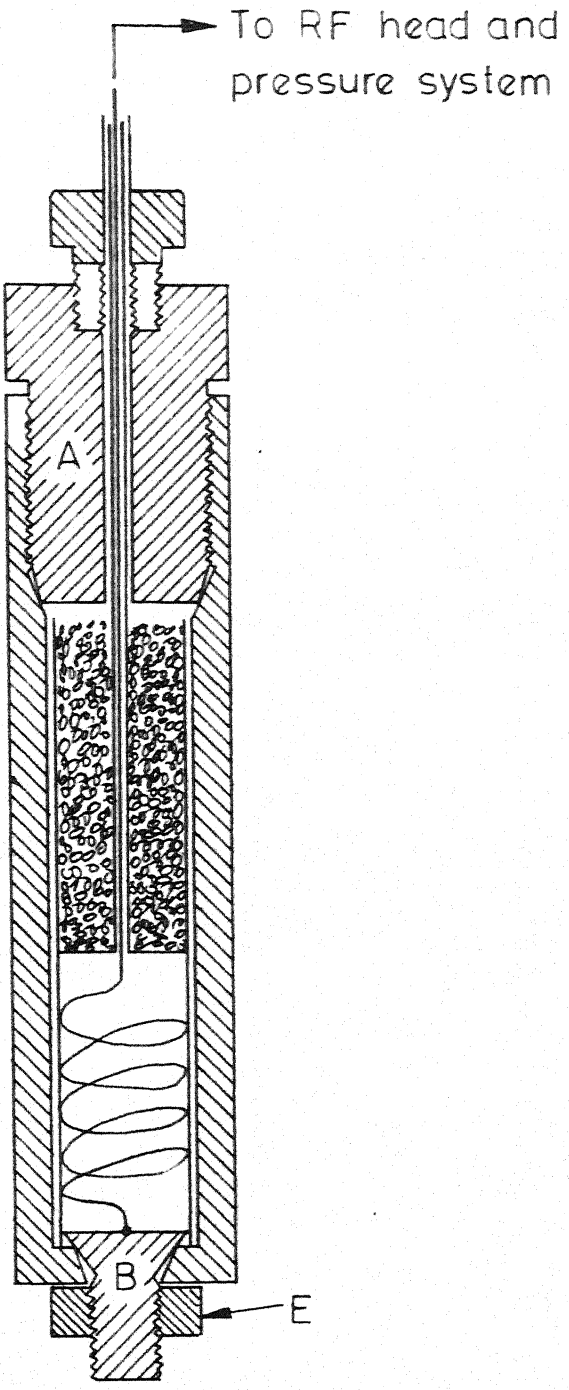

Fig. 7 - Sample holder.

element was wound non-inductively on the outside of the pressure vessel using a thin mica sheet for insulation. A liquid porcelain called "saureisin" was used to hold the windings in place. D.C. was used to heat the sample holder since small 50 Hz noise was observed when A.C. was used. About 80 watts of electrical power had to be dissipated in order to maintain the sample holder at about 600°K. The pressure vessel along with the heater was kept inside a vacuum jacket to keep the conduction and convection current losses to a minimum. The leads from the heater were taken outside the vacuum jacket through Kovar seals.

k) Temperature Measurements:

The temperature was measured using calibrated Chromel-Alumel thermo-couple embedded on the top portion of the pressure vessel away from the heater element. The thermo-couple leads were also taken outside the vacuum jacket through kovar seals. A Honeywell temperature controller model no. R7086 A (millivolt operated) was used to control the temperature. Whenever the temperature was changed atleast 8 to 10 hours were allowed before taking the measurements to ensure that the sample was at equilibrium with the vessel. The temperature was measured with a Leeds and Northrup potentiometer, type 8087. The temperature measurements were accurate to at least $\pm$ 2°.

II.4 i) Mixing of Gases: Composition Determination:

All the gases that were used in the experiments except Argon were of research grade and were obtained from Matheson Gas Co., Argon was obtained from Indian Oxygen Co., and was of 99.97% purity. A mixture of the two gases was prepared in a cylinder by first introducing the low concentration component and then the second component to bring the total pressure to the required value. The total pressures were noted before and after the introduction of the second component. The gases were left together for about 48 hours after mixing to obtain a homogeneous mixture. The composition of the gases was estimated from the partial pressures and was checked experimentally by comparing the signal strength of the mixture with that of pure CH_4 under identical conditions. The number density of CH_4 was obtained from the compressibility data by Petroleum Research Institute.[37]

ii) Experimental Determination of Composition:

The height of the spin-echo $A(2\tau)$ where τ is the time between 90° and 180° pulses is given by[38]

$$A(2\tau) = A(0) \exp\left(-\frac{2\tau}{T_2} - \frac{D\gamma^2 G^2 (2\tau)^3}{12}\right) \quad (2.4)$$

in a magnetic field of constant gradient along the Z axis. In eq. 2.4,

$A(2\tau)$ = echo amplitude at time 2τ

$A(0)$ = echo amplitude at time $\tau = 0$

T_2 = spin-spin relaxation time

D = self-diffusion coefficient of the molecule

γ = gyromagnetic ratio of the spins considered

G = constant gradient of the external magnetic-field

At moderate densities both T_2 and $\frac{1}{D}$ are proportional to ρ, the density of the gas in amagat units, where an amagat is 2.69×10^{19} molecules/cc. Assuming $\frac{T_1}{\rho} = \frac{T_2}{\rho}$ and neglecting $\frac{D\gamma^2 G^2 (2\tau)^3}{12}$ where τ was about 0.5 msec, the equation 2.4 becomes

$$A(2\tau) = A(0) \exp(-2\tau / T_1) \qquad (2.5)$$

If the number of spins per molecule is denoted by n_I, then

$$A(0) \propto M(0) \quad \text{where} \quad M(0) = \frac{\rho n_I \hbar^2 \gamma^2 I(I+1)}{3 KT} \qquad (2.6)$$

or $A(0) = C\rho$ where C is a constant, then eq. 2.5 becomes,

$$A(2\tau) = C\rho \exp(-2\tau / T_1) \qquad (2.7)$$

Therefore $(C\rho)_{Mix}/(C\rho)_{pure\ CH_4}$ gives the fractional composition of CH_4 in the mixture. Since the mixture pressures involved

in all the experiments were not high, the composition determined by the experimental method agreed within 3 to 4% to the value determined by partial pressures. In other words though the non-ideality was taken into account while determining the composition the ideal gas law was adequate enough to determine the same. Typical plots of signal strength vs density of CH_4 and signal strength vs pressure of CH_4-CO_2 mixture are shown in Figs. 9 and 10.

All densities of the mixtures were calculated using the ideal gas law

$$\rho = \frac{273}{T} \times P \quad \text{(in atmospheres)} \qquad (2.8)$$

where T is the temperature in degree Kelvin and P, the pressure in atmospheres.

* * *

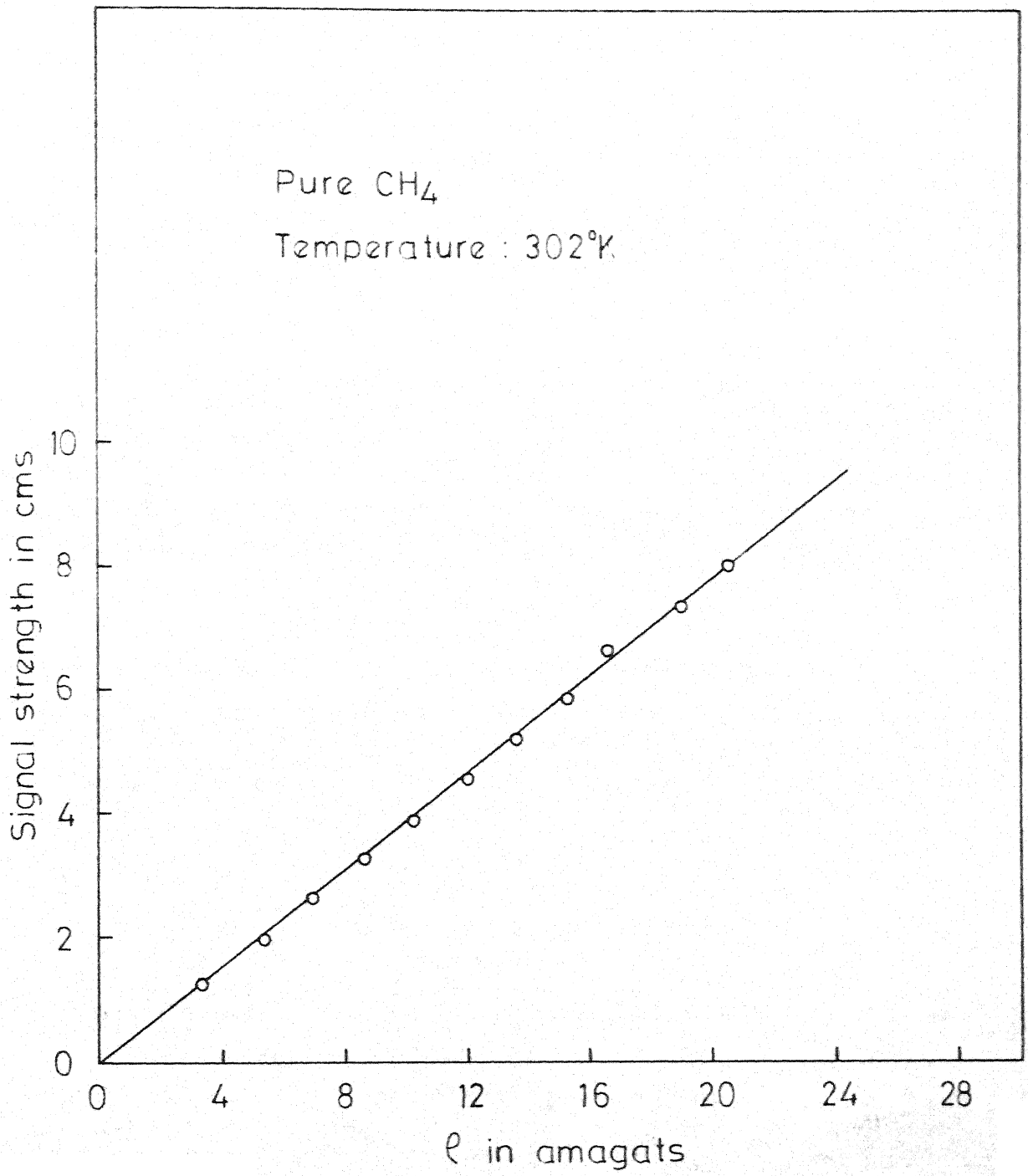

Fig. 9 - Signal strength vs. density.

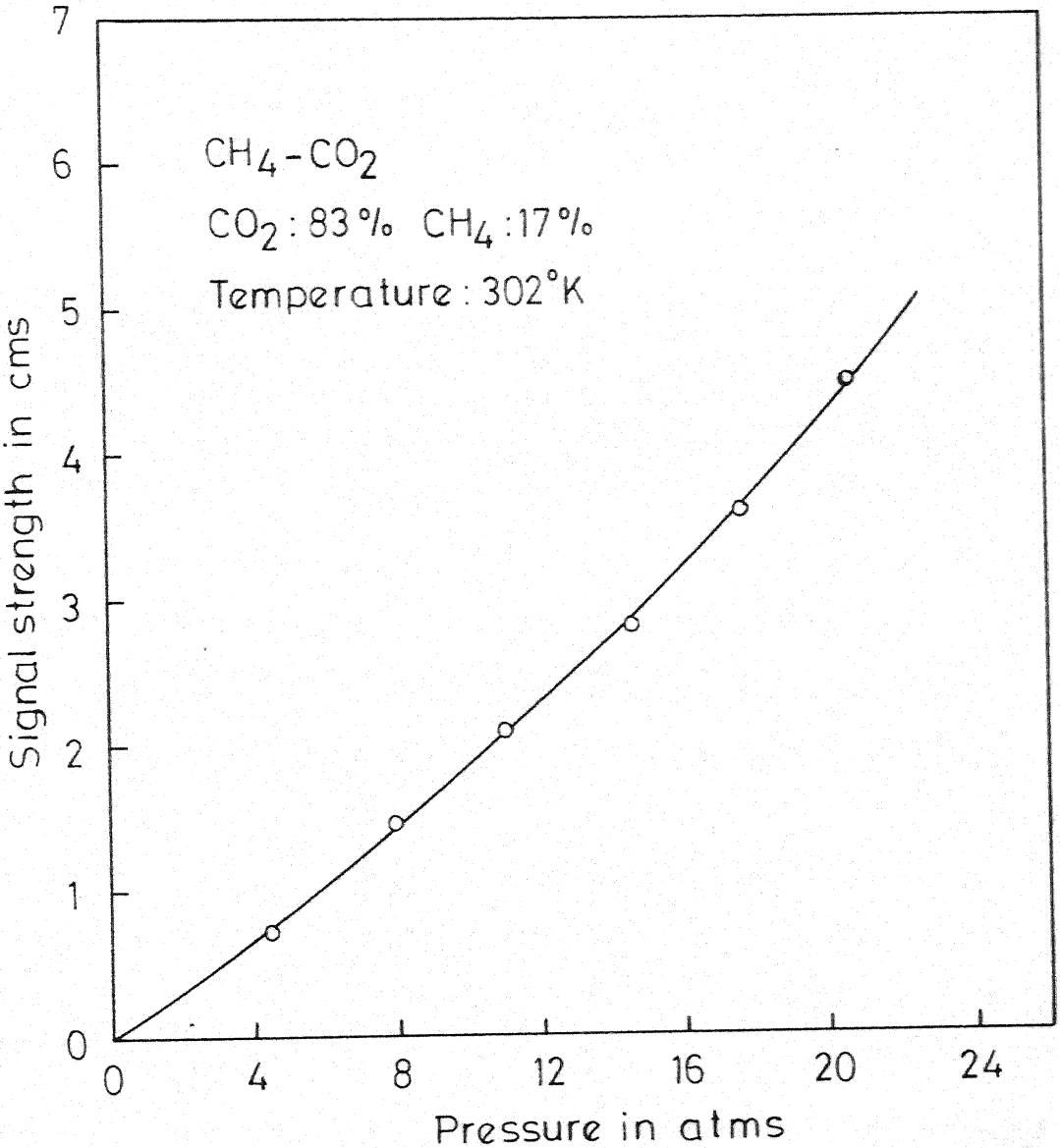

Fig. 10 - Signal strength vs. pressure.

CHAPTER III

THEORY

III.1 Intramolecular Interactions:

The spin-lattice relaxation rate T_1^{-1} for most molecular liquids and gases receives contribution from the inter molecular and intra molecular interactions. For gases which are not too dense, the inter molecular contribution is negligibly small because of the large average separation between molecules. The intra molecular interactions which contribute to T_1^{-1} in dilute gases are of two types, a dipole-dipole interaction between the different spins ($I = 1/2$ only) within a molecule and a spin-rotational interaction between the spins and rotational magnetic moment of the molecule. In case of H_2, the strengths of these two interactions are comparable. The strengths of the coupling constants in H_2 for the intra molecular dipolar interaction and spin-rotation interaction are 34 gauss and 27 gauss respectively.[39] But in the case of polyatomic molecules such as CH_4, Bloom et. al[19] have established, as would be shown later in this chapter, that only spin-rotation interaction is the dominant mechanism of relaxation.

Collisions between molecules give rise to transitions between the rotational states of the molecules. In case of symmetric top or spherical top molecules, these rotational

states are denoted by the quantum numbers J,K and M which are the values of the total angular momentum J , the projection of J on the symmetry axis of the molecule and the projection of J on a space fixed Z axis respectively.

As a result of the transitions between different rotational states, the intra-molecular spin dependent interactions fluctuate with time. These fluctuations enable the nuclear spin system to exchange energy with the rotational and translational degrees of freedom of the molecules. These non-spin degrees of freedom constitute the lattice at a constant temperature T to the nuclear spins. The nuclear spin system thereby approaches equilibrium at temperature T at a rate which is governed by the strength of the intra molecular interactions and the spectrum of frequencies associated with the fluctuations of these interactions.

The eigen functions $|JKM\rangle$ of the rotational Hamiltonian $\mathcal{H}_J$ of a symmetric top or spherical top molecule are characterised by the quantum numbers J, K and M.

$$\mathcal{H}_J \; |J\,K\,M\rangle = \hbar\omega_{JK} \; |J\,K\,M\rangle \qquad (3.1)$$

where

$$\hbar\omega_{JK} = \frac{\hbar^2}{2I_o} J(J+1) + \frac{\hbar^2}{2}\left(\frac{1}{I_A} - \frac{1}{I_o}\right) K^2 \qquad (3.2)$$

for a symmetric top molecule. I_o and I_A denote the two principal moments of enertia.

For spherical top molecules $I_A = I_o$ and hence

$$\hbar \omega_{JK} = \frac{\hbar^2}{2I_o} [(J(J+1))] \qquad (3.3)$$

where ω_{JK} is independent of K.

i) Magnetic Dipolar Interaction:

The Hamiltonian for the intra molecular dipolar and quadrupolar interactions can be written in terms of products of nuclear spin operators and the $Y_{2m}(\Omega)$. From the general theory of nuclear spin relaxation[25], one obtains R_A, the relaxation rate due to intra molecular dipolar and quadrupolar interactions, in terms of Fourier transforms $J_{2,m}(\omega)$ of the correlation functions $G_{2,m}(\tau)$ of the $Y_{2,m}(\Omega)$ (t)),

$$R_A = 4\pi \; K_A \left[J_{21}(\omega_o) + 4 J_{22}(2\omega_o) \right] \qquad (3.4)$$

where ω_o is the nuclear Larmor frequency and

$$G_{2,m}(\tau) = \mathrm{Re} \left\langle Y_{2,m}(\Omega(0)) \; Y^{\dagger}_{2,m}(\Omega(t)) \right\rangle \qquad (3.5)$$

where $\langle \; \rangle$ represents an ensemble average. The quantity K_A depends on the type of interaction considered.

Bloom et.al[19] have evaluated $[G_{2,m}(\tau)]_{\text{free}}$ for spherical top molecules;

For spherical top molecules,

$$\left[G_{2,m}(\tau)\right]^{\text{Sph}}_{\text{free}} = \frac{1}{4\pi} \sum_{J=0}^{\infty} \frac{(2J+1)^2}{5} P_{JKM} \sum_{\substack{n=-2 \\ n+J \geq 0}}^{+2} \left(1+\frac{2n}{2J+1}\right) \times$$

$$\text{Cos}\left[\frac{nK T_o \tau}{\hbar}(2J+n+1)\right] \qquad (3.6)$$

where $n = J'-J$ and T_o is the characteristic temperature defined by $T_o = \hbar^2/2K\,I_o$.

The Fourier transform or "spectral density" $J(\omega)$ of the free molecule correlation function is a series of delta functions at $nKT_o(2J+n+1)/\hbar$ for spherical top molecules. The effect of collisions among molecules is to limit the lifetime of the molecules in their rotational states and hence to spread the 'spectral density' associated with each δ -function over a range of frequencies of the order of collision frequency. Since the lowest rotational frequency is often much larger than the nuclear Larmor frequencies at which the spectral densities are calculated, the contribution to $J(\omega_o)$ from δ functions centered at frequencies other than zero can be safely neglected. Then the oscillating term in eq. 3.6 is dropped and the free molecule correlation functions become independent of time. The effect of molecular collisions is to cause $G_{2,m}(\tau)$ to decay to zero

in a time of the order of τ_c. In polyatomic molecules it was assumed that the effect of collisions could be adequately described by writing

$$G_{2,m}(\tau) = [\, G_{2,m}(\tau) \,]_{free}\, g_2(\tau) \qquad (3.7)$$

where $g_2(0) = 1$ and $g_2(\tau)$ is a function which decreases monotonically to zero as τ is increased. It is seen that in eq. 3.6, $[\, G_{2,m}(\tau)]_{free}$ is independent of m. Hardy[39] has shown that under quite general conditions, which should apply to gaseous methane

$$G_{1,m}(\tau) = G_{1,0}(\tau)\, \exp\left(i\, m\, \omega_J(\tau)\right) \qquad (3.8)$$

where ω_J is the rotational Larmor frequency of the molecule. Then the spectral density of $G_{2,m}(\tau)$ can be written as,

$$J_{2,m}(\omega) = \int_{-\infty}^{+\infty} G_{2,0}(\tau)\, e^{im\omega_J \tau}\, e^{-i\omega\tau}\, d\tau \qquad (3.9)$$

$$= \frac{1}{4\pi}\, f_2\, j_2(\omega - \omega_J) \qquad (3.10)$$

where $$j_2(\omega) = \int_{-\infty}^{+\infty} g_2(\tau)\, \exp(-i\omega\tau)\, d\tau \qquad (3.11)$$

The quantity f_2 must take on a value between 0 and 1. When the oscillating term in eq. 3.6 is dropped, using eqs. 3.6, 3.7 and 3.8 it is shown[19] that $f_2 = 0.2$ for spherical top molecules.

Using eqs. 3.9 and 3.4 one gets,

$$R_A = K_A f_2 \left[j_2 (\omega_o - \omega_J) + 4 j_2 (2\omega_o - 2\omega_J) \right] \quad (3.12)$$

ii) Spin-Rotation Interaction:

The spin-rotation interaction arises from the fact that the rotating electron cloud of the molecule establishes a local magnetic field at the sites of the nuclei. The transitions in the rotational states of the molecule caused by collisions modulate randomly these magnetic fields, thereby causing the nuclear spin transitions which bring the spin system to equilibrium.

In polyatomic molecules, the spin-rotation interaction is in general characterised by six independent parameters, the three principal values of the spin-rotation tensor and the three Euler angles required to specify the orientation of the principal axis coordinate system. In spherical top molecules such as CH_4 where the principal axis coordinate system of the spin-rotation tensor coincides with the molecular principal axis coordinate system, the number of independent parameters is reduced to only two which are denoted by C_{11} and $C_{\perp}^{40}$.

The spin-rotation Hamiltonian $\mathcal{H}_R$ of a single spin is given by[19, 41, 42]

$$\hbar^{-1} \mathcal{H}_R = C_a \sum_{k=-1}^{+1} (-1)^k I'_k J'_{-k} - C_d \left(I'_o J'_o - \frac{1}{3} \sum_{k=-1}^{+1} (-1)^k I'_k J'_k \right) \quad (3.13)$$

where

$$I_1 = -\frac{1}{\sqrt{2}}(I_x + i\,I_y) \qquad J_1 = -\frac{1}{\sqrt{2}}(J_x + i\,J_y)$$

$$I_{-1} = \frac{1}{\sqrt{2}}(I_x - i\,I_y) \qquad J_{-1} = \frac{1}{\sqrt{2}}(J_x - i\,J_y)$$

$$I_o = I_z \qquad J_o = J_z$$

$$C_a = \frac{1}{3}(C_{\parallel} + 2\,C_{\perp}) \qquad C_d = C_{\perp} - C_{\parallel} \tag{3.14}$$

The primes in eq. 3.13 indicate that the components of $\bar{I}$ and $\bar{J}$ are referred to a coordinate system fixed in the molecule with the Z axis along the symmetry axis of the molecule.

Transforming $\bar{I}'$ and $\bar{J}'$ into a SFF, Hubbard[41] has obtained

$$\hbar^{-1} H_R = \sum_m I_m K_{1,m} \tag{3.15}$$

where

$$K_{1,m} = (-1)^m C_a J_{-m} - \left(\frac{2}{3}\right)^{\frac{1}{2}} C_d \sum_{\mu} (-1)^{\mu} C(112 \mid m\ \mu)\ x$$

$$D^2_{o,-(m+\mu)}\ J_{\mu} \tag{3.16}$$

The operators $D^2_{m_1 m_2}$ and J_μ and hence $K_{1,m}$ are time-dependent because of changes of molecular state as a result of collisions among molecules. From the general theory of nuclear spin relaxation[25]

$$R_c = 4\pi^2 J_{11}(\omega_o) = 4\pi^2 \int_{-\infty}^{\infty} G_{11}(\tau)\, e^{-i\omega_o \tau}\, d\tau \qquad (3.17)$$

where $G_{11}(\tau)$ is the correlation function of $K_{11}(\tau)$, defined as,

$$G_{1,m}(\tau) = \mathrm{Re} \left\langle K_{1,m}(0)\, K^{\dagger}_{1,m}(\tau) \right\rangle \qquad (3.18)$$

The bracket $\langle\ \rangle$ denotes an ensemble average of the molecules at the temperature T.

The contribution to the relaxation rate T_1^{-1} in spherical top molecules due to spin-rotation interaction has been calculated by Bloom et.al using time correlation function method[19,43]. They have neglected the contribution to the spectral density of G(t) from $\Delta J \neq 0$ transitions which fall in the infra-red region. Also they have assumed that the effect of molecular collisions is to cause the correlation functions associated with the freely rotating molecule to decay to zero exponentially. In the short correlation time limit ($\omega_o\ \tau_1 \ll 1$) where the rotational lines are broadened by an amount larger than the average centrifugal distortion splittings ($\simeq$ 200 MHz), the theory in which the centrifugal distortion effects are neglected may be used. Following their theory T_1 may be written as,

$$\frac{1}{T_1} = \left\langle \left(\frac{1}{T_1} \right)_J \right\rangle \simeq \frac{8\pi^2}{3} C^2_{eff} \left\langle J(J+1)\ \tau_1^J \right\rangle \qquad (3.19)$$

where $C^2_{eff} = \left[C_a^2 + (4/45)\, C_d^2 \right]$ for a spherical top molecule.[19]

C_a and C_d are the spin-rotation interaction coupling constants having values 10.4 KHz and 18.5 KHz respectively[44] for CH_4; τ_1^J is the correlation time of the spin-rotation interaction corresponding to the J state.

Considering the relative contributions of the intra molecular dipolar interaction R_A and the spin-rotation interaction R_C, Bloom et.al[19] have concluded that in the case of CH_4, R_A contributes 8% of T_1^{-1} for $\tau_1 = 3\,\tau_2$ and 20% for $\tau_1 = \tau_2$ at T = 100°K and 3% and 8% respectively at T = 300°K. τ_1 and τ_2 are the time constants of the exponentially decaying reduced correlation functions $g_1(\tau)$ of the spin-rotation interaction and intra molecular dipolar interaction respectively. It may also be noted that there are quite general arguments[45] for believing that τ_1/τ_2 lies between the values of 1 and 3. This establishes that the spin-rotation interaction is the dominant mechanism of relaxation in CH_4 at room temperature and above; hence the parameters used to fit the experimental data as a function of temperature (300°K-600°K) would be associated with R_C only to a good approximation in all the cases studied.

III.2 Intermolecular Potential and Intramolecular Correlation Time:

From the foregoing discussion it is obvious that nuclear spin relaxation cannot take place in the absence of collisions. The effect of collisions is to limit the lifetime of a molecule in a J state. For a two level system Bloom and Oppenheim[5] have related the intra molecular correlation functions explicitly to the intermolecular anisotropic interactions. The proton relaxation data in pure H_2 and in mixtures of H_2 with other gases were interpreted to obtain information on the anisotropic intermolecular potentials.[5,8] In polyatomic molecules such as CH_4, because of its large moment of enertia, appreciable number of rotational levels are populated even at room temperature. Hence the results of H_2 are not applicable to polyatomic molecules. In fact it does not seem that the two level results of H_2 and its isotopic modifications are applicable to any other gaseous system as the number of rotational levels involved is quite large.

In the absence of a detailed molecular theory for polyatomic molecules, the theory of Bloom and Oppenheim has been used in a modified way to obtain information about the intermolecular potential. Since there is no simple theory to relate the correlation time of the intra-molecular interactions to the inter molecular potential, it is assumed, a priori, that τ_1^J, the correlation time of the spin-rotation interaction is equal to the average lifetime of the molecule in that J state. The

average lifetime of the molecule in a J state may then be evaluated for a given anisotropic potential using first order perturbation theory and the results of Bloom and Oppenheim for intermolecular correlation functions. The justification for this assumption must then come a posteriori and will be discussed later. Under this approximation, it is then possible to obtain the anisotropic potential parameters using eq. 3.19.

III.3 General Procedure for the Evaluation of the Average Lifetime of a Molecule in a J State:

Defining A(J'M'; JM) as the transition rate for the transitions $JM \longrightarrow J'M'$, τ_1^J can be expressed as[11]

$$\frac{1}{\tau_1^J} = \frac{1}{2J+1} \sum_{M=-J}^{+J} \sum_{J'} \sum_{M'=-J'}^{+J'} A(J'M';JM) \qquad (3.20)$$

$M' \neq M$ for $J=J'$

It is assumed that the collisions are weak[46] in the sense that first order perturbation theory may be used to evaluate the transition rates A(J'M'; JM). Then the transition rate A(J'M';JM) is given by

$$A(J'M';\ JM) = \frac{1}{(2J'+1)} \sum_{KK'} A(J'K'M';\ JKM) \qquad (3.21)$$

and

$$A(J'K'M';\ JKM) = \frac{1}{\hbar^2}\int_{-\infty}^{+\infty} e^{-i\omega_{JJ'}t} \times \left\langle (JKM \mid V_A(0) \mid J'K'M')\ (J'K'M' \mid V_A(t) \mid JKM) \right\rangle dt \qquad (3.22)$$

where $|JKM\rangle$ are the eigen states of the unperturbed rotational Hamiltonian (eq. 3.1) and

$$\hbar\omega_{JJ'} = E_J - E_{J'} \qquad (3.23)$$

is the energy difference between the rotational states J and J' $\left\langle (JKM \mid V_A(0) \mid J'K'M')\ (J'K'M' \mid V_A(t) \mid JKM) \right\rangle$ is the correlation function of the matrix element of V_A between states J'K'M' and JKM where the average is performed with the density matrix $e^{-\beta H_L^o} / Tr\,[e^{-\beta H_L^o}]$ and

$$V_A(t) = e^{i/\hbar\, H_L^o t}\ V_A(0)\ e^{-i/\hbar\, H_L^o t} \qquad (3.24)$$

where

$$H_L^o = H_L - V_A \qquad (3.25)$$

is that part of the lattice Hamiltonian which contains the kinetic energy of the centres of mass of the molecules and the isotropic intermolecular potential.

i) Intermolecular Potentials:

The intermolecular potential V between two molecules separated by distance r is given by

$$V = V_o(r) + V_A(r, \theta') \qquad (3.26)$$

where the isotropic part $V_o(r)$ depends only on r and the anisotropic part $V_A(r,\theta')$ depends both on r and θ' where θ' denotes the orientation of the molecule relative to a space fixed frame.

Two models of isotropic intermolecular potentials will be considered:

Model 1: Hard sphere potential

$$\begin{aligned} V_o(x) &= \infty \qquad x < 1 \\ V_o(x) &= 0 \qquad x \geq 1 \end{aligned} \qquad (3.27)$$

where $x = r/a$ is a dimensionless quantity and a is a potential parameter.

Model 2: Lennard-Jones potential:

$$V_o(x) = 4\varepsilon\,(x^{-12} - x^{-6}) \qquad (3.28)$$

ε , and $a = r/x$ are appropriate energy and distance parameters;

ii) Anisotropic Intermolecular potentials:

The anisotropic intermolecular potential is in general written by considering the electrostatic interaction appropriate to the colliding pair. Specific forms of the anisotropic potentials appropriate for the different systems will be discussed in the following:

The most general form of the attractive anisotropic interaction is given by[47]

$$V_\lambda = \frac{4\pi C_\lambda}{R^{l+1}} \sum_{m_1,m_2} C(l_1 l_2 l;\ m_1 m_2 m)\ Q_{l_1,m_1}(\Omega_1)\ Q_{l_2 m_2}(\Omega_2)\ Y^*_{l,m}(\Omega) \qquad (3.29)$$

The orientations of Ω_1, Ω_2 and Ω are all relative to a SFF (Fig. 11). The vector connecting O_1 to O_2 is denoted by $\bar{R} = (R, \Omega)$ representing the intermolecular axis where $\Omega = (\theta, \phi)$ give the orientation of $\bar{R}$. The molecules have been considered as having rigid non-overlapping charge distributions centred around origins O_1 and O_2.

$\lambda = l_1 l_2$, $l = l_1 + l_2$, l_1 and l_2 indicate the order of the electric moment; for dipole $l_1=1$, quadrupole $l_1=2$ etc.,

$$C_\lambda = C_{l_1,l_2} = \frac{(-1)^{l_2}}{(2l+1)} \left[\frac{4\pi(2l+1)!}{(2l_1+1)!\ (2l_2+2)!} \right]^{1/2} \qquad (3.30)$$

The multipole moments $Q_{l,m}$ are defined by[47]

$$Q_{l,m} = \sum er^l\ Y_{l,m}(\bar{r}) \qquad (3.31)$$

the sum extending over all the charges in the distribution with $\bar{r} = (r, \bar{r})$, the position of the charge e relative to the origin of the distribution. For a continuous distribution of charge,

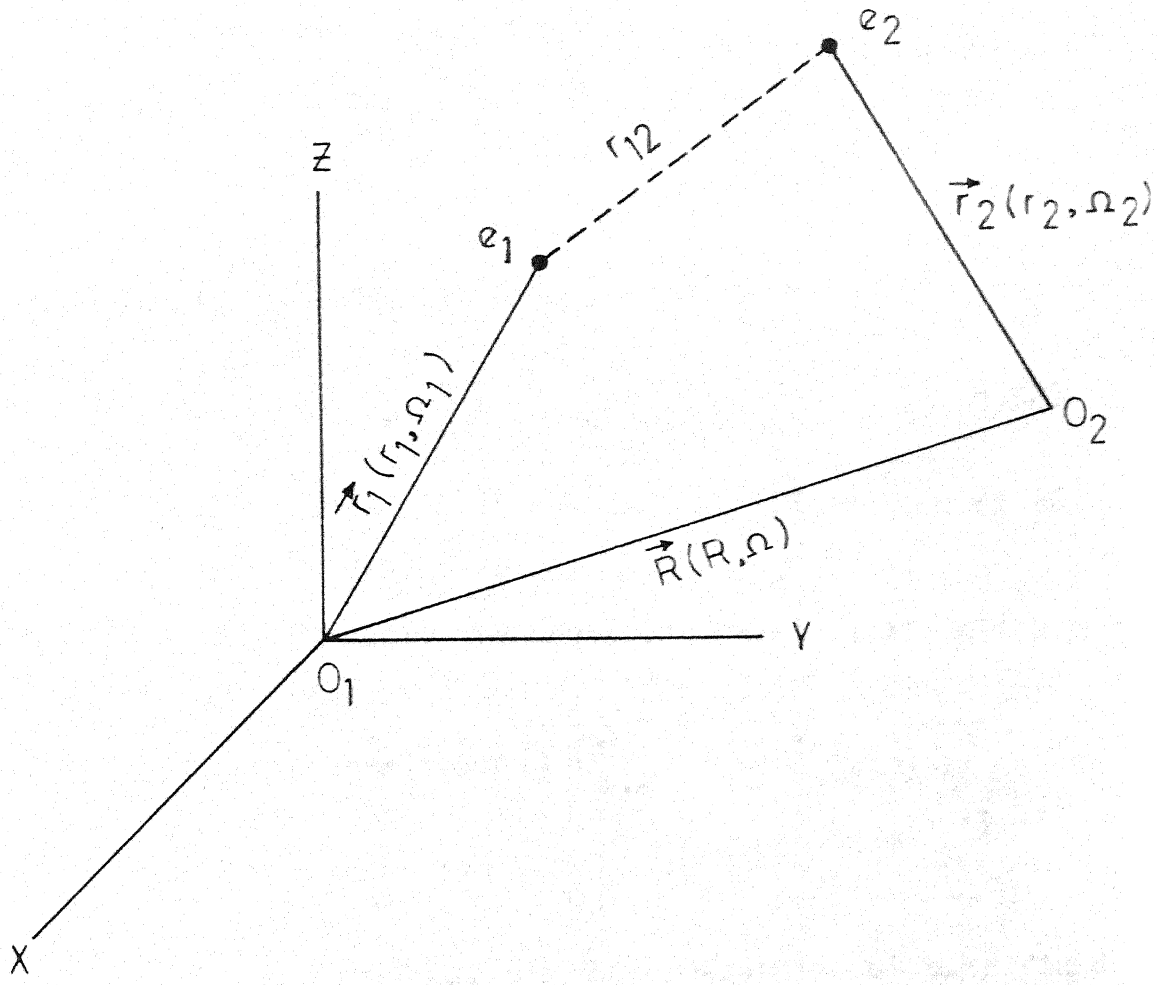

Fig. 11 - Orientation of Ω_1, Ω_2 and Ω relative to SFF

the sum in definition 3.31 is replaced by an integral over the charge density $\rho(r)$. When the intermolecular potential is considered for definite electric moments, $Q_{l,m}$, for a fixed l, would then form the components of an irreducible tensor of rank l. It is shown[47] for systems having axial symmetric charge distribution such as N_2 or CO_2.

$$Q_{l,m} = Q_l \, Y_{l,m}(\Omega) \tag{3.32}$$

where Q_l is a constant; Ω denotes the orientation of the symmetry axis of the charge distribution. In case of CH_4 where there is a T_d symmetry the octopole moment is given[47] by

$$Q_{3,m} = i \left(\frac{7}{4\pi}\right)^{\frac{1}{2}} \left(\frac{6}{5}\right)^{\frac{1}{2}} \hat{\Omega} \left[D^3_{m,2}{}^*(\Omega) - D^3_{m,-2}{}^*(\Omega) \right] \tag{3.33}$$

where

$\Omega = (\theta, \phi, \chi)$ denotes the orientation of body fixed frame relative to a SFF. D's are the corresponding rotation matrices[48] $\hat{\Omega}$ is the scalar value of the octopole moment.

a) Spherical Top Molecules (CH_4, CF_4 and SiF_4):

The attractive part of the anisotropic intermolecular potential in spherical top molecules such as CH_4 (also CF_4 and SiF_4) is given by the electrostatic interaction between the permanent octopoles resident on the molecules whereas the

repulsive part is assumed to have an r^{-12} dependence and the same angle dependence as that of the attractive part. Then using eqs. 3.29, and 3.30, the anisotropic potential is given by

$$V_A(r,\Theta') = \left(\frac{4\pi \times 1716}{7}\right)^{\frac{1}{2}} \frac{42}{65}\, b(ax) \sum_{m_1 m_2 m} C(336;\, m_1 m_2 m) \times$$

$$\left[\left(D^{3*}_{m_1,2}(\Omega_1) - D^{3*}_{m_1,-2}(\Omega_1)\right)\left(D^{3*}_{m_2,2}(\Omega_2) - D^{3*}_{m_2,-2}(\Omega_2)\right) Y^*_{6,m}(\Omega\right. \tag{3.34}$$

where

$$b(ax) = (a_1/x^{12} - a_2/x^7) \tag{3.35}$$

$$x = r/a, \quad \text{and}$$

$$a_2 = \hat{\Omega}^2/a^7 \tag{3.37}$$

a_1 is the measure of the strength at r=a of the repulsive part in the anisotropic potential.

b) CH_4-N_2 and CH_4-CO_2 Mixtures:

The attractive part of the anisotropic potential in these systems is considered to be given by the interaction between the octopole moment of CH_4 and quadrupole moment of N_2 or CO_2.

Using eqs. 3.29, 3.32 and 3.33 and assuming an r^{-12} dependence for the repulsive part of the anisotropic potential

having the same angle dependence as that of the attractive part,

$$V_A(r,\Theta') = 4\pi \; i\left(\frac{252}{55}\right)^{\frac{1}{2}} b(ax) \sum_{m_1 m_2 m} C(325;\, m_1 m_2 m) \times$$

$$\left[\left(D^{3*}_{m_1,2}(\Omega_1) - D^{3*}_{m_1,-2}(\Omega_1)\right) \left(Y_{2,m_2}(\Omega_2)\right) Y^*_{5,m}(\Omega) \right] \qquad (3.38)$$

where $b(ax) = (a_1/x^{12} - a_2/x^6)$ (3.39)

and $a_2 = (\hat{\Omega}\,\Phi\,/a^6)$ (3.40)

where Φ is the scalar value of the quadrupole moment of N_2 or CO_2.

iii) CH_4-Inert Gas Atom:[49]

Buckingham[50] has derived an expression for the long range attractive part of the intermolecular potential between a tetrahedral molecule and a spherically symmetric atom by expanding the Coulomb interaction in terms of multipole moments, the leading terms of which are,

$$V_{att}(r,\Theta) = -\frac{3U_1U_2}{2(U_1+U_2)} \left[\frac{\alpha_1\,\alpha_2}{r^6} + \frac{8\,\alpha_1\,A}{r^7} \cos\Theta_x \cos\Theta_y \cos\Theta_z + \ldots \right] \qquad (3.41)$$

α_1 and α_2 are the polarizabilities of the inert gas atom and methane molecule respectively. The angles Θ_x, Θ_y and Θ_z are as shown in Fig. 12. A is the hyperpolarizability of the

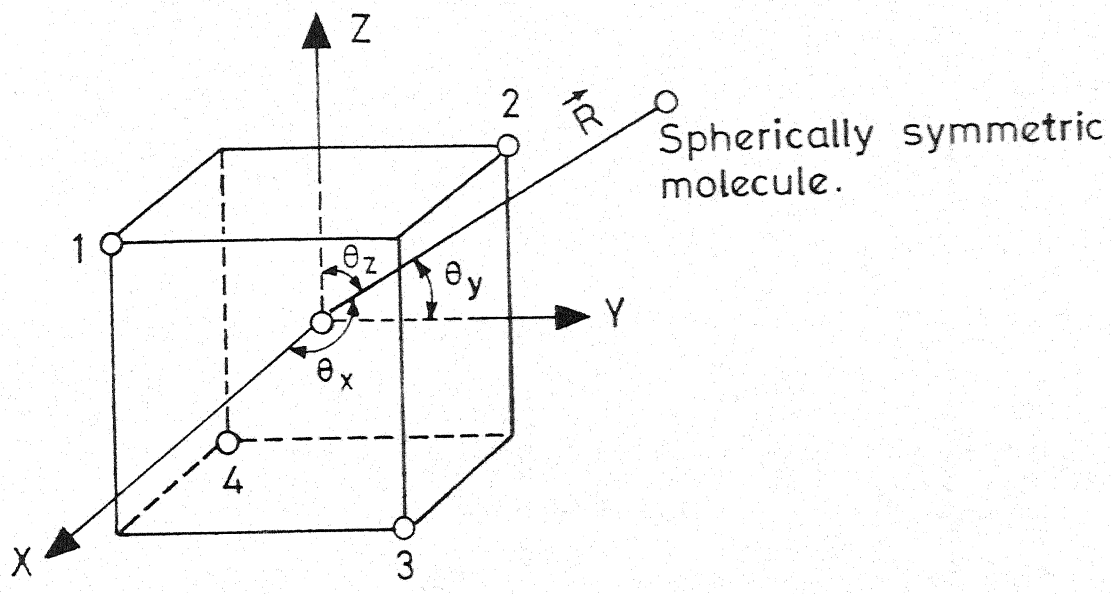

Fig. 12 - Orientation of CH_4 molecule w.r. to a spherically symmetri
atom in MFF

methane molecule describing the distortion of the molecule due to an external electric field and field gradient. U_1 and U_2 have the units of energy and it was suggested by Buckingham that they might be taken as the first ionisation potentials of the two molecules.

The first term in eq.3.41 is the isotropic part of the long-range interaction and hence must be identical with the attractive part in eq.3.28. Therefore (U_1U_2/U_1+U_2) has been chosen such that

$$\left[\frac{3\ U_1U_2}{2(U_1+U_2)}\right] \quad \alpha_1 \quad \alpha_2 \quad = 4\varepsilon \quad a^6 \qquad (3.42)$$

where ε and a are taken from viscosity data. It is worth pointing out here that this choice gives for (U_1U_2/U_1+U_2), a value approximately twice as that would be obtained following Buckingham's suggestion. This difference is due to the fact that r^{-6} term is only the leading part of the potential derived by Buckingham while in the (12-6) potential it is the only term.

It is also assumed that an r^{-12} dependence on r for the repulsive part of the anisotropic potential and the same angle dependence as that of the attractive part. The intermolecular potential may then be written as,

$$V = 4\varepsilon \ (x^{-12} - x^{-6}) + b(ax) \ \mathrm{Cos}\ \theta_x \ \mathrm{Cos}\ \theta_y \ \mathrm{Cos}\ \theta_z \quad (3.43)$$

where

$$b(ax) = (a_1/x^{12} - a_2/x^7),\ x = r/a \qquad (3.44)$$

and

$$a_2 = 32\ A\varepsilon / \alpha_2\ a \qquad (3.45)$$

In order to calculate the transition rates A(J'M', JM), the anisotropic potential $V_A(r,\Theta)$ is rewritten in the molecule fixed frame (MFF) in terms of the spherical harmonics as,

$$V_A(r,\Theta) = \frac{b(ax)}{i} \left(\frac{2\pi}{105}\right)^{\frac{1}{2}} (Y_{3,2} - Y^*_{3,2}) \qquad (3.46)$$

Using Eqs. 4.22 and 4.28 a of Rose[48] the above equation can be transformed to a space fixed frame (SFF) as

$$V_A(r,\Theta') = \frac{b(ax)}{i} \left(\frac{2\pi}{105}\right)^{\frac{1}{2}} \left[\sum_M D^{3*}_{M,2}(\alpha\beta\gamma)\ Y_{3,M}(\Theta',\phi') - \sum_M D^{3*}_{M,-2}(\alpha\beta\gamma)\ Y^*_{3,M}(\Theta',\phi') \right] \qquad (3.47)$$

where ($\alpha\beta\gamma$) are the Euler angles of rotation, D's are the corresponding rotation matrices and Θ' is the orientation of r in the SFF.

The details of the calculations for the different systems studied in order to obtain the appropriate anisotropic potential parameters and the related molecular quantities such

as the scalar value of the octopole moment of CH_4 and the hyperpolarizability of CH_4 from the experimental data are presented in Chapters IV and V.

* * *

CHAPTER IV

EXPERIMENTAL RESULTS AND ANALYSIS (PURE GASES)

IV.1 Results:(CH_4, CF_4 and SiF_4)

Proton spin-lattice relaxation times, T_1 were measured in pure CH_4 as a function of density ($1 < \rho < 12$ amagats) in the temperature region 300-600°K. At each temperature T_1/ρ was plotted as a function of ρ and the extrapolated value to $\rho = 0$ was taken as true value. In general it was observed that T_1 is proportional to density in the region $1 < \rho < 10$ amagats, but slight deviations occur for densities greater than 10 amagats, approximately. Since at the moment it is believed that these deviations are due to surface effects, all the measurements were restricted to about 10-12 amagats only. The value of T_1/ρ obtained at 300°K (21.8 msec/amagat) is in good agreement with the value obtained from the low-density data of Beckmann et al.[51] They have reported that it is likely that the earlier results of Lalita and Bloom[52] in pure CH_4 were influenced by a small contribution ($\simeq$ 10%) to the relaxation rate due to surface effects. Gerritsma et. al[53] have reported T_1 measurements in the region 108-549 amagats. They found that T_1 is proportional to density upto about 400 amagats and obtained a value of $T_1/\rho \simeq$ 22 msec/amagat at 298°K. One important difference between the pressure vessel used by Gerritsma et.al and the vessels used by others

is that Gerritsma et.al encased their rf coil in glass whereas others had their rf coils immersed in the gas sample. Also Gerritsma et.al went through an elaborate cleaning procedure for their sample containers. If the surface effects are coming from the collision of the gas molecules with the surface of the vessel, made of glass in all the cases, Gerritsma's results should have been affected to the same extent as those of others. Since they are not, it is likely that the surface effects might be coming from the collision of the gas molecules with the coil. Typical plots of T_1 versus ρ and corresponding T_1/ρ vs ρ are shown in Fig. 13. The temperature dependence of $(T_1/\rho)_{\text{pure } CH_4}$ is shown in Fig. 14. The data can be fitted with a power law of the form $T_1/\rho \propto T^{-n}$ where the T is the temperature. The value of the index n is found to be 1.47 ± 0.03.

Armstrong et.al [18] have studied ^{19}F relaxation in CF_4 and SiF_4 in a limited temperature region 230-370°K. The temperature dependences of T_1/ρ in these systems are found to be the same as in CH_4 with the index n taking the value 1.5. The present values of T_1/ρ at different temperatures in CH_4 along with the values of (T_1/ρ) in CF_4 and SiF_4 reported by Armstrong et.al are tabulated in Table 1. The effective cross section σ_{eff} for spin-rotation interaction along with the corresponding kinetic cross sections σ_{kin} and the ratios $\sigma_{kin}/\sigma_{eff}$ for CH_4, CF_4 and SiF_4 are tabulated in Table 2.

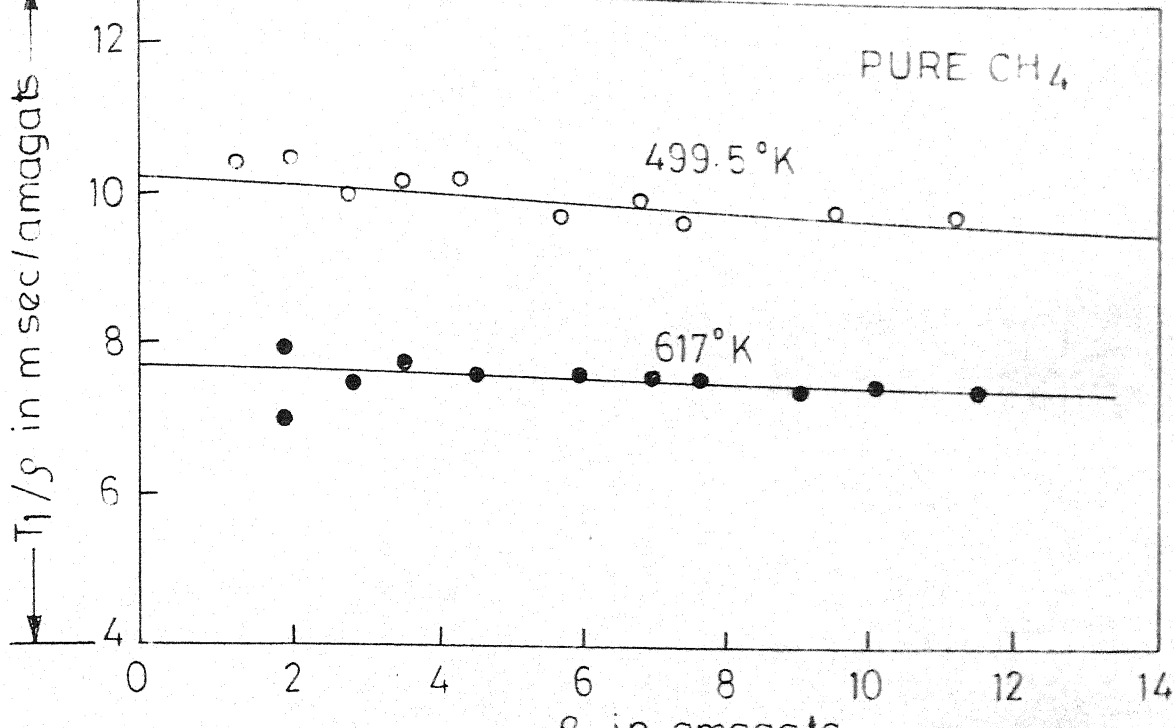

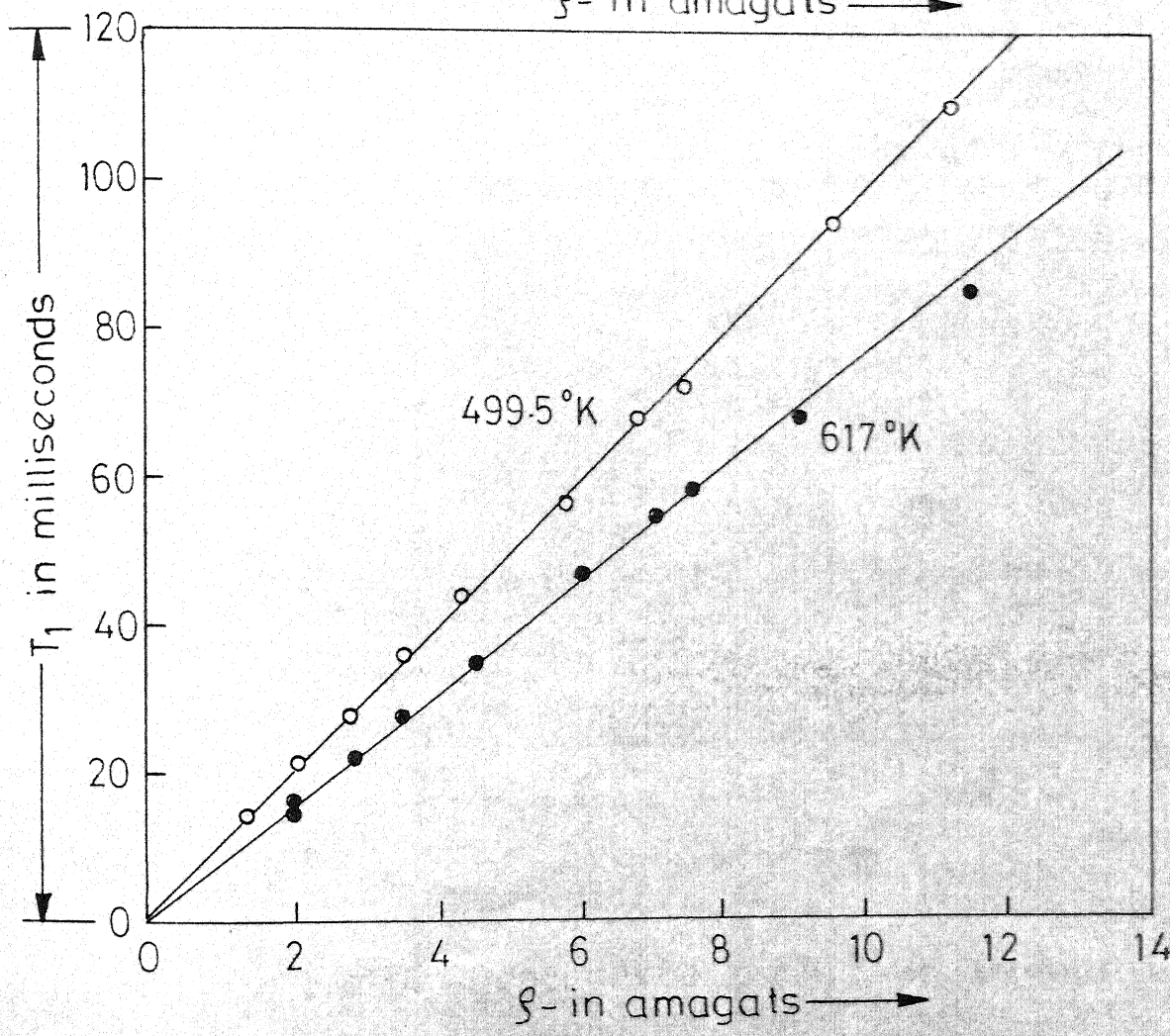

Fig. 13 - Typical plots of T_1 versus ρ and T_1/ρ versus ρ.

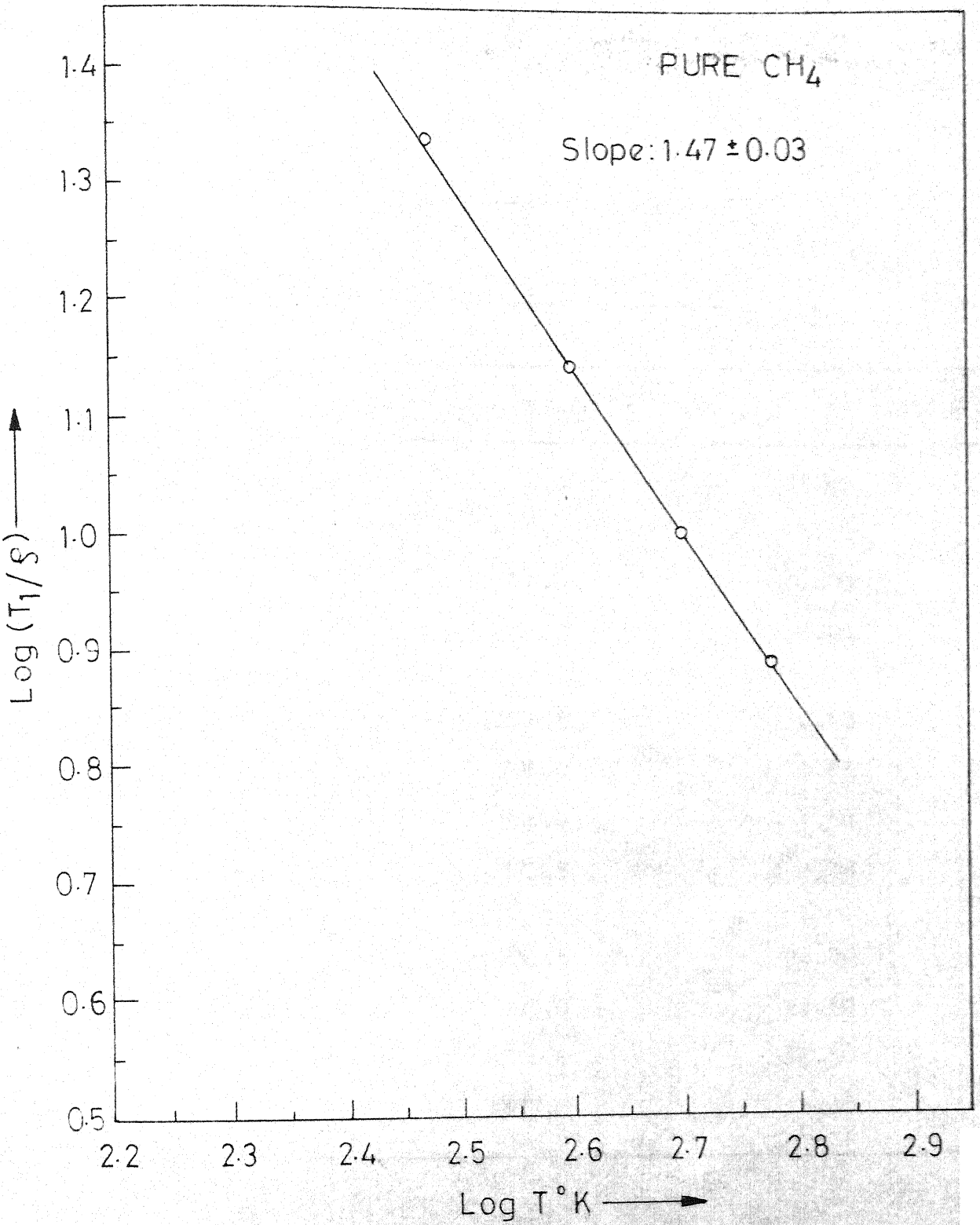

Fig. 14 - Dependence of T_1/S on temperature.

TABLE 1

T_1/ρ VALUES OF CH_4, CF_4 AND SiF_4

System	Temperature °K	(T_1/ρ) msec/amagat
CH_4	300.0	21.80
	400.0	13.80
	500.0	10.20
	600.0	7.80
CF_4	244.5	2.65
	300.0	2.03
	334.0	1.59
	371.5	1.36
SiF_4	231.5	26.00
	295.0	18.60
	320.5	15.50
	337.5	13.60

TABLE 2

COMPARISON OF KINETIC CROSS SECTIONS AND COLLISION CROSS SECTIONS

System	Kinetic cross section $\sigma_{kin} = a^2(\text{Å}^2)$	Temperature, °K	Collision cross sections $\sigma_{eff}(\text{Å}^2)$	Mean Number of collisions ($\sigma_{kin}/\sigma_{eff}$)
CH_4	45.27	300.0	19.46	2.32
		400.0	14.27	3.17
		500.0	11.80	3.84
		600.0	9.88	4.58
CF_4	69.5	244.5	40.5	1.72
		300.0	34.3	2.03
		334.0	28.4	2.45
		371.5	25.6	2.71
SiF_4	88.0	231.5	86.5	1.02
		295.0	73.1	1.20
		320.5	61.2	1.44
		337.5	54.5	1.61

IV.2 Interpretation:

As it was pointed out in the introduction, the temperature dependence of nuclear spin-lattice relaxation times, T_1, available until now in pure gases for which the spin-rotation interaction is the dominant interaction, can be fitted by a power law $T_1/\rho \propto T^{-3/2}$ where T is the temperature and ρ is the density. These results for such spherical and symmetric top molecules are in accord with the theory based on hard-sphere intermolecular potential and weak collision approximation; In fact such a temperature dependence results irrespective of the form of the anisotropic potential assumed. Hence such data were used so far only to establish the dominance of spin-rotation interaction and the adequacy of the hard sphere potential to describe the isotropic part[16-23] and no attempt has been made to obtain the parameters of the anisotropic part of the intermolecular potential.

In the following analysis the temperature dependences of proton T_1 in CH_4 and fluorine T_1 in CF_4 and SiF_4[18] have been interpreted to obtain anisotropic potential parameters and corresponding scalar value of the octopole moment. The isotropic part of the intermolecular potential is considered to be described by a hard-sphere potential as given by eq.3.27. Since in this case a $T^{-3/2}$ dependence results independent of the form of the anisotropic potential, it is not possible, knowing only the temperature dependence of T_1/ρ, to determine the strengths of

both the repulsive and attractive parts of the anisotropic potential. Hence only an attractive part of the anisotropic potential given in eq. 3.34 will be assumed.

In view of the fact that 12-6 Lennard-Jones potential is more realistic than a hard sphere potential, the data on pure gases CH_4, CF_4 and SiF_4 would also be analysed using a Lennard-Jones isotropic potential for the isotropic part. The form of Lennard-Jones potential is given in eq. 3.28. In this model, in order to explain the observed temperature dependence of T_1/ρ in pure gases, it is necessary to assume as it is explained in the following discussion that the anisotropic potential contains both the repulsive and attractive parts.

The effect of the anisotropic potential (eq. 3.34) is to produce transitions of molecule 1 (eg. CH_4) from the state J', K', M' to the state JKM while the molecule 2 (eg. another CH_4) simultaneously undergoes a transition from J"', K"', M"' to J", K", M". Denoting the transition rate for this process by, $A((JKM, J'K'M')\ (J"K"M"; J"'\ K"', M"'))$ one could write

$$A(JKM,\ J'K'M') = \sum_{\substack{J",J"' \\ M",M"' \\ K",K"'}} A((JKM;J'K'M')(J"K"M";J"'K"'M"')) \qquad (4.1)$$

The transition rates A(JKM; J'K'M') to be evaluated are those associated with molecule 1.

Using the anisotropic potential as given in eq.3.34 and using eqs. 4.1 and 3.22 we write,

$$A(JKM;\ J'K'M') = \sum_{J'',J'''} \sum_{M''} \sum_{M'''} \sum_{M'} \sum_{K''} \sum_{K'''} \sum_{M_2} \left(\frac{4\pi \times 33264}{325}\right) j(\omega_{JJ';J''J'''}) \left[C(336;M_1M_2M)\right]^2 \frac{P_{J'''}}{(2J'''+1)^2} \left\{ \left[\left| \left\langle (J''K''M'' \middle| D^{3*}_{M_2,2}(\Omega_2) \middle| J'''K'''M''') \right\rangle \right|^2 + \left| \left\langle (J''K''M'' \middle| D^{3*}_{M_2,-2}(\Omega_2) \middle| J'''K'''M''') \right\rangle \right|^2 \right] \left[\left| \left\langle (JKM \middle| D^{3*}_{M_1,2}(\Omega_1) \middle| J'K'M') \right\rangle \right|^2 + \left| \left\langle (JKM \middle| D^{3*}_{M_1,-2}(\Omega_1) \middle| J'K'M') \right\rangle \right|^2 \right] \right\} \quad (4.2)$$

where

$$j(\omega_{JJ';J''J'''}) = \frac{1}{\hbar^2} \int_{-\infty}^{+\infty} e^{i\omega_{JJ';J''J'''}t} \left\langle b(R(0))Y_{6,-m}(\Omega(0))\, b(R(t)Y_{6m}(\Omega(t)) \right\rangle \quad (4.3)$$

The bar denotes an average over the equilibrium ensemble and

$$\hbar\omega_{JJ';J''J'''} = (E_J - E_{J'}) + (E_{J''} - E_{J'''}) \quad (4.4)$$

and

$$P_{J'''} = \frac{(2J'''+1)\, e^{-J'''(J'''+1)\theta_o/T}}{\sum_{J'''} (2J'''+1)\, e^{-J'''(J'''+1)\theta_o/T}} \quad (4.5)$$

where θ_o is the characteristic temperature of the molecule in degree Kelvin. In Eq. 4.2 C is a clebsch-Gordon coefficient.

We use normalized symmetric top wave functions

$$\left| JKM \right\rangle = \frac{(2J+1)^{\frac{1}{2}}}{\sqrt{8\pi}} \quad D^{J*}_{M,K}(\Omega) \qquad (4.6)$$

to evaluate the matrix elements in eq. 4.2. After carrying out the summations over M_2, M" and M"' using standard methods of Rose and using eq. 3.21 one obtains

$$A(JM;J'M') = \sum_{J",J"'} \sum \left(\frac{4\pi \times 33264 \times 52}{325 \times 49 \times 49}\right) P_{J"'}\left(\frac{2J"+1}{2J"'+1}\right)\left(\frac{2J+1}{2J'+1}\right) \times$$

$$C(J3J';M,-M_1M')^{\,2}\, j(\omega) \qquad (4.7)$$

The spacing between the rotational levels of CH_4 (also CF_4 and SiF_4) is such that at temperatures of our experiment we can assume $j(\omega) \simeq j(0)$.[5] Now using the expression for $1/\tau_{J'}$ as in eq. 3.20 and summing over J" with J" = J"' + 3 to J"'-3 we arrive at

$$1/\tau_{J'} = 1337\, j(0) \qquad (4.8)$$

The function j(0) has been evaluated by Bloom et.al using constant Acceleration Approximation (CAA).[5] It is given by

$$j(0) = \frac{\rho\, a^4 (2\pi\beta\mu)^{1/2}\, I(p)}{\hbar^2} \qquad (4.9)$$

where

$$I(p) = a_1^2\, I(p,n') + a_2^2\, I(p,n) - 2a_1a_2 I(p,n,n') \tag{4.10}$$

and

$$I(p,n) = \int_0^\infty dy \left\{ \int_0^\infty dx\, [g(x)]^{\frac{1}{2}}\, J_{p+\frac{1}{2}}(xy)\, x^{3/2-n} \right\}^2 \tag{4.11}$$

$$I(p,n,n') = \int_0^\infty dy \left\{ \left[\left(\int_0^\infty dx [g(x)]^{\frac{1}{2}}\, J_{p+\frac{1}{2}}(xy) x^{3/2-n} \right) x \right.\right.$$
$$\left.\left. \left(\int_0^\infty dx\, [(g(x)]^{\frac{1}{2}}\, J_{p+\frac{1}{2}}(xy)\, x^{3/2-n'} \right) \right] \right\} \tag{4.12}$$

In above expressions μ and a are the reduced mass and distance parameters of the system under consideration respectively. ρ is the number density of the mixture, $\beta = 1/KT$ where K is the Boltzmann's constant, T, the absolute temperature, $x=r/a$ and y are the dimensionless variables of integration. Also

$$g(x) = \exp\left[-V_o(x)/KT\right] \tag{4.13}$$

is the radial distribution function and $J_{p+\frac{1}{2}}(xy)$ is a Bessel function of order p. For octopole-octopole interaction p takes the value of 6; the radial dependence of the attractive part of the anisotropic potential is given by the index n = 7. The repulsive radial dependence n' is assumed to be 12.

Using eqs. 3.19, 4.8, and 4.9, T_1/ρ can be written as,

$$\frac{T_1}{\rho} = \frac{\theta_o}{4\pi^2} \times \frac{1}{C_{eff}^2} \times \frac{1337.0 \times \rho_1 a^4 (2\pi\beta\mu)^{\frac{1}{2}}}{T} I(6) \qquad (4.14)$$

The values of θ_o, C_{eff}^2, a and μ are tabulated in Table 3 for the three molecules CH_4, CF_4 and SiF_4; $\rho_1 = 2.69 \times 10^{19}$ mols/cc and I(6) is given by eq. 4.10 with p=6, n=7 and n'=12.

Since in case of the pure gases CH_4, CF_4 and SiF_4 the experimental data fits a 3/2 law it can be seen from eq. 4.14 that $[I(6)]_{expt}$ is temperature independent. The temperature dependences of I(p,n) and I(p,n,n') in eqs. 4.11 and 4.12 come only through the radial distribution as given in eq. 4.13; If $V_o(x)$ is given by a hard sphere potential I(p,n) and I(p,n,n') would be independent of temperature. Therefore it is not possible in this case to determine both the parameters a_1 and a_2 in eq. 4.10 from only the temperature dependence of T_1/ρ as can be seen from eq. 4.14. Hence it was assumed that the anisotropic potential in this model is purely attractive. The anisotropic potential parameter a_2 was obtained by fitting the expression given by eq. 4.14 to the experimental values of T_1/ρ in each system over the entire temperature region using least squares criterion. For the hard-sphere isotropic potential the value of I(6,7) is tabulated by Bloom et.al and is 0.0104. The anisotropic potential parameter a_2 for the three systems along with the scalar values of the octopole moments obtained using the equation,

TABLE 3

VALUES OF θ_R^o, C_{eff}^2, a AND μ

System	θ_R^o(K)	C_{eff}^2 (MHz)	a (10^{-8}cm)	μ (gms)
CH_4	7.680	138.60	3.80	13.40
CF_4	0.270	39.80	4.70	73.60
SiF_4	0.1970	5.94	5.59	87.00

$$\hat{\Omega} = (a_2\, a^7)^{\frac{1}{2}} \qquad (4.15)$$

for the hard sphere isotropic potential are tabulated in Table 5.

If the isotropic part is given by a Lennard-Jones potential I(p,n), and I(p,n,n') would be temperature dependent. Though I(p,n) and I(p,n,n') are temperature dependent it is possible to make I(6) temperature independent by choosing the strengths of the repulsive and attractive parts of the anisotropic potential appropriately and explain the observed temperature dependence in pure gases. For the isotropic Lennard-Jones potential, the values of I(6,12), I(6,7) and I(6,7,12) were evaluated as a function of temperature given by $\beta\varepsilon$ and are tabulated in Table 4. The anisotropic potential parameters a_1 and a_2 for this realistic model obtained from eqs. 4.14, 4.10 and Table 4, using a least squares fit of the experimental data over the entire temperature region along with the respective octopole moment obtained using eq. 4.15 are tabulated in Table 5. For purposes of comparison Table 5 also contains values of octopole moments obtained from other techniques.

IV.3 Remarks on the Numerical Integrations:

The integrals given by eqs. 4.8 and 4.9 for a given p,n and n' were evaluated numerically by Gaussian quadrature techniques on an IBM 7044 computer. The subroutines were

TABLE 4

VALUES OF I(p,n'), I(p,n) AND I(p,n,n') FOR THE CLASSICAL DILUTE GAS FOR LENNARD-JONES ISOTROPIC POTENTIAL

$\beta\varepsilon$	I(6,12)	I(6,7)	I(6,7,12)
0.621	0.01677	0.02571	0.01958
0.505	0.01861	0.02561	0.02051
0.480	0.01917	0.02566	0.02084
0.360	0.02346	0.02669	0.02340
0.288	0.02827	0.02818	0.02630
0.240	0.03350	0.02986	0.02950

ANISOTROPIC POTENTIAL PARAMETERS AND OCTOPOLE MOMENTS

System	$V=V_o(r)+V_1(r,\theta)$* $V_o(r)$:Hard Sphere $a_2 \times 10^{16}$ (ergs)	$\hat{\Omega} \times 10^{34}$ (esu cm^3)	$V=V_o(r)+V_1(r,\theta)$ $V_o(r)$:Lennard-Jonnes $a_1 \times 10^{16}$ (ergs)	$a_2 \times 10^{16}$ (ergs)	$\hat{\Omega} \times 10^{34}$ (esu cm^3)	Other experiments. $\hat{\Omega} \times 10^{34}$ (esu cm^3)
CH_4-CH_4	3.86	2.10	5.6	6.36	2.69	3.0[a], 2.5[b] 2.6[c], 5.0[d]
CF_4-CF_4	1.39	2.12	1.82	2.19	3.33	4.4[a], 4.6[e] 4.4[f]
SiF_4-SiF_4	1.28	5.30	0.25	1.00	4.14	-

*$V_1(r,\theta)$ is only attractive.

[a] Bose, T.K., Sochanski, J.S., and Cole, R.H., 1971, J. Chem. Phys., 57, 3592.
[b] Birnbaum, G., and Rosenberg, A., 1968, Phys. Lett., 27A, 272.
[c] Ozier, I., and Fox, K., 1970, J. Chem. Phys., 52, 1416.
[d] Tejwani, G.D.T., and Varanasi, P., 1971, J. Chem. Phys., 55, 1075.
[e] Rosenberg, A., and Birnbaum, G., 1968, J. Chem. Phys., 48, 1396.
[f] Parsonage, N.G., and Scott, R.L., 1962, J. Chem. Phys., 37, 304.

developed for the Gaussian quadrature and for the generation of the half-order Bessel functions. Convergence and accuracy of the integrations were checked by extending the upper limits of the variables of the integration and increasing the point densities until results of successive integrations agreed to the desired accuracy. Appendix B contains the details. The accuracy of the generated half-order Bessel functions was tested by a comparison with standard tables. Also the results are in agreement for the selected integrals I(p,n) and I(p,n,n') tabulated as a function of temperature by Bloom et al[8]. It is to be noted that Bloom et.al have tabulated the numerical values of these integrals for the case I(p,n) for Lennard-Jones isotropic potential where p = 0,2 and 4 and for I(p,n,n') where p=2 only.

IV.4 Discussion:

Two model intermolecular isotropic potentials, a hard-sphere potential and (12-6)L-J potential, with appropriate anisotropic potentials have been considered for the analysis of the experimental data on pure gases CH_4, CF_4 and SiF_4 and the results are tabulated in Table 5. Both these models successfully explain the temperature dependence of the spin relaxation data in the region of interest. It is seen from the Table 5 that the octopole moments of CH_4 and CF_4 obtained from the hard sphere

model are somewhat 'less' (20-30%) compared to a more realistic model consisting of a Lennard-Jones potential and an anisotropic potential having both the attractive and repulsive parts. The scalar values of the octopole moments of CH_4 and CF_4 obtained from the latter model are in better agreement with the reported values from other techniques. However in case of SiF_4, a hard sphere model predicts a value of 5.3×10^{-34} esu cm^3 for the scalar value of the octopole moment, whereas the Lennard-Jones potential model gives a value of 4.14×10^{-34}. There is little to choose between these two models as no experimental value of octopole moment is known from other techniques.

* * *

V.2. CH_4-N_2 and CH_4-CO_2 Mixtures: Results:

Plots of T_1/ρ versus ρ are shown in Figs. 15 and 16 for CH_4-N_2 and CH_4-CO_2 systems respectively. Figures 17 and 18 represent T_1/ρ as a function of N_2 and CO_2 concentrations at different temperatures. Solid lines in all the plots indicate least square fit of the data. The error bars in Figs. 17 and 18 are the standard deviations in (T_1/ρ). The extrapolated values of $(T_1/\rho)_{CH_4-N_2}$ and $(T_1/\rho)_{CH_4-CO_2}$ are tabulated in Table 6. The temperature dependence of the extrapolated values of (T_1/ρ) for the two systems are shown in Figs. 19 and 20. The data can be fitted with a power law of the type $(T_1/\rho)_{CH_4-X} \propto T^{-n}$ where $n=0.87 \pm 0.14$ for CH_4-N_2 and $n=0.91 \pm 0.1$ for CH_4-CO_2. The effective cross sections σ_{eff} for spin-rotation interactions along with the kinetic cross sections are presented in Table 7. The ratio $(\sigma_{kin}/\sigma_{eff})$ give the mean number of collisions required for randomizing rotational angular momentum.

V.3 Interpretation:

The anisotropic intermolecular potential as given by eq. 3.38 is used to calculate the average lifetime of a molecule in a J state. Using eqs. 3.22, and 4.1 the transition rate could be written as,

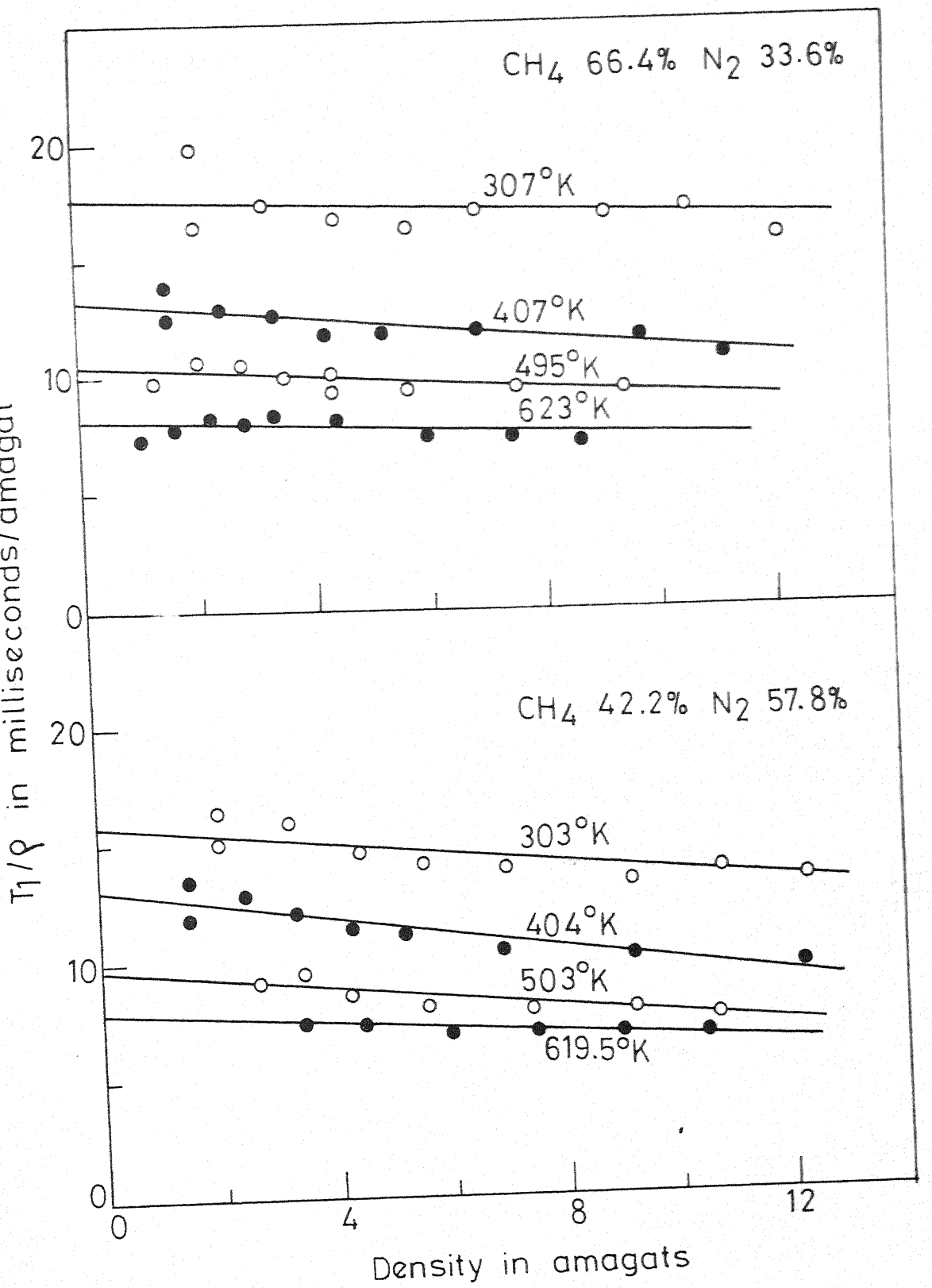

Fig.15 - Plots of T_1/ρ versus ρ.

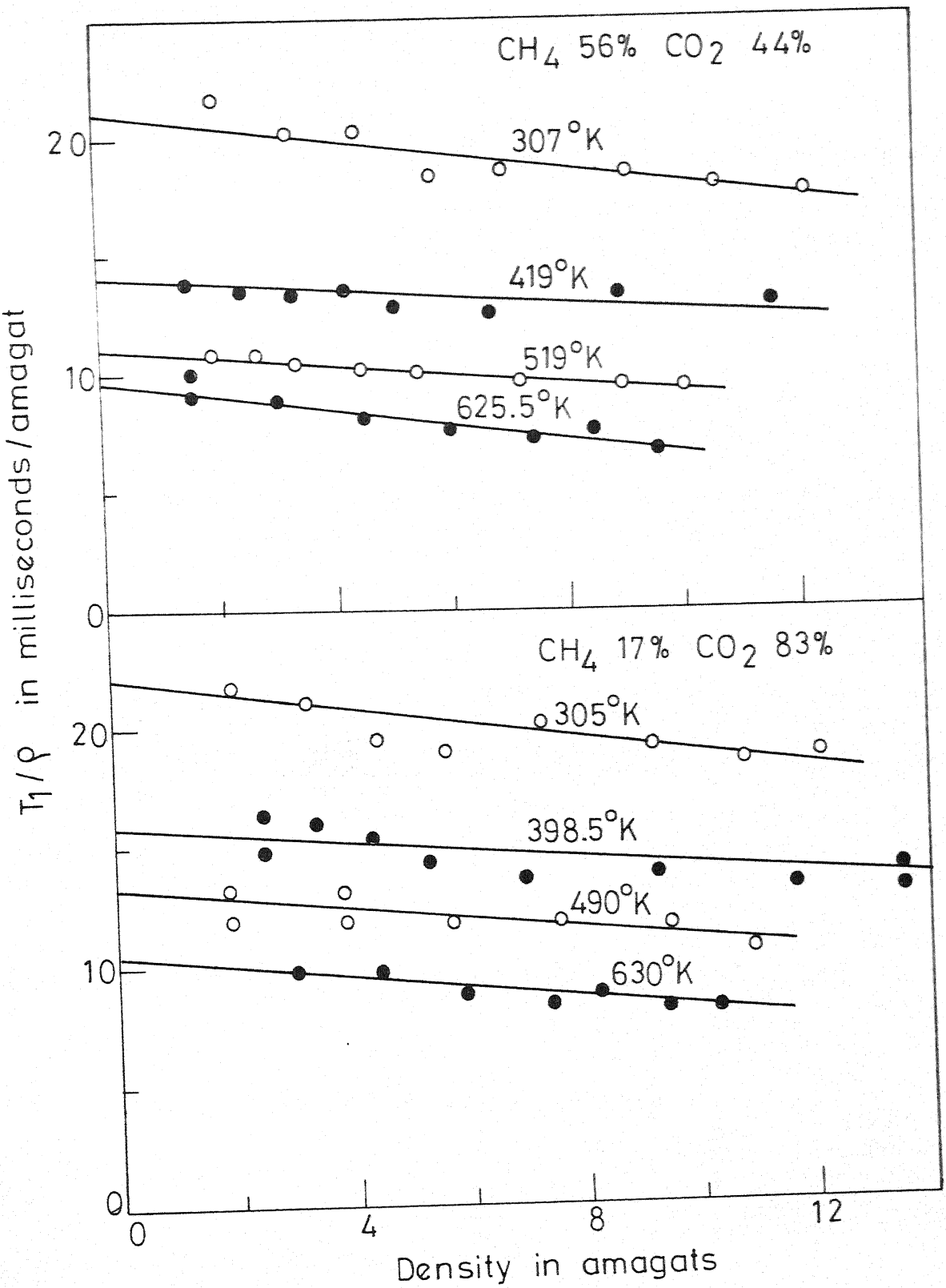

Fig. 16 - Plots of T_1/ρ versus ρ.

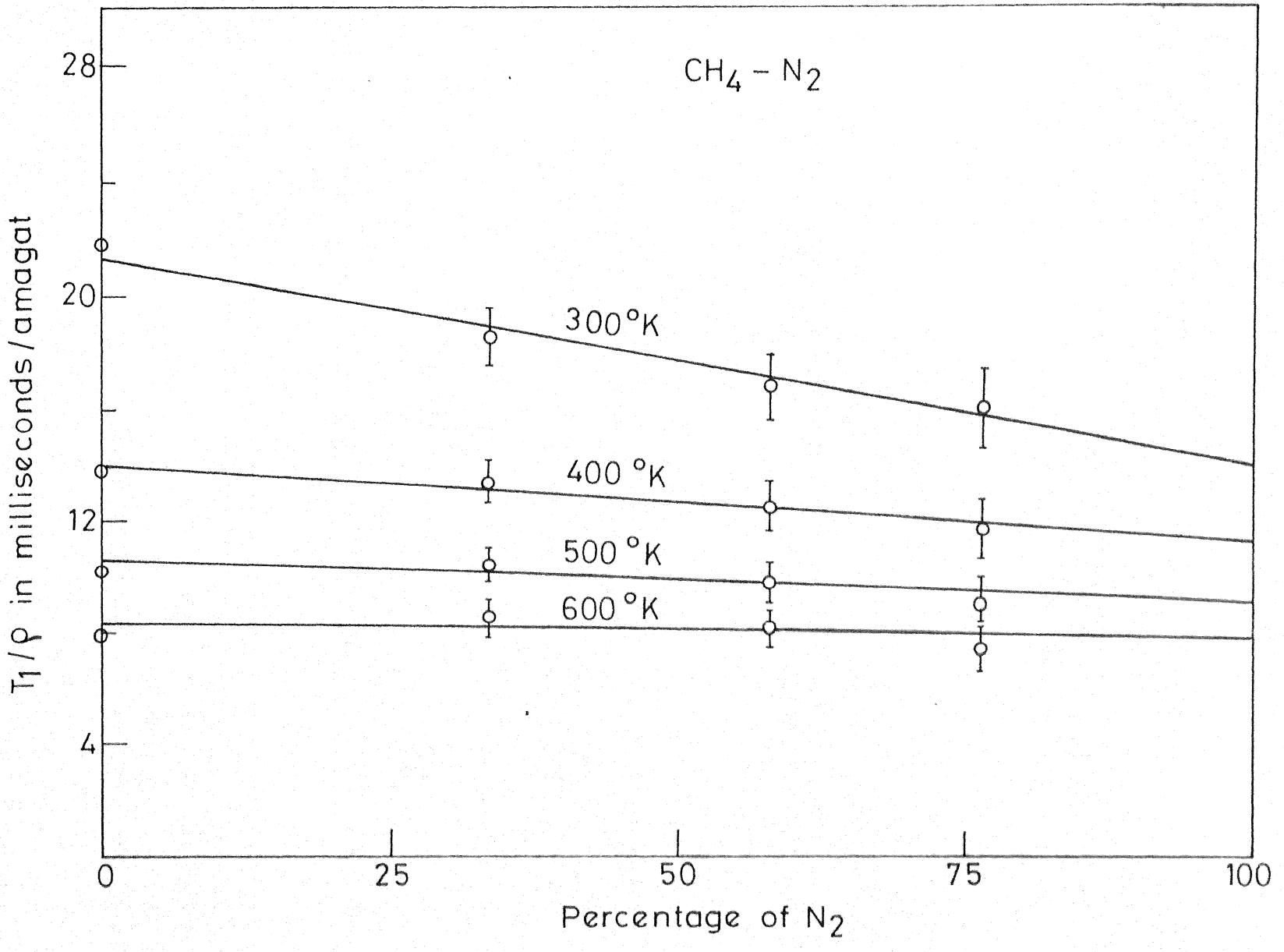

Fig. 17 - Dependence of T_1/ρ on N_2 concentration at different temperatures.

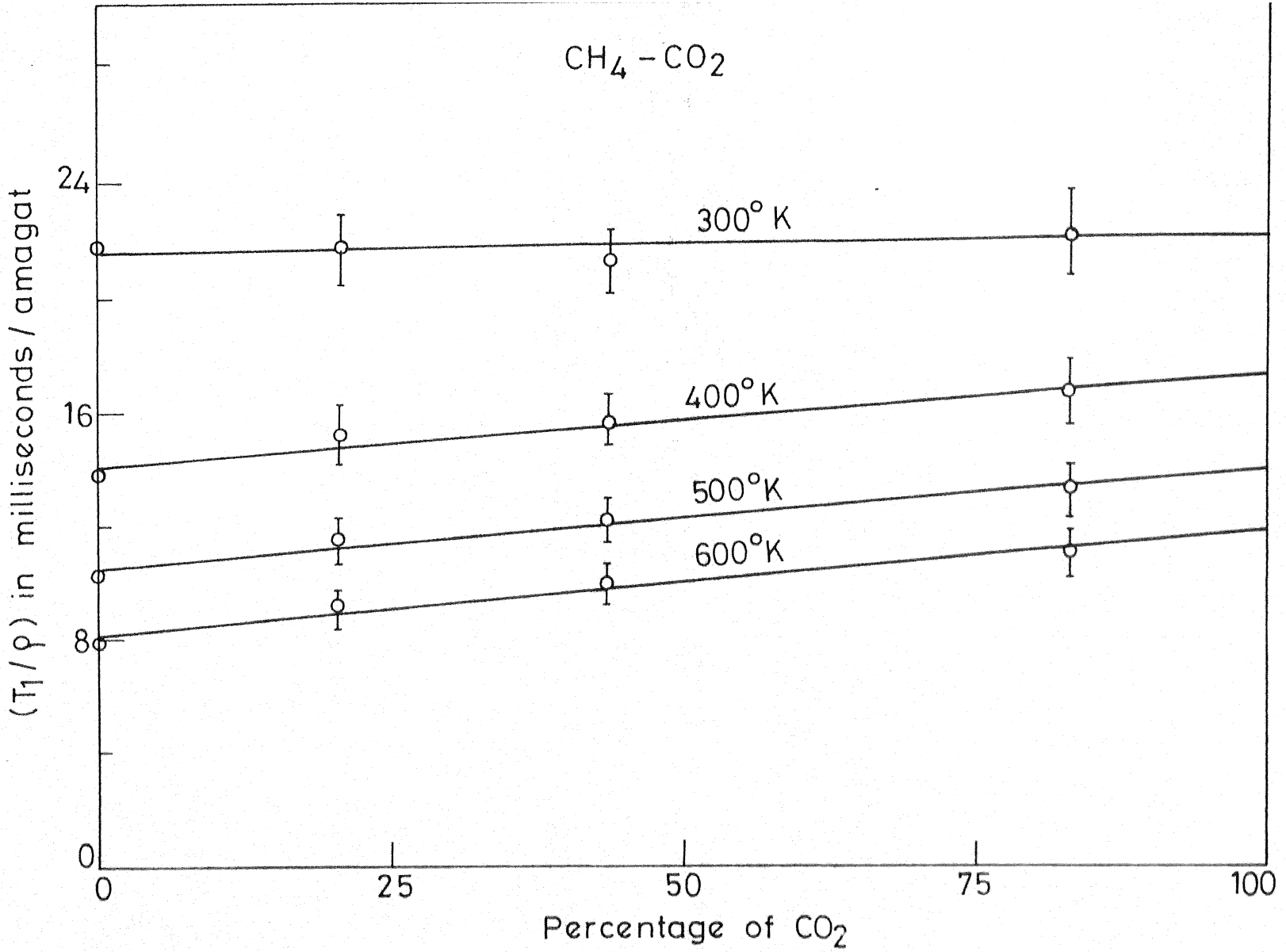

Fig.18 - Dependence of T_1/ρ on CO_2 concentration at different temperatures.

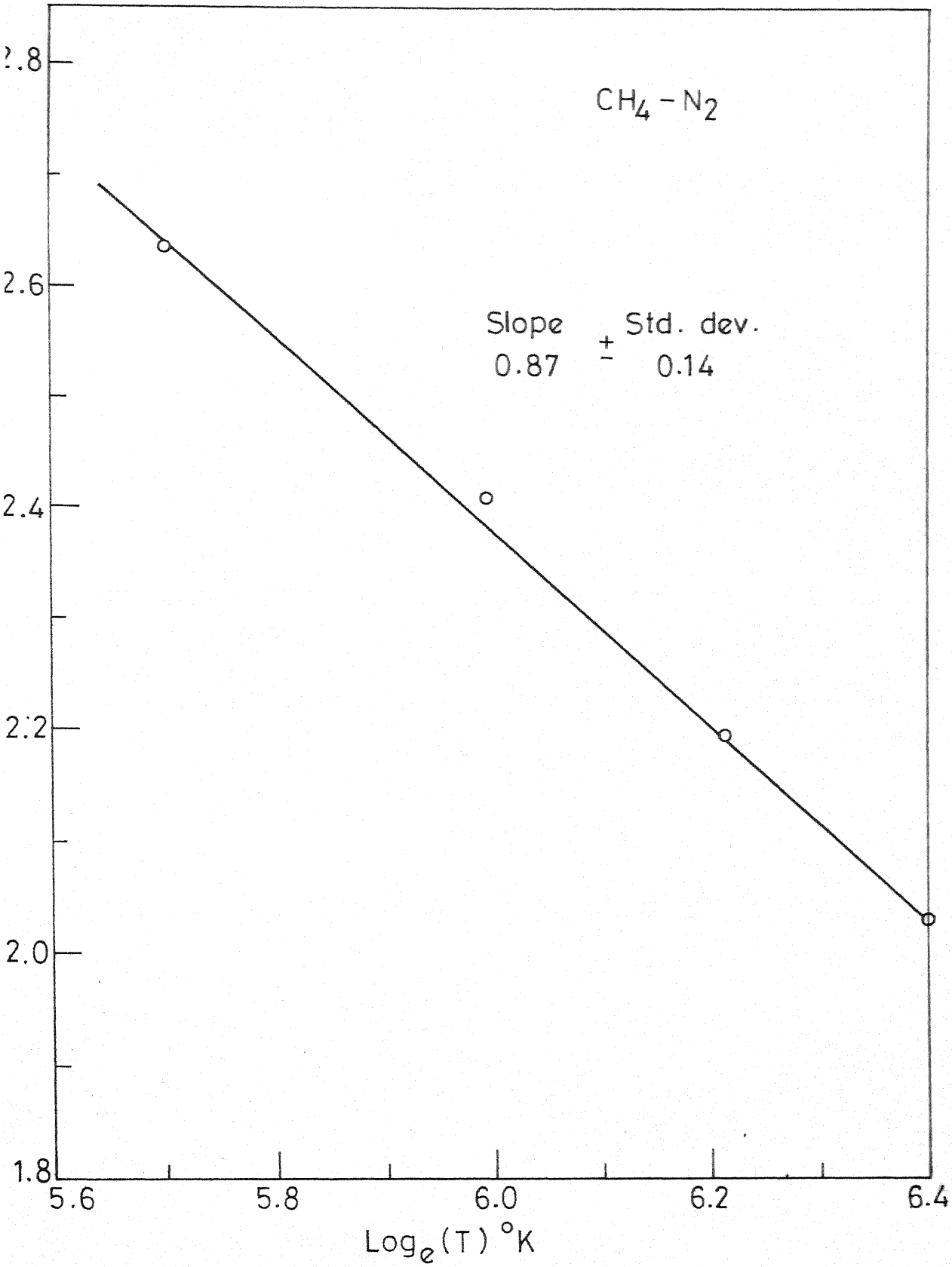

Fig.19 - Dependence of (T_1/ temperature.

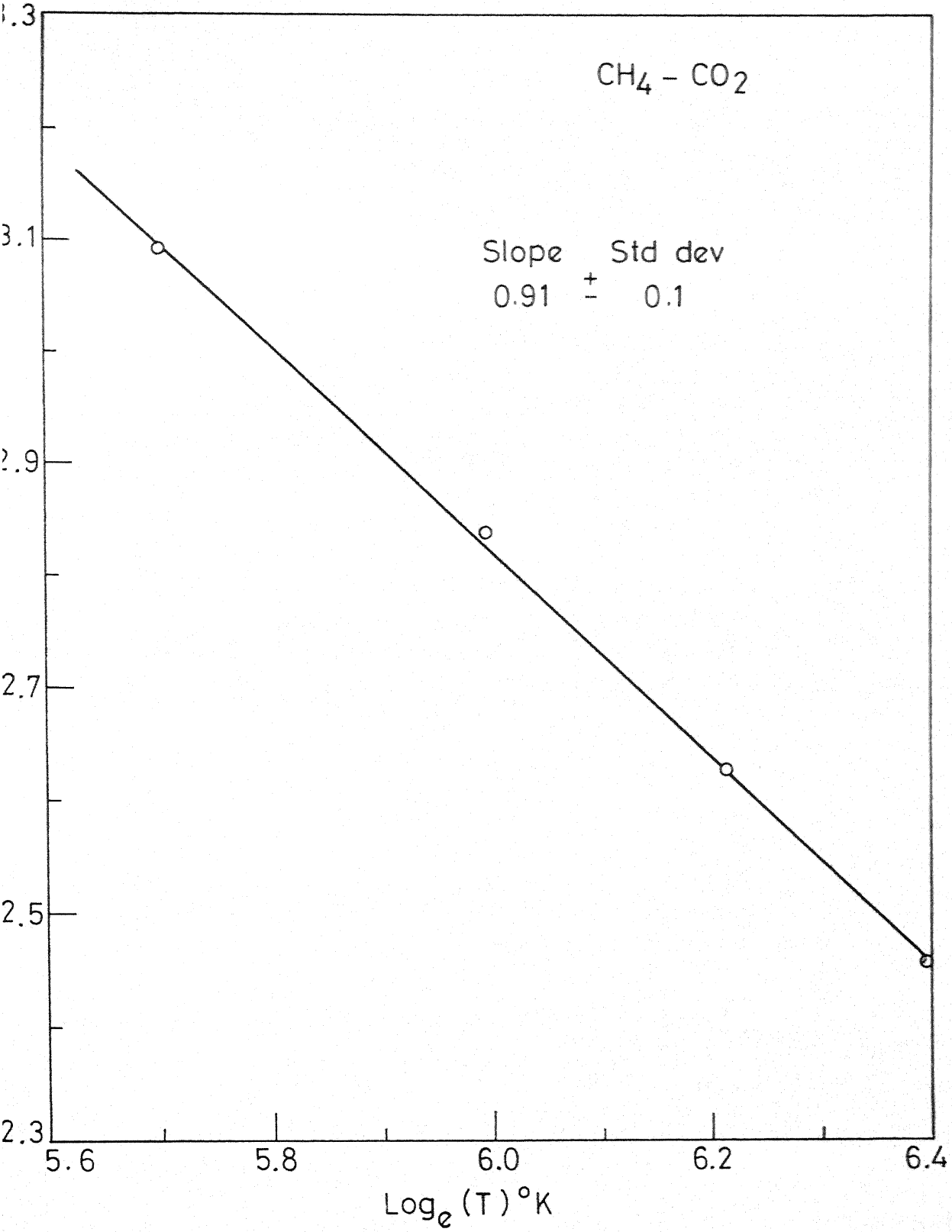

Fig.20 - Dependence of $(T_1/\rho)_{CH_4-CO_2}$ on temperature.

TABLE 6

EXTRAPOLATED VALUES OF (T_1/ρ) TO 100% N_2 AND CO_2 AT VARIOUS TEMPERATURES

Temperature °K	$(T_1/\rho)_{CH_4-N_2}$ ± Standard Deviation	$(T_1/\rho)_{CH_4-CO_2}$ ± Standard Deviation
300	13.94 ± 1.21	21.97 ± 1.35
400	11.15 ± 0.84	17.14 ± 0.96
500	9.00 ± 0.67	13.86 ± 0.74
600	7.63 ± 0.58	11.70 ± 0.61

TABLE 7

COMPARISON OF KINETIC CROSS SECTIONS AND COLLISION CROSS SECTIONS

System	Kinetic cross section $\sigma_{kin} = a^2 (\mathring{A}^2)$	Temperature °K	Collision cross section σ_{eff} ($\mathring{A}^2$)	Mean number of collisions $\sigma_{kin} / \sigma_{eff}$
CH_4-N_2	44.65	300	14.07	3.17
		400	13.00	3.43
		500	11.73	3.80
		600	10.89	4.10
CH_4-CO_2	46.48	300	23.81	1.95
		400	21.45	2.17
		500	19.39	2.40
		600	17.93	2.59

$$A((JKM;\ J'K'M')(J''M'';J'''M''')) = \sum_{m_1 m_2} \pi^2 \left(\frac{252x16}{55}\right) j(\omega_{J'J''J'''}) \times$$

$$[C(325;\ m_1 m_2)]^2 \frac{P_{J'''}}{(2J'''+1)} \left|\left\langle (J''M'' \mid Y_{2,m_2}(\Omega_2) \mid J'''M''') \right\rangle\right|^2 \times$$

$$\left\{ \left|\left\langle (JKM \mid D^{3*}_{m_1,2}(\Omega_1) \mid J'K'M') \right\rangle\right|^2 + \left|\left\langle (JKM \mid D^{3*}_{m_1,-2}(\Omega_1) \mid J'K'M') \right\rangle\right|^2 \right\}$$

(5.1)

where

$$j(\omega_{JJ'J''J'''}) = \frac{1}{\pi^2} \int_{-\infty}^{+\infty} d\tau\, e^{-i\omega_{JJ'J''J'''}\tau} \times$$

$$\overline{\left\langle b(r(0))\, Y^*_{5,m}(\Omega(0))\, b(r(t))\, Y_{5,m}(\Omega(t)) \right\rangle}$$

(5.2)

Using Rose[48]

$$\left|\left\langle (J''M'' \mid Y_{2,m_2}(\Omega_2) \mid J'''M''') \right\rangle\right|^2 = \frac{5(2J'''+1)}{4\pi(2J''+1)} [C(J'''2J'';M''',m_2)]^2 \times$$

$$[C(J'''2J'';00)]^2$$

$$(M''' + m_2 = M'') \qquad (5.3)$$

$$\left|\left\langle (JKM \mid D^{3*}_{m_1,2}(\Omega_1) \mid J'K'M') \right\rangle\right|^2 = \left(\frac{2J+1}{2J'+1}\right)[C(J3J';M,-M_1,M')]^2 \times$$

$$[C(J3J';\ K,-2,\ K')]^2$$

(5.4)

It is to be noted that the sum

$$\sum_{J''} [C(J'''\ 2J'';\ 00)]^2 = 1 \qquad (5.5)$$

Substituting eqs. 5.3, 5.4 in eq. 5.1 and using eqs. 5.2, 5.5 and carrying out the summations using standard methods, it is written

$$A(JM;J'M') = \left(\frac{16\times18\ \pi}{35}\right) j(0)\frac{2J+1}{(2J'+1)^2}\left[C(J3J',M,-m_1)\right]^2 \tag{5.6}$$

with the approximation $j(\omega) \simeq j(0)$. Now using eq. 3.20 the average lifetime of the molecule in a given J' state can be written as

$$\tau_{J'} = \frac{245}{864 \times 16\pi\ j(0)} \tag{5.7}$$

where $j(0)$ is given by 4.9 using eqs. 3.19, 5.7, $(T_1/\rho)_{CH_4-X}$ at a temperature T is given by

$$(T_1/\rho)_{CH_4-X} \simeq \frac{216 \times 16\alpha\rho_1\ a^4(2\pi\beta\mu)^{\frac{1}{2}}}{245\pi\ C_{eff}^2\ \hbar^2}\ I(p) \tag{5.8}$$

where X could be N_2 or CO_2 and $\alpha = 7.68°K/T°K$; $I(p)$ is given by equation 4.10 with p=5, n=6 and n'=12. The values of the integrals I(5,6), I(5,12) and I(5,6,12) at different temperatures are tabulated in Table 8.

Using eq.4.10 and the numerical values of Table 8 the parameters a_1 and a_2 were obtained by fitting the expression given by eq. 5.8 to the experimental data of (T_1/ρ) over the entire temperature region using least squares criterion. The

TABLE 8

VALUES OF I(p,n'), I(p,n) AND I(p,n,n') FOR DILUTE CLASSICAL GAS MIXTURE FOR LENNARD-JONES ISOTROPIC POTENTIALS

$\beta\varepsilon$	I(5,12)	I(5,6)	I(5,6,12)
0.19850	0.04536	0.03926	0.03760
0.21420	0.04235	0.03844	0.03580
0.26775	0.03370	0.03646	0.03142
0.29200	0.03119	0.03585	0.02999
0.35040	0.02676	0.03491	0.02749
0.35700	0.02637	0.03484	0.02727
0.43800	0.02248	0.03436	0.02520
0.58600	0.01919	0.03413	0.02350

octopole moment is then given by

$$\hat{\Omega} = \frac{a_2 \, a_{CH_4-X}^6}{\Phi_X} \qquad (5.9)$$

where Φ_X is the scalar value of the quadrupole moment of N_2 or CO_2.

The anisotropic potential parameters a_1 and a_2 for the systems CH_4-N_2 and CH_4-CO_2 are tabulated in Table 9 along with the scalar value of the octopole moment obtained.

V.4 Discussion of the Results:

It can be seen from the Table 9 that $\hat{\Omega}$ obtained from the analysis of CH_4-N_2 system is in reasonable agreement with the reported values. The value obtained from CH_4-CO_2 system is, however, small by a factor of 2 approximately. Billingslay and Krauss[54] have pointed out that the hyperpolarizability of the molecule is not taken into account while obtaining the quadrupole moments of the molecule and hence the recommended values of the quadrupole moments are over estimated by 20% approximately. If the quadrupole moments of N_2 and CO_2 obtained from birefriengence method[55,56] are used after correcting for the hyperpolarizability by decreasing the quoted values by 20%, we obtain $\hat{\Omega} = 2.64 \times 10^{-34}$ esu cm^3 from CH_4-N_2 and $\hat{\Omega} = 1.33 \times 10^{-34}$ esu.cm^3 from CH_4-CO_2. This value of

TABLE 9

ANISOTROPIC POTENTIALS PARAMETERS FOR CH_4-N_2 AND CH_4-CO_2 SYSTEMS AND OCTOPOLE MOMENT OF CH_4

System	$a_1 \times 10^{15}$ (ergs)	$a_2 \times 10^{15}$ (ergs)	Quadrupole moment of N_2 or CO_2 used $\Phi \times 10^{26}$ esu cm^2	Octopole moment of CH_4 obtained $\hat{\Omega} \times 10^{34}$ csu cm^3	Other experiments $\hat{\Omega} \times 10^{34}$ esu cm^3
CH_4-N_2	1.05	1.03	1.4 1.12	2.12 2.64	3.0[a], 2.5[b], 2.6[c],
CH_4-CO_2	1.51	1.31	4.1 3.28	1.04 1.33	0.94 - 6.0[d], 5.0[e]

[a] Bose, T.K., Sochanski, J.S., and Cole, R.H., 1971, J.Chem. Phys., 57, 3592.

[b] Birnbaum, G., and Rosenberg, A., 1968, Phys. Lett., 27 A, 272.

[c] Ozier, I., and Fox, K., 1970, J.Chem. Phys., 52, 1416.

[d] Spurling, T.H., De Rocco, A.G., and Storvick, T.S., 1968, J. Chem. Phys., 48, 1006.

[e] Tejwani, G.D.T., and Varanasi, P., 1971, J. Chem. Phys., 55, 1075.

2.64×10^{-34} is in good agreement with the value obtained from the analysis of T_1 data in pure CH_4 presented in Chapter IV.

Analysis of the data for radial dependences such as r^{-15} and r^{-8} for the repulsive part in anistropic potentials yield values of octopole moments of CH_4 30-40% smaller than the values obtained from an r^{-12} dependences for both CH_4-N_2 and CH_4-CO_2 systems. This suggests that collision cross-sections are sensitive to form of the repulsive potential. In the analysis it is assumed that the angle dependence of the repulsive part is the same as that of the attractive part without any justification. It might be that they are sensitive to the angle dependence also. CO_2 being a triatomic linear molecule longer in size than N_2 it might be more sensitive to the angle dependence than N_2 molecule.

V.5 CH_4-Inert Gas Atom: Results:

Typical plots of T_1 versus ρ are shown in Fig. 21 for 77.3% CH_4 and 22.7% Ar mixture at three different temperatures. Figs.22,23 and 24 represent T_1/ρ as a function of inert gas atom concentration for the three systems (He, Ne and Ar) at different temperatures. The extrapolated values of (T_1/ρ) to 100% He, Ne and Ar are tabulated in Table 10. The temperature dependence of $(T_1/\rho)_{CH_4\text{-}X}$ where X could be either He, Ne or Ar is shown in Fig. 25. In all the cases the data

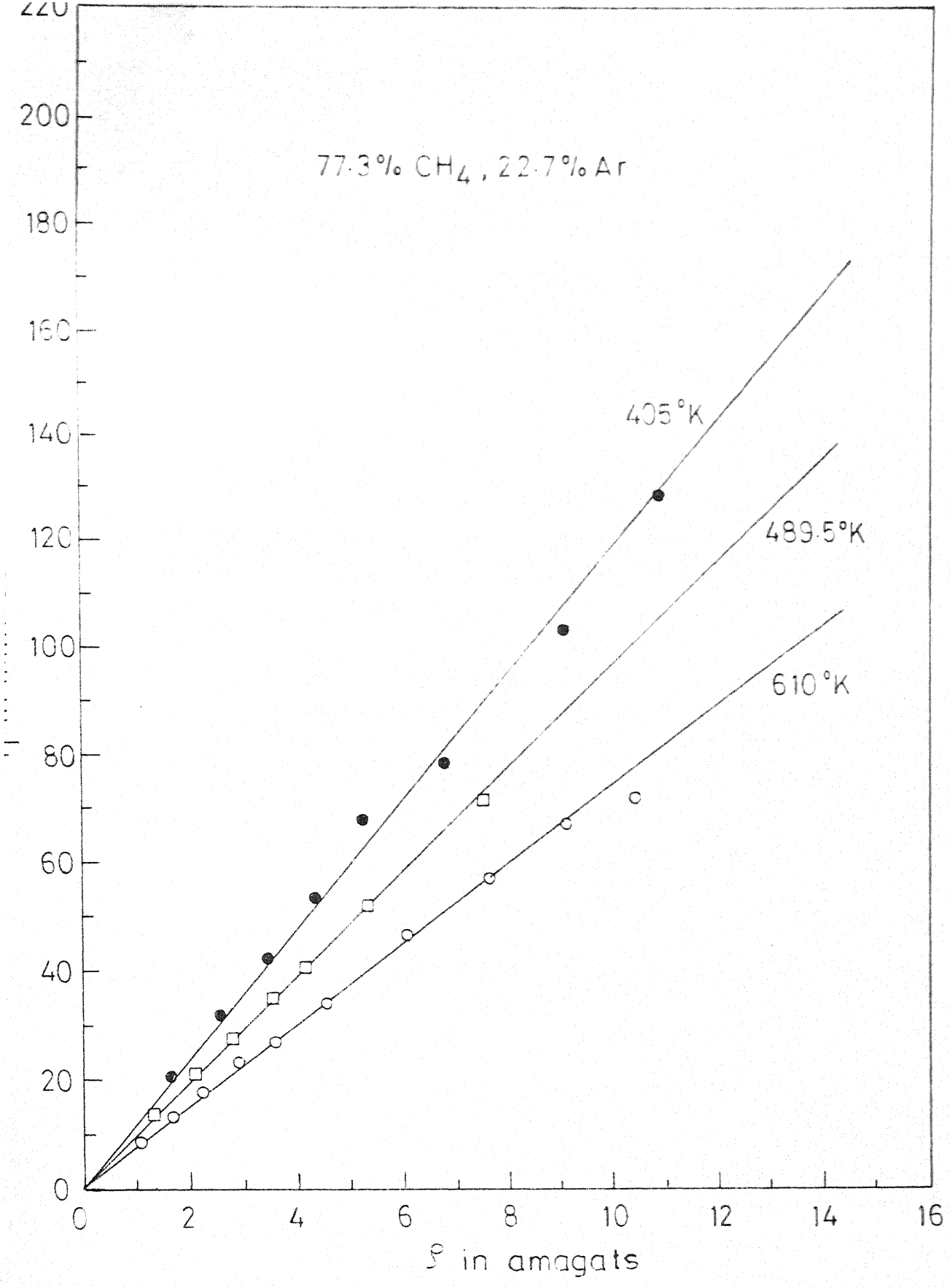

Fig. 21 - Typical plots of T_1 versus ρ.

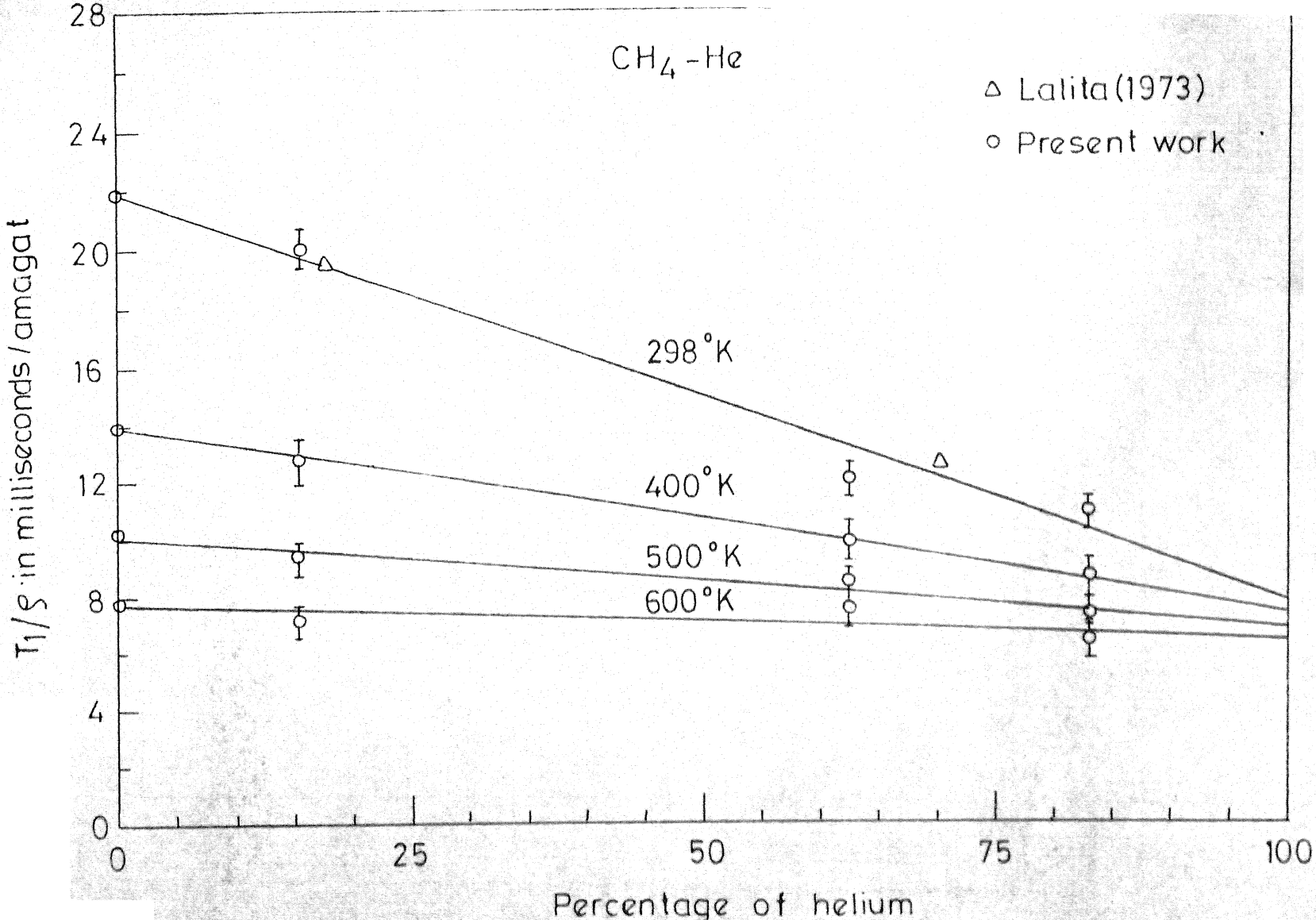

Fig. 22 - Dependence of T_1/ρ on Helium concentration at different temperatures.

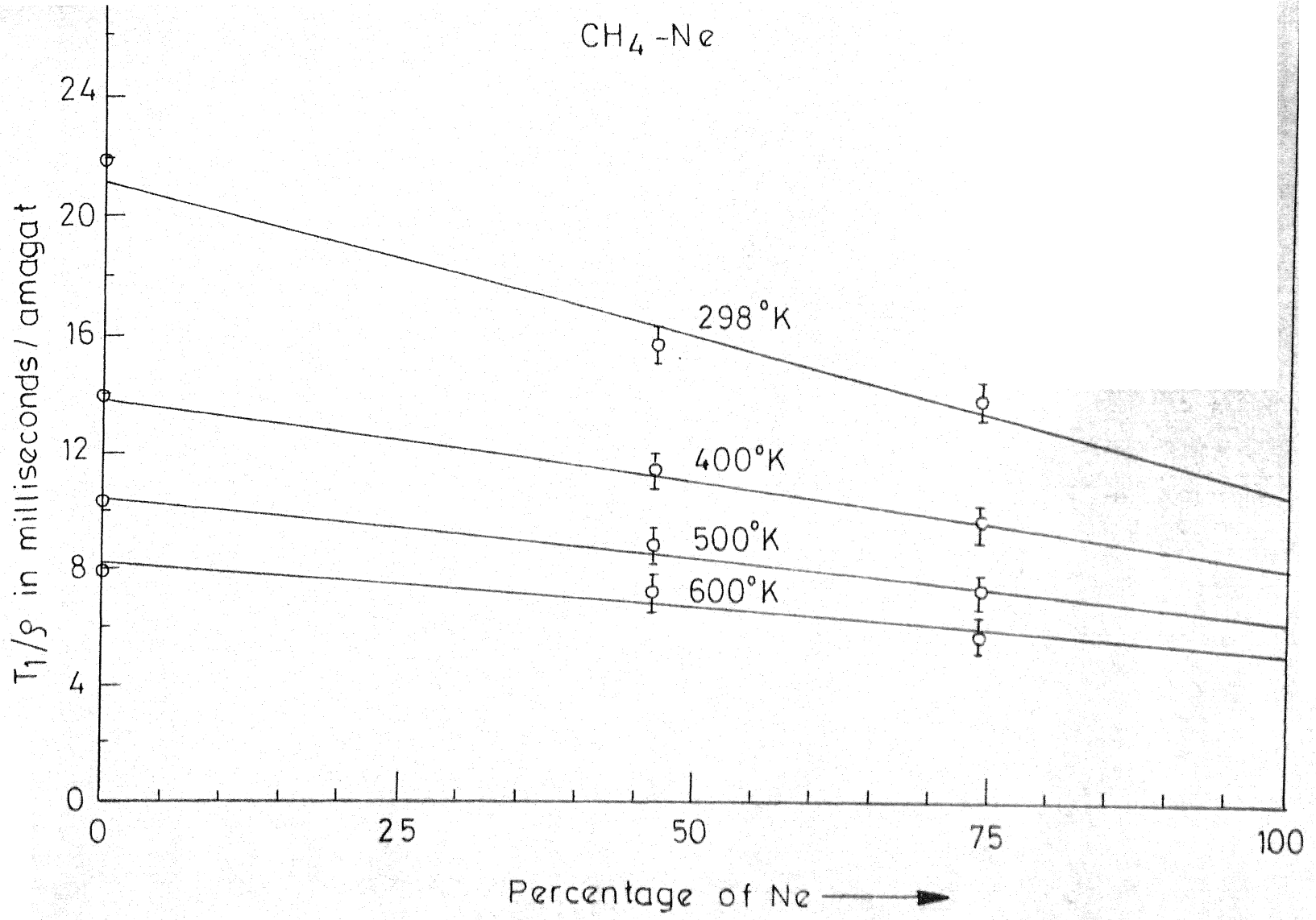

Fig. 23 - Dependence of T_1/ρ on Neon concentration at different temperatures.

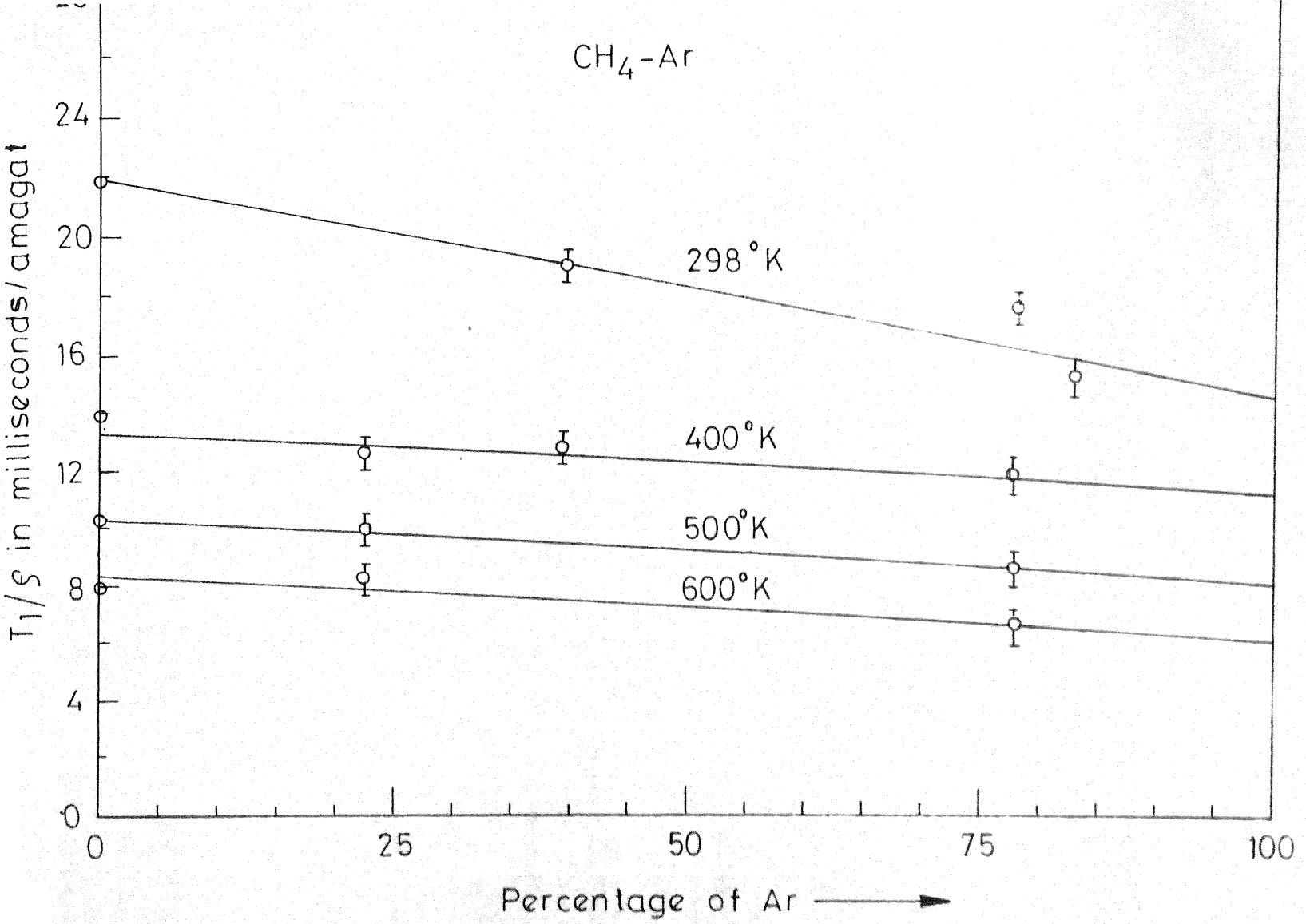

Fig. 24 - Dependence of T_1/S on Argon concentration at different temperatures.

TABLE 10

VALUES OF $(T_1/\rho)_{CH_4-X}$ ± STANDARD DEVIATION AT DIFFERENT TEMPERATURES

Temperature °(K)	$(T_1/\rho)_{CH_4-He}$ (msec/amagat)	$(T_1/\rho)_{CH_4-Ne}$ (msec/amagat)	$(T_1/\rho)_{CH_4-Ar}$ (msec/amagat)
298	7.7 ± 0.63	10.5 ± 0.89	14.3 ± 0.86
400	7.4 ± 0.57	8.0 ± 0.74	11.2 ± 0.70
500	6.84± 0.58	6.15± 0.78	7.9 ± 0.67
600	6.36± 0.61	5.06± 0.79	6.05± 0.70

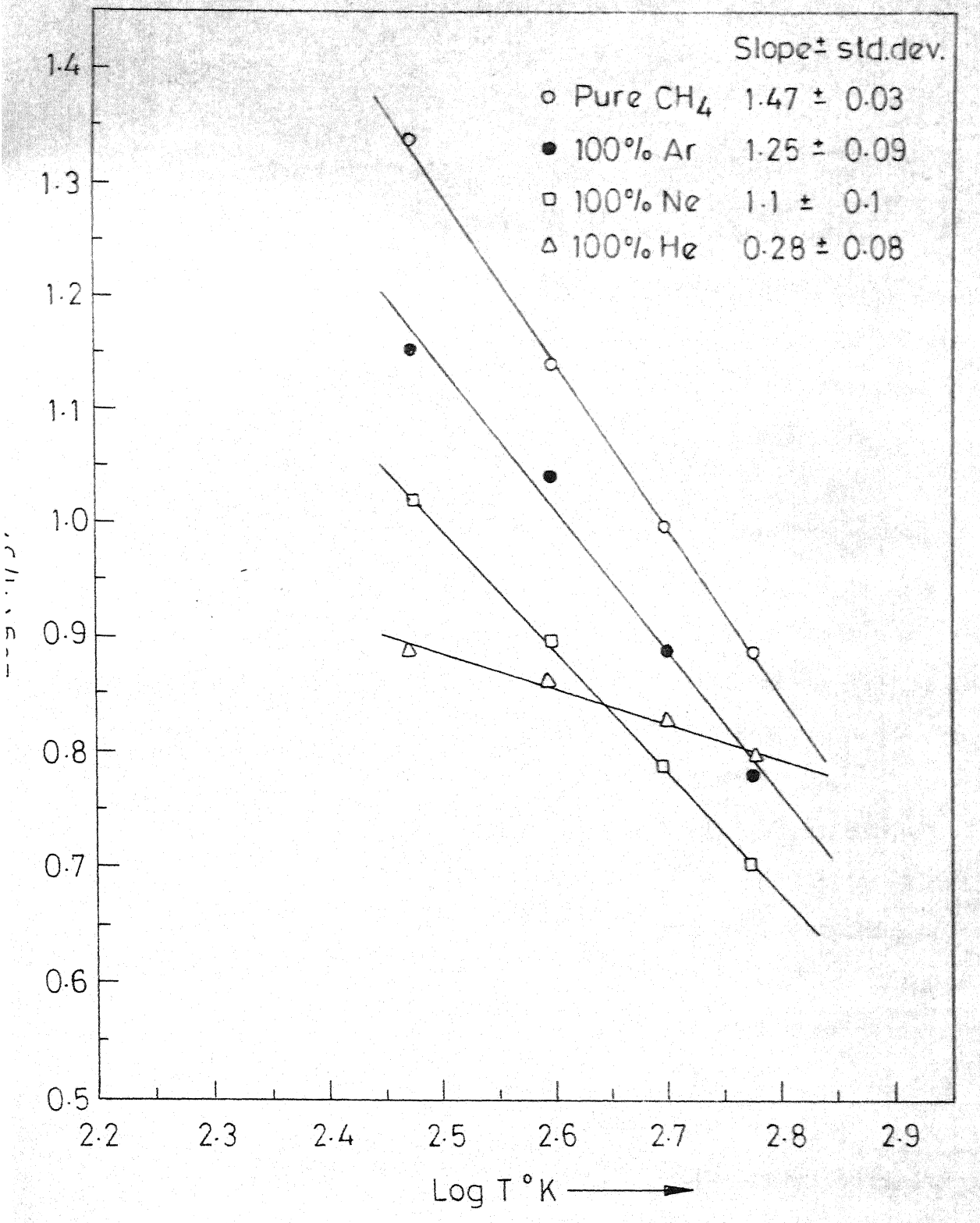

Fig. 25 - Dependence of $(T_1/\rho)_{pure\ CH_4}$ and $(T_1/\rho)_{CH_4-X}$ on temperature.

can be fitted by a power law, as in the earlier systems of the form $(T_1/\rho)_{CH_4\text{-}X} \propto T^{-n}$ where n=0.28 ± 0.08 for CH_4-He, 1.1 ± 0.1 for CH_4-Ne and 1.25 ± 0.09 for CH_4-Ar. The cross sections σ_{eff} for spin-rotation interactions along with the kinetic cross section σ_{kin} are tabulated in Table 11.

Lalita and Bloom[24] reported a value of 0.8 for the index n in CH_4-He. They also have reported that T_1/ρ is not linear with composition for small concentrations of He and assumed that these small departures do not appreciably affect the values of T_1/ρ extrapolated to 100% He. Their values of T_1/ρ were consistently smaller than the present values. It is possible that their results in the mixture were also influenced by the surface effects, as in pure CH_4. Fig. 22 shows that the present values of T_1/ρ in CH_4-He mixtures fit very well the data reported by Lalita[46] at room temperature for two different concentrations of He, where surface effects were believed to be eliminated. In the present results no non-linear dependence of T_1/ρ on the concentration of inert gas atom is found. Hence the extrapolated values of T_1/ρ to 100% inert gas atom can be taken as the real contribution to (T_1/ρ) due to CH_4-X collisions only where X could be He, Ne or Ar.

TABLE 11

COMPARISON OF KINETIC CROSS SECTIONS AND COLLISION CROSS SECTIONS

System	Kinetic cross section $\sigma_{kin} = a^2(\mathring{A}^2)$	Temperature °K	Collision cross section σ_{eff} ($\mathring{A}^2$)	Mean number of collisions ($\sigma_{kin}/\sigma_{eff}$)
CH_4-He	32.15	298	5.07	6.34
		400	4.98	6.45
		500	4.81	6.67
		600	4.31	7.43
CH_4-Ne	35.05	298	9.84	3.56
		400	8.68	4.03
		500	7.46	4.69
		600	6.72	5.21
CH_4-Ar	41.62	298	15.19	2.74
		400	13.78	3.02
		500	10.87	3.83
		600	9.12	4.56

V.6 Interpretation:

As before, defining A(J'M';JM) as the transition rate for the transitions JM $\rightarrow$ J'M' (CH_4 molecule), it is given by

$$A(J'M';JM) = \frac{1}{\hbar^2}\frac{1}{2(J+1)} \sum_{KK'} \int_{-\infty}^{+\infty} e^{-i\omega_{JJ'}\tau} \quad x$$

$$\left\langle \overline{(JKM \mid V_A(t) \mid J'K'M')} \quad (J'K'M' \mid V(t+\tau) \mid JKM) \right\rangle d\tau \qquad (5.10)$$

The anisotropic potential $V_A(r, \theta')$ is given by eq. 3.48. After carrying out the summations over K and K' one obtains

$$A(J'M';JM) = \frac{4\pi}{735}\, j(\omega_{JJ'})\, [C(J3J';\, M,M'-M)]^2 \qquad (5.11)$$

where

$$j(\omega_{JJ'}) = \frac{1}{\hbar^2} \int_{-\infty}^{+\infty} d\tau\, e^{-i\omega_{JJ'}\tau} \quad x$$

$$\left\langle b(r(t)\, Y^*_{3,M}(\theta'(t))\; b(r(t+\tau)\, Y_{3,M}(\theta'(t+\tau)) \right\rangle \qquad (5.12)$$

with $j(\omega_{JJ'}) \simeq j(0)$. The function j(0) is given by eq. 4.9. In case of CH_4-Inert gas system, the index p which is determined by the angular variation of the anisotropic interaction is given by 3. The radial dependence of the attractive part of the

anisotropic intermolecular potential which is given by the index n = 7; the repulsive part of the anisotropic potential is assumed to vary as r^{-12}. The values of integrals 'I(3,12), I(3,7) and I(3,7,12) required for the CH_4-Inert gas atom potential are listed in Table 12 as a function of $\beta\varepsilon$.

Now using eqs. 3.20, 3.21, 4.4 and 4.6, and the properties of Clebsch-Gordon coefficients, the life time of a molecule in a J state is obtained as,

$$1/\tau_J = \frac{192\ \pi\ j(0)}{5145} \qquad (5.13)$$

and the relaxation time per unit density can be written as,

$$\frac{T_1}{\rho} \simeq \frac{\rho_1\ a^4 (2\ \pi\beta\mu\ )^{\frac{1}{2}}}{5\times10^{-53}\ T\ C_{eff}^2}\ I(3) \qquad (5.14)$$

where

$$I(3) = a_1^2\ I(3,12) + a_2^2\ I(3,7) - 2\ a_1 a_2\ I(3,7,12) \qquad (5.15)$$

V.7 Anisotropic Potential Parameters for CH_4-Inert Gas Systems and Hyperpolarizability of Methane:

The spin-rotation coupling constants were determined by Yi et.al[44] for methane molecule from molecular beam experiments. The values are C_a = 10.4 KHz, C_d=18.5 KHz. The value of $C_{eff}^2 = (C_a^2 + (4/45)\ C_d^2)^{19}$ = 138.6 MHz (Refer Table 3). The parameters

TABLE 12

VALUES OF I(p,n'), I(p,n), AND I(p,n,n') FOR DILUTE CLASSICAL GAS MIXTURE FOR LENNARD-JONES ISOTROPIC POTENTIALS

$\beta\varepsilon$	I(3,12)	I(3,7)	I(3,7,12)
0.06570	0.2403	0.0888	0.1390
0.07884	0.1830	0.0819	0.1160
0.10500	0.1280	0.0670	0.0882
0.13140	0.0969	0.0612	0.0730
0.15750	0.0780	0.0560	0.0620
0.21000	0.0568	0.0493	0.0495
0.25640	0.0460	0.0458	0.0435
0.32050	0.0380	0.0433	0.0380
0.42733	0.0297	0.0405	0.0325

a_1 and a_2 were obtained by fitting the expression 4.11 to the experimental data of $(T_1/\rho)_{CH_4-X}$ over the entire temperature region using least squares criterion. The hyperpolarizability A is given by (Refer Eq. 3.28),

$$A = \frac{\alpha_2 \, a_{CH_4-X} \, a_2}{32 \, \varepsilon_{CH_4-X}} \qquad (5.16)$$

where α_2 is the polarizability of methane. The values a_1, a_2 and A are tabulated in Table 13 along with the value obtained for CH_4-Ar mixtures from infra-red spectral line broadening by Gray.[57]

V.8 Discussion of the Results:

The value of the hyperpolarizability of methane, A, obtained from CH_4-Ne and CH_4-Ar data agree well with the theoretical value of 0.97×10^{-32} cm^4 obtained from $A = 4(\alpha_{11} - \alpha_\perp)R_o/\sqrt{3}$, a relation derived from a molecular model in which the tetrahedron is comprised of four atoms at a distance R_o from the center and having polarizabilities α_{11} and $\alpha_\perp$ along and at right angles to their bonds to the central atom[5]. The value obtained from CH_4-He data is somewhat higher. Helium being the lighter atom than the other two, might be probing more of the repulsive part of the anisotropic potential than Ne and Ar at these temperatures. Hence it is likely that in this case the value of A is more

TABLE 13

VALUES OF ANISOTROPIC POTENTIAL PARAMETERS AND HYPERPOLARIZABILITY OF CH_4

System	$a_1 \times 10^{14}$ (ergs)	$+a_2 \times 10^{14}$ (ergs)	$A \times 10^{32}$ (cm^4)	$A \times 10^{32}$ (cm^4) (other experiment)	Theoretical estimate of $A \times 10^{32}$
CH_4-He	3.2	5.5	2.71	-	
CH_4-Ne	2.0	2.8	0.88	-	0.97
CH_4-Ar	4.8	4.8	0.89	2.0	

sensitive to the form of the repulsive potential. Further experiments at low temperature should clarify this point.

The value of A obtained from CH_4-Ar data may be compared with the value obtained by Gray[57] from the mean squared torque $\langle \tau^2 \rangle$ on a CH_4 molecule in a bath of Ar atoms as determined from Infra-red band moments. He has obtained a value of 2.0×10^{-32} esu cm^4 for A as compared to the present value of 0.89×10^{-32} esu cm^4. Gray has the data only at 295°K and he could estimate only one of the two parameters involved, assuming the other to be zero. Hence it is possible that his value of A is overestimated.

* * *

CHAPTER VI

CONCLUSIONS

It has been realized for quite sometime that the nuclear spin-lattice relaxation measurements can be interpreted to obtain information on the intermolecular potentials, particularly the anisotropic part. T_1 measurements were indeed interpreted earlier in simple systems like hydrogen, where the number of rotational states that are appreciably populated at temperatures of interest are restricted to one or two, to obtain precise information on the intermolecular potentials. So far such an analysis has not been done in polyatomic molecules and their mixtures where the number of rotational levels are quite large. The present analysis is an attempt to obtain information on the intermolecular potentials, especially the anisotropic intermolecular potentials in polyatomic molecules and their mixtures from the experimental data of nuclear spin-lattice relaxation times, T_1s.

Measurements of proton spin-lattice relaxation times were made in pure CH_4, mixtures of CH_4-N_2, CH_4-CO_2 and CH_4-inert gas atom as a function of density and composition in the temperature region 300-600°K, using a phase coherent spin-echo spectrometer constructed for the purpose. The data

available in pure CF_4 and SiF_4 have also been interpreted to obtain similar information as in other systems studied.

In the absence of a detailed molecular theory for polyatomic molecules to relate the correlation time to the intermolecular potentials, it is assumed that τ_1^J, the correlation time of the spin-rotation is equal to the average lifetime of a molecule in that J state, which can be evaluated interms of the intermolecular potential using Bloom and Oppenheim's theory and 'weak collision approximation.'

In analysing the experimental data on pure gases CH_4, CF_4 andSiF_4, two models of isotropic intermolecular potentials have been considered, with appropriate anisotropic potentials, i) A hard sphere potential; ii) A Lennard-Jones potential. In case of hard sphere isotropic potential, the anisotropic part is assumed to be described by an attractive term only and no repulsive part is considered. This is necessary because when the isotropic potential is described by a hard sphere potential, certain integrals involving anisotropic intermolecular functions become independent of temperature. Hence it is not possible to evaluate both the potential parameters, repulsive as well as attractive, of the anisotropic potential from the temperature dependence of T_1/ρ alone. However, in Lennard-Jones isotropic model, in order to explain the observed temperature dependence of T_1/ρ, it is necessary to have a repulsive term also in the

anisotropic part along with an appropriate attractive term.

The scalar values of the octopole moments of CH_4 and CF_4 obtained from the analysis of a hard sphere isotropic model are 20-30% less compared to the values from a Lennard-Jones isotropic model. The octopole moments obtained from this model are in better agreement with the values reported from other techniques such as collision induced infrared absorption. In case of SiF_4 the value of the octopole moment obtained from a hard sphere model is about 25% higher compared to the value from a Lennard-Jones model. So far no value of octopole moment of SiF_4 is known from other techniques.

The temperature dependence of the proton spin relaxation data in CH_4-N_2, CH_4-CO_2 and CH_4-inert gas atom mixtures is different from a 3/2 law which is found to be the case in pure gases reported so far where spin-rotation interaction is the dominant mechanism of relaxation. These results have been interpreted as the failure of the hard sphere potential to adequately describe the isotropic potential. Hence a Lennard-Jones potential which is more realistic than a hard-sphere potential, is chosen to represent the isotropic part, with appropriate anisotropic potentials. The analysis yields anisotropic potential parameters and molecular quantities such as the octopole moment and hyperpolarizability of CH_4. The octopole moment of CH_4 obtained from the analysis of CH_4-N_2

data is found to be 2.12×10^{-34} esu cm^3 when the quadrupole moment of N_2 is taken to be 1.5×10^{-26} esu cm^3. This generally accepted value of quadrupole moment of N_2, when corrected for hyperpolarizability effects, is decreased by 20%. If the corrected value is used, the present analysis gives a value of 2.64×10^{-34} esu cm^3 for the octopole moment of CH_4. This value of 2.64×10^{-34} esu cm^3 is in good agreement with the value obtained from our analysis on pure CH_4 where Lennard-Jones isotropic potential was used with an appropriate anisotropic potential. The octopole moment of CH_4 obtained from the analysis of CH_4-CO_2 data is however smaller by a factor of two compared to the value from CH_4-N_2 data. In case of CH_4-inert gas atom the value 0.89×10^{-32} cm^4 that was obtained for the hyperpolarizability A from CH_4-Ne and CH_4-Ar measurements is in good agreement with the theoretical estimate of 0.97×10^{-32} cm^4. However hyperpolarizability obtained from CH_4-He data is larger by a factor of two. In case of CH_4-CO_2 and CH_4-He systems it is likely that the assumptions made regarding the radial term in the anisotropic potentials are not justified.

It can be concluded that the present analysis of the experimental data on different systems studied indicate that the identification of the correlation time τ_1^J of the spin-rotation interaction with the average lifetime of a molecule in that J state is indeed a reasonable approximation. The

evaluation of the average lifetime τ_J under weak collision approximation for appropriate anisotropic potentials within the frame work of Bloom-Oppenheim theory, serves as a preliminary estimate of the magnitude of the correlation time for spin-rotation interaction. It is also interesting to note that though the ratio of kinetic cross section to the effective cross section for spin-rotation interaction in all the systems considered indicate that the collisions are not really 'weak' (mean number of collisions ranging from two to ten), 'the weak collision approximation' can be successfully applied.

* * *

REFERENCES

1. J.O. Hirschfelder (Ed.) "Advances in Chemical Physics", 7 (1967).
2. H. Margenau and N.R. Kestner, "Theory of Intermolecular Forces" (Pergamon, New York, 1968).
3. B.Stevens, "Collisional Activation in Gases" (Pergamon, New York, 1967) Chapter 5.
4. R.G. Gordon, W. Klemperer and J.I.Steinfeld, Annu. Rev. Phys. Chem., 19, 215 (1968).
5. M. Bloom and I. Oppenheim "Advances in Chemical Physics", 12, 549 (1967).
6. C.S. Johnson and J.S. Waugh, J.Chem. Phys., 36, 2266 (1962).
7. R.G. Gordon, J. Chem. Phys., 44, 228 (1966).
8. M. Bloom, I. Oppenheim, M. Lipsicas, C.G. Wade and C.F. Yarnell, J.Chem. Phys. 43, 1036 (1965).
9. M. Lipsicas and M. Bloom, Can. J. Phys., 39, 881 (1961).
10. M. Lipsicas and A. Hartland, Phys. Rev., 131, 1187 (1963).
11. K. Lalita and M. Bloom and J.D. Noble, Can. J. Phys., 47, 1355 (1969).
12. K. Lalita, M. Bloom, Can. J. Phys., 49, 1018 (1971).
13. K.R. Foster and J.H. Rugheimer, J. Chem. Phys., 56, 2632 (1972)
14. J.W. Riehl, C.J.Fisher, J.D. Baloga and J.L. Kinsey, J. Chem. Phys., 58, 4571 (1973).

15. J.W. Riehl, J.L. Kinsey, J.S. Waugh and J.H. Rugheimer, J.Chem. Phys., 49, 5276 (1968).

16. C.S. Johnson, J.R. and J.S. Waugh, J.Chem. Phys., 35, 2020 (1961).

17. J.A. Courthey and R.L. Armstrong, Can. J. Phys., 50, 1252 (1972).

18. R.L. Armstrong and E. Tward, J.Chem. Phys., 48, 332 (1968).

19. M. Bloom, F.B. Bridges and W.N. Hardy, Can. J. Phys., 45, 3533 (1967).

20. R.L. Armstrong and J.A. Courtney, Can. J. Phys., 50, 1262 (1972).

21. R.Y. Dong and M. Bloom, Phys. Rev. Lett., 20, 981 (1968).

22. R.L.Armstrong and J.A. Courtney, Can. J. Phys., 51, 457(1969).

23. R.L. Armstrong and T.A.J. Hanrahan, J.Chem. Phys., 49, 4777 (1968).

24. K. Lalita and M. Bloom, Chem. Phys. Lett., 8, 285 (1971).

25. A. Abragam, "The Principles of Nuclear Magnetism" (Oxford University Press, 1961)

26. N. Bloembergen, E.M. Purcell and R.V. Pound, Phys. Rev., 73, 679 (1948).

27. G.T. Needler and W. Opechowski, Can. J. Phys., 36, 870 (1961).

28. J.L. Kinsey, J.W. Riehl and J.S. Waugh, J. Chem. Phys., 49, 5269 (1968).

29. E.L. Hahn, Phys. Rev., 80, 980 (1950).

30. T.C. Farrar and E.D. Becker, "Pulse and Fourier Transform Spectroscopy" (Academic Press, New York and London, 1971).

31. F. Bloch, Phys. Rev., 70, 460 (1946).

32. W.N. Hardy, Ph.D. Thesis, University of British Columbia (1964).

33. W.G. Clark, Rev. Sci. Instr., 35, 316 (1964).

34. R.J. Blume, Rev. Sci. Instr., Notes 32, (1961).

35. J.D. Noble, Ph.D., Thesis University of British Columbia(1964).

36. Handbook, Preferred Circuits, Nav Weps 16-1-519-1 NBS.,

37. American Petroleum Institute, Project 44, Selected Values of Properties of Hydrocarbons and Related Compounds, Table 1ja.

38. H.Y. Carr and E.M. Purcell, Phys. Rev., 94, 630 (1954).

39. W.N. Hardy, Can. J. Phys., 44, 265 (1966).

40. P. Yi, I. Ozier and C.H.Anderson, Phys. Rev., 165, 92 (1968).

41. P.S. Hubbard, Phys. Rev., 131, 1155 (1963).

42. J.S. Blicharski, Acta Phys. Polon. 24, 817 (1963).

43. R.Y.Dong and M. Bloom, Can. J. Phys., 48, 793 (1970).

44. P. Yi, I. Ozier and N.F. Ramsay, J.Chem. Phys., 55, 5215 (1971).

45. M. Bloom and I. Oppenheim, Can. J. Phys., 41, 1580 (1963).

46. K. Lalita, Can. J. Phys., 52, 876 (1974).

47. C.G. Gray, Can. J. Phys., 46, 135 (1966).

48. M.E. Rose, "Elementary Theory of Angular Momentum" (John Wiley & Sons, Inc., 1957).

49. S. Rajan, K. Lalita and S.V. Babu, J. Mag. Res., 16, 115 (1974).

50. A.D. Buckingham, "Advances in Chemical Physics", Vol.12 p.131 (Interscience publishers, New York 1967).

51. P.A. Beckmann, M. Bloom and E.E. Burnell, Can. J. Phys., 50, 251 (1972).

52. K. Lalita, Ph.D., Thesis, University of British Columbia (1967).

53. C.J.Gerritsma, P.H. Oosting and N.J. Trappeniers, Physica, 51, 365 (1971).

54. F.B. Billingslay and M. Krauss, J.Chem. Phys., 60, 2767 (1974).

55. A.D. Buckingham, R.L. Disch and D.A. Dunmur, J.Am.Chem. Soc., 90, 3104 (1968).

56. A.D. Buckingham and R.L.Disch, Proc. Roy.Soc., (London), A 273, 275 (1963).

57. C.G. Gray, J.Chem. Phys., 50, 549 (1969).

...

APPENDIX A

CIRCUIT DIAGRAMS

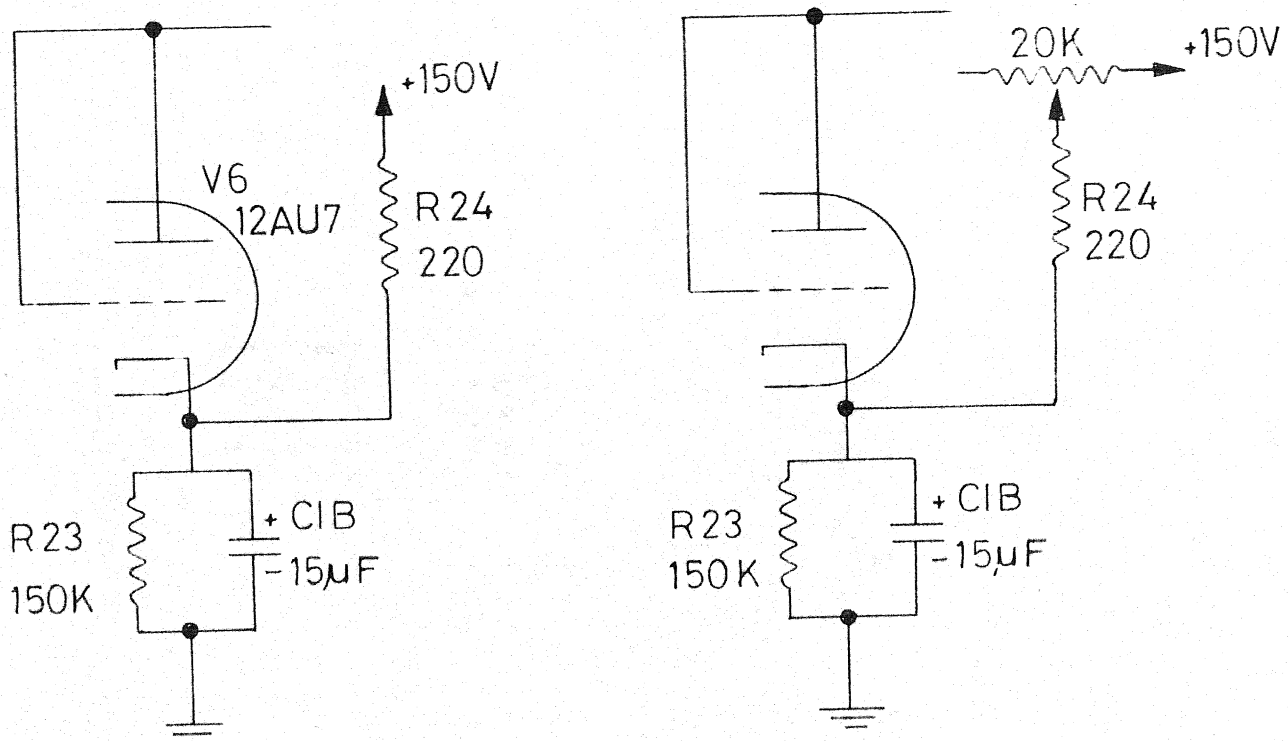

Portion as in Tek. 162 waveform generator

Modification

Fig. A1 - Saw tooth d-c level variation.

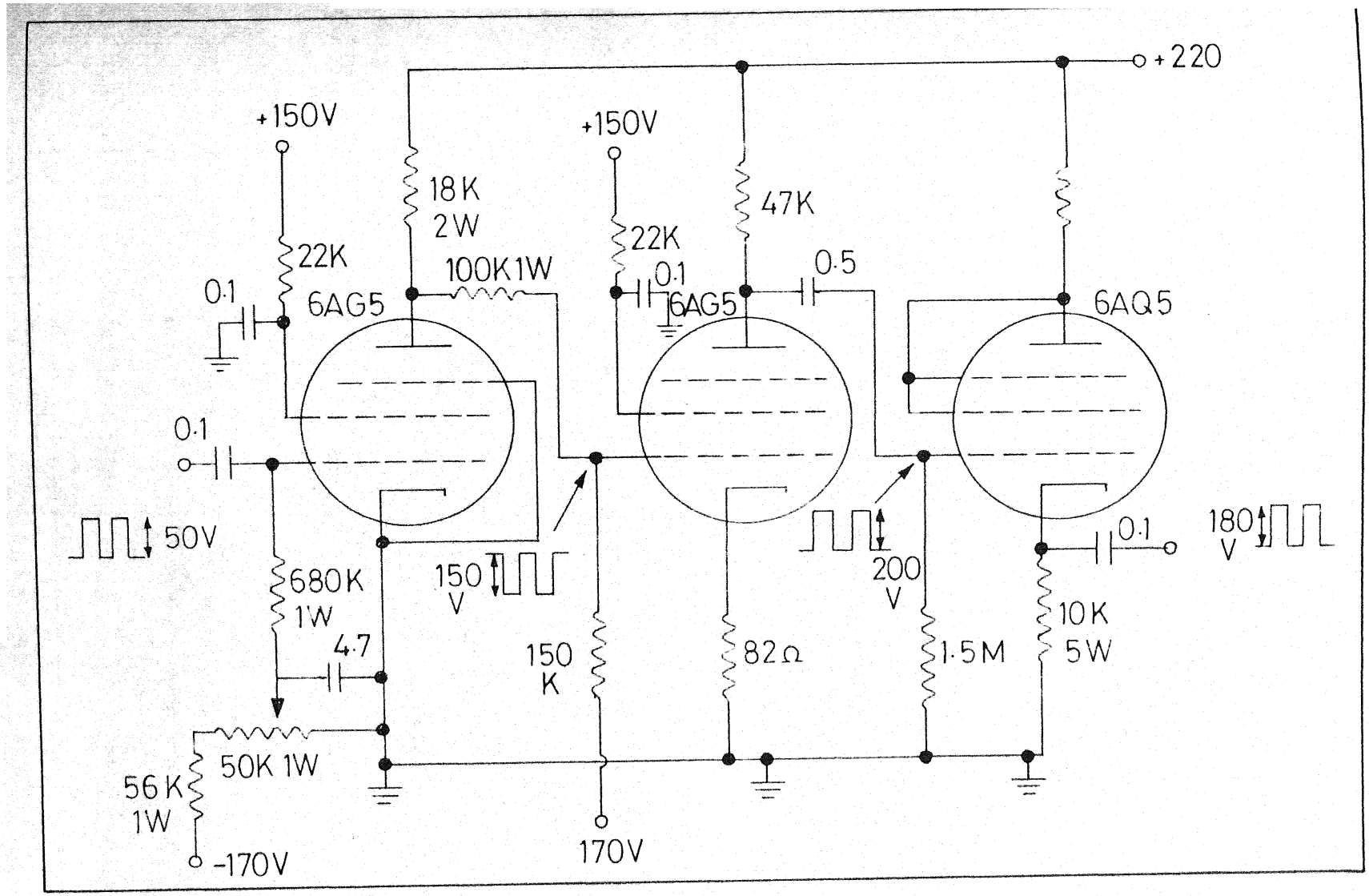

Fig. A4- Pulse shaper and amplifier.

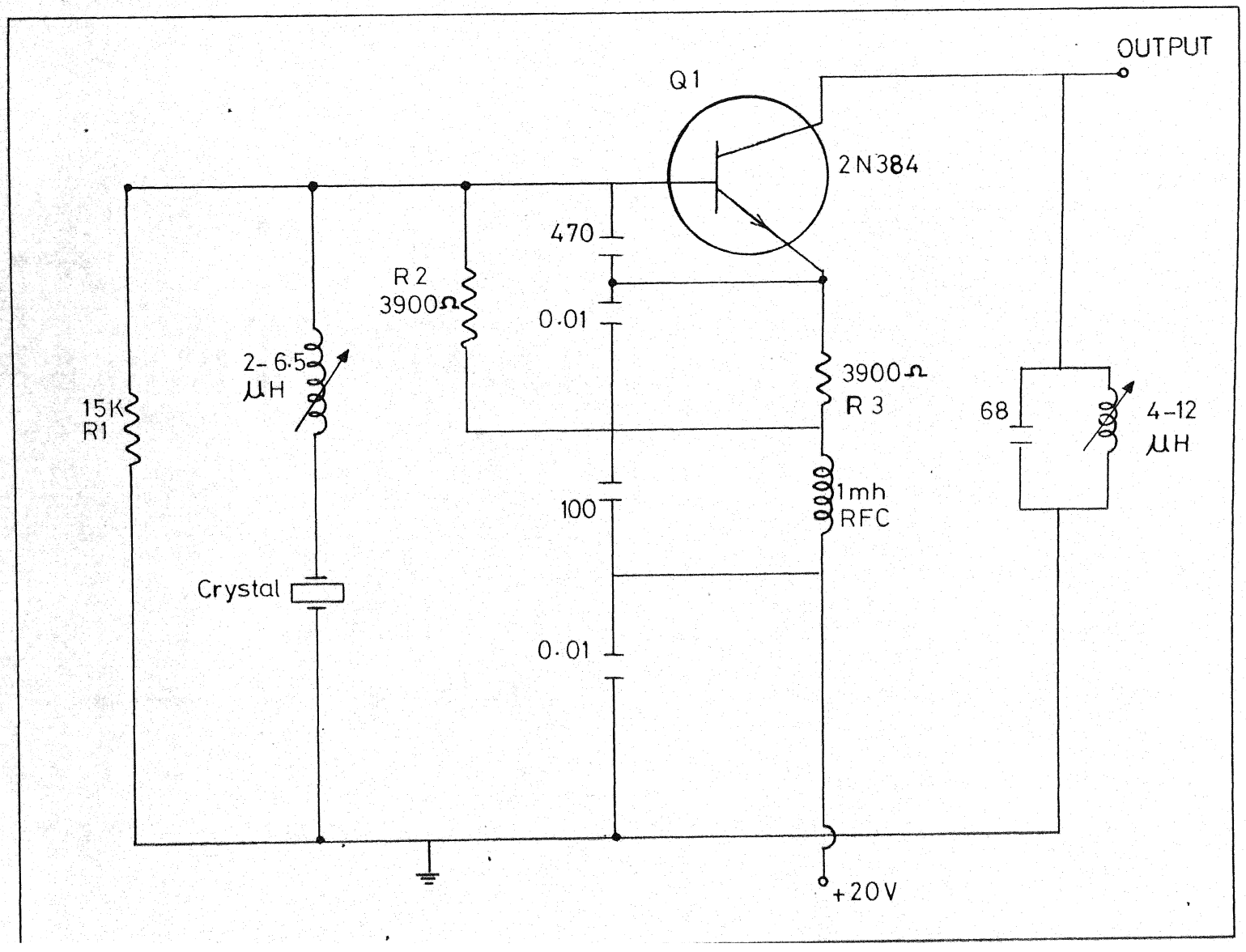
OUTPUT
Q1
2N384
470
R 2
3900Ω
0·01
2-6·5
μH
15K
R1
3900Ω
R 3
68
4-12
μH
1mh
RFC
100
Crystal
0·01
+20V

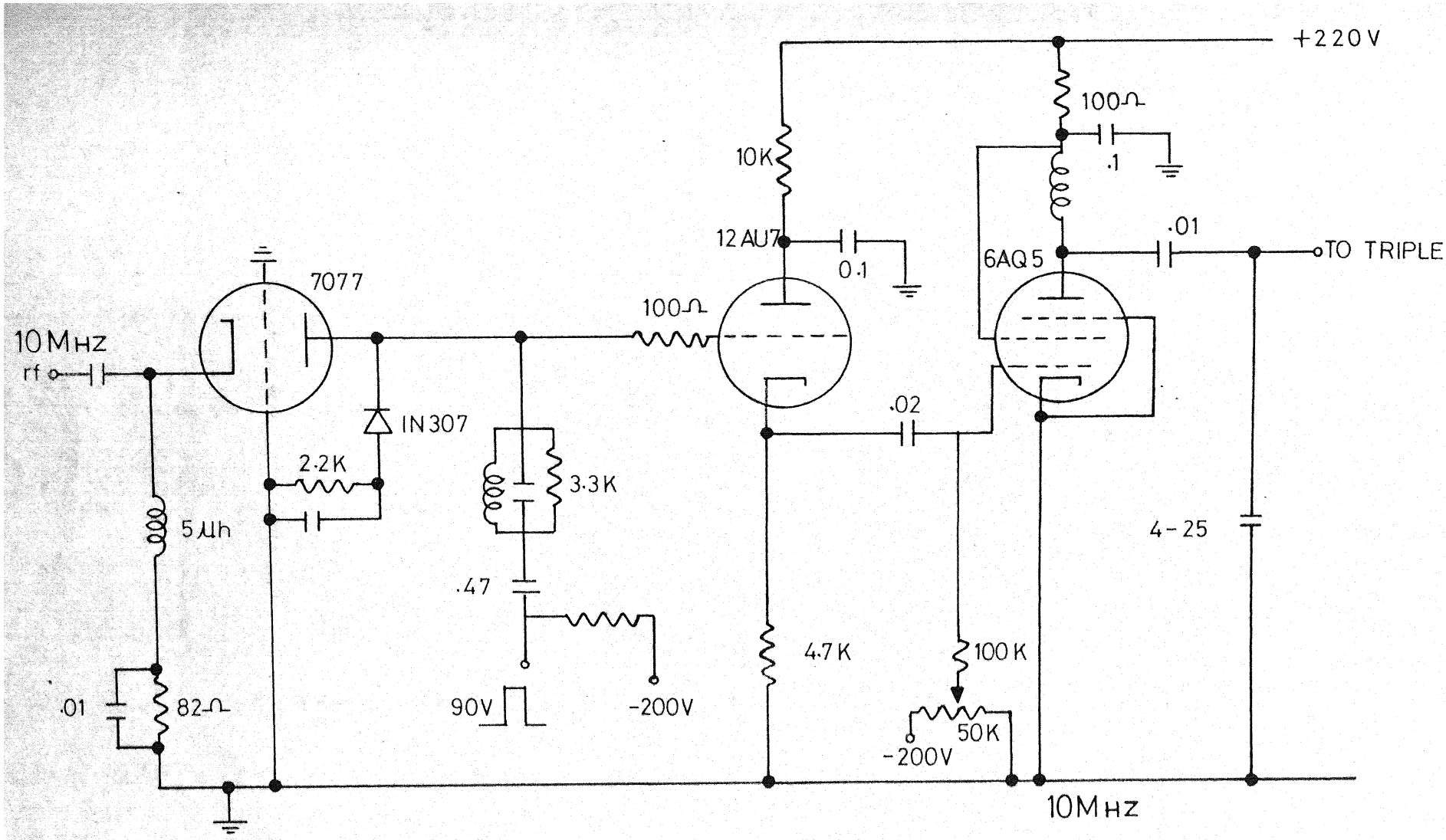

Fig. A6-Coherence gated and 10 MHz amplifier.

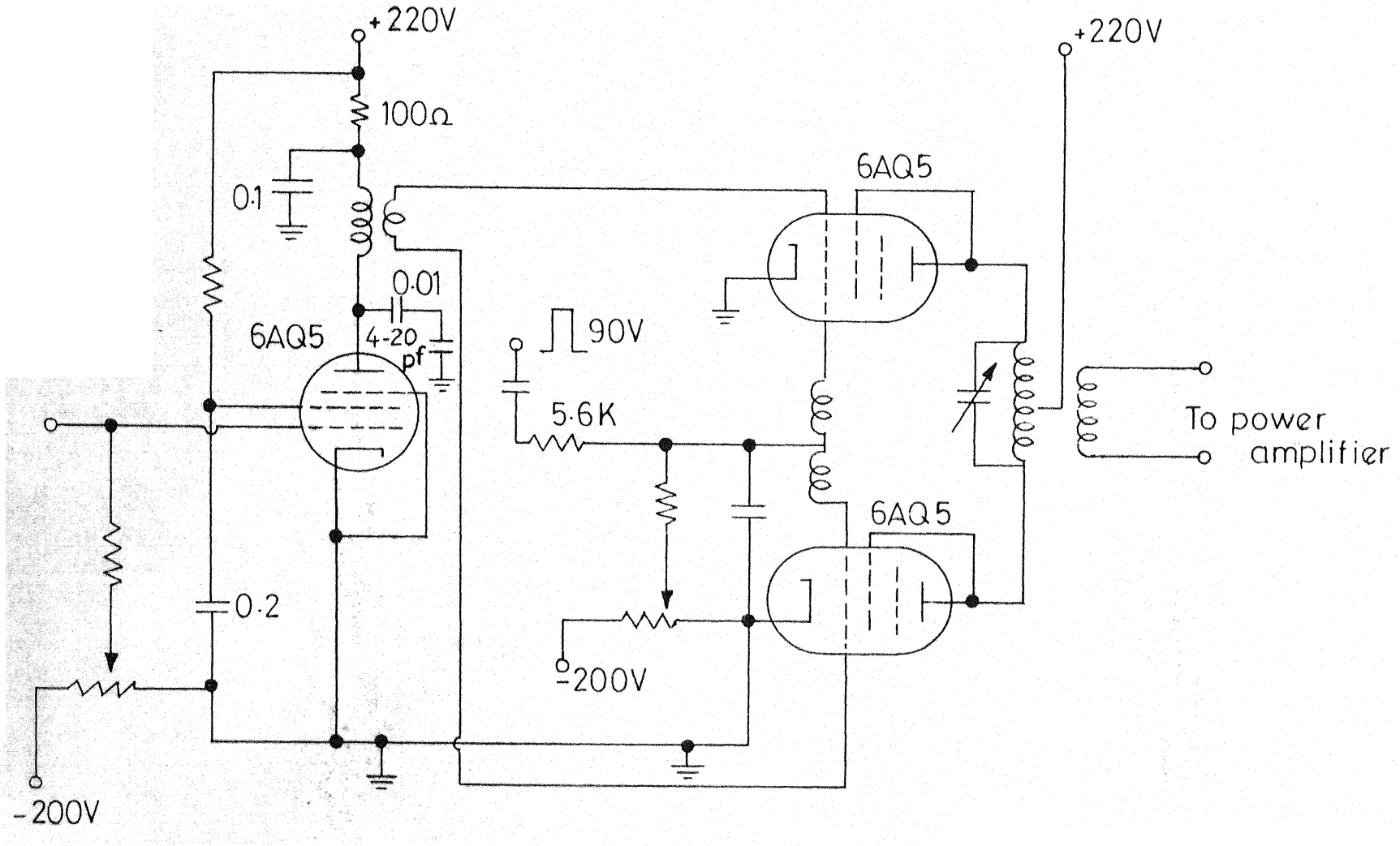

Fig.A7- 30 MHz tripler.

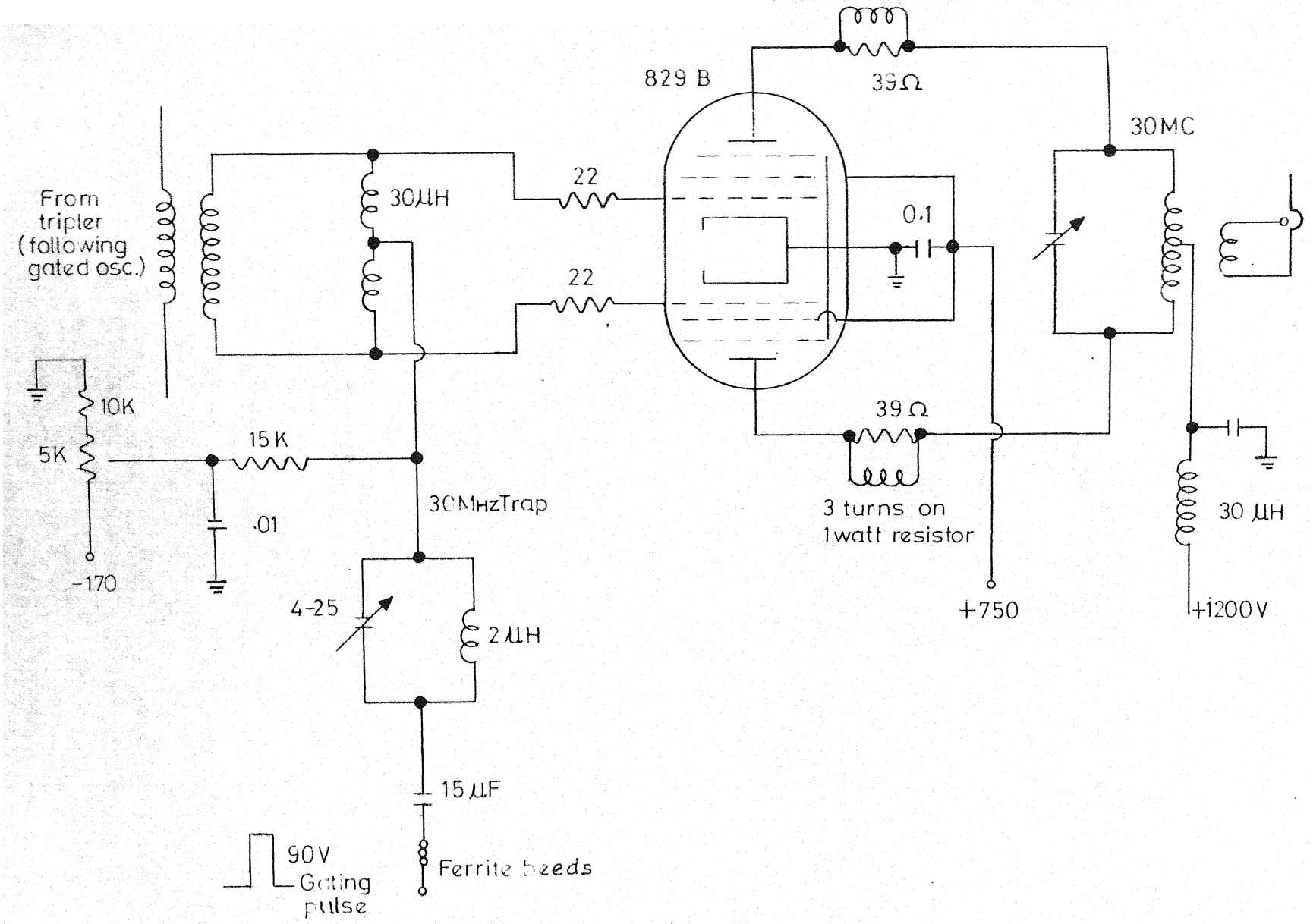
From tripler (following gated osc.)
30µH
22
22
829 B
39Ω
30MC
0.1
10K
5K
15 K
.01
-170
30MHzTrap
39 Ω
3 turns on 1watt resistor
+750
30 µH
+1200V
4-25
2µH
15µF
90V Gating pulse
Ferrite beeds

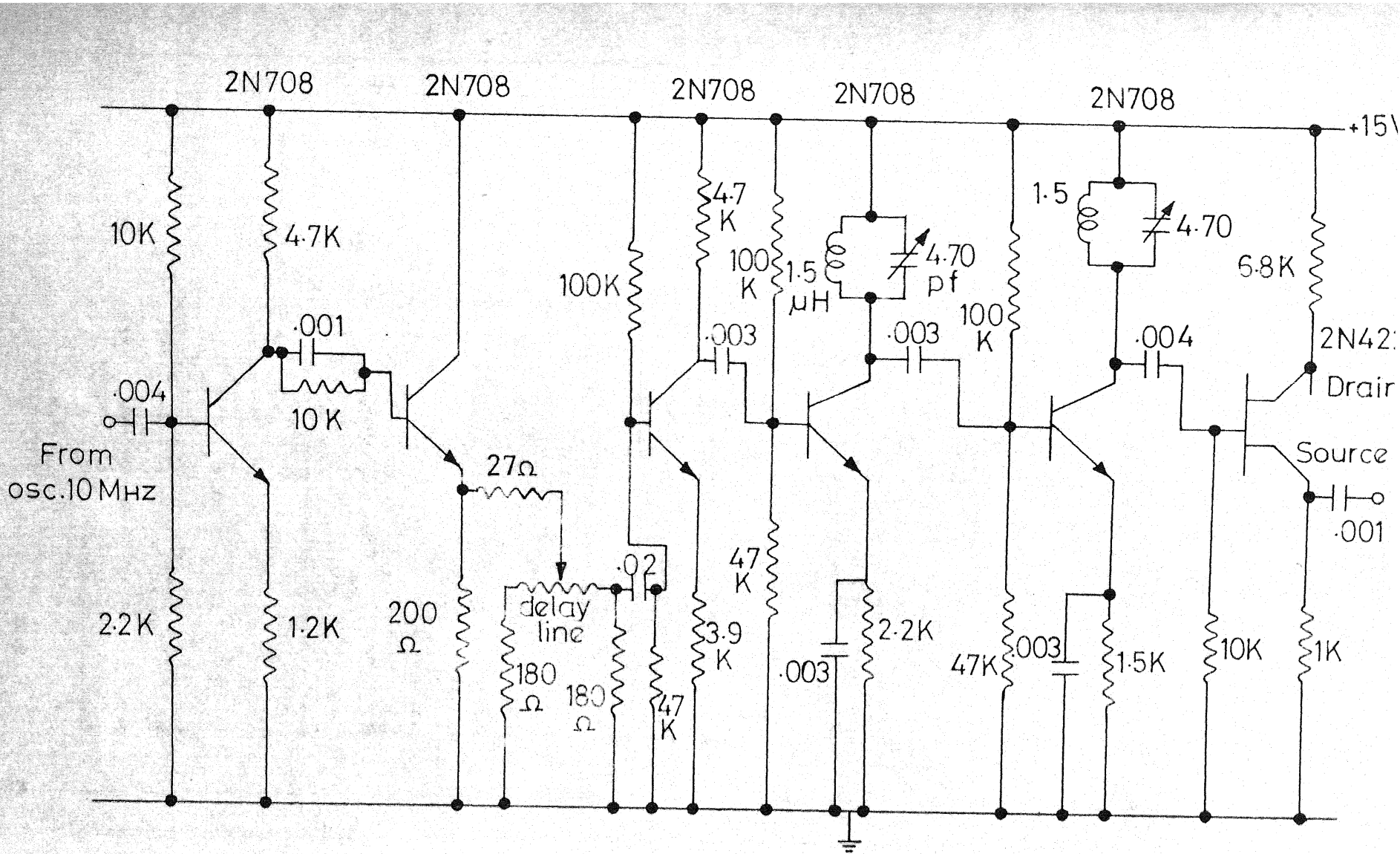

Fig. A9- Tripler.

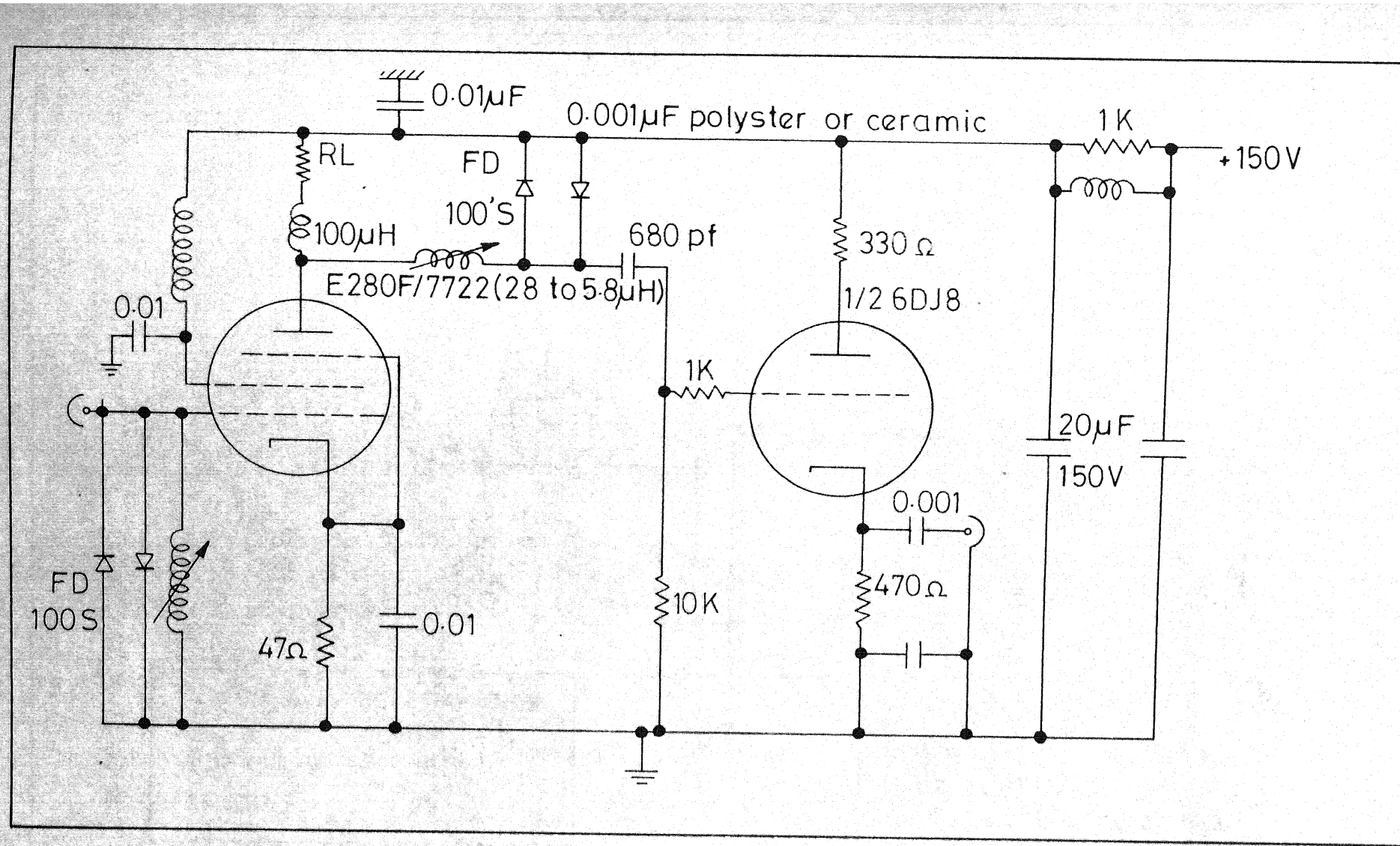

Fig.A10- Pre-amplifier.

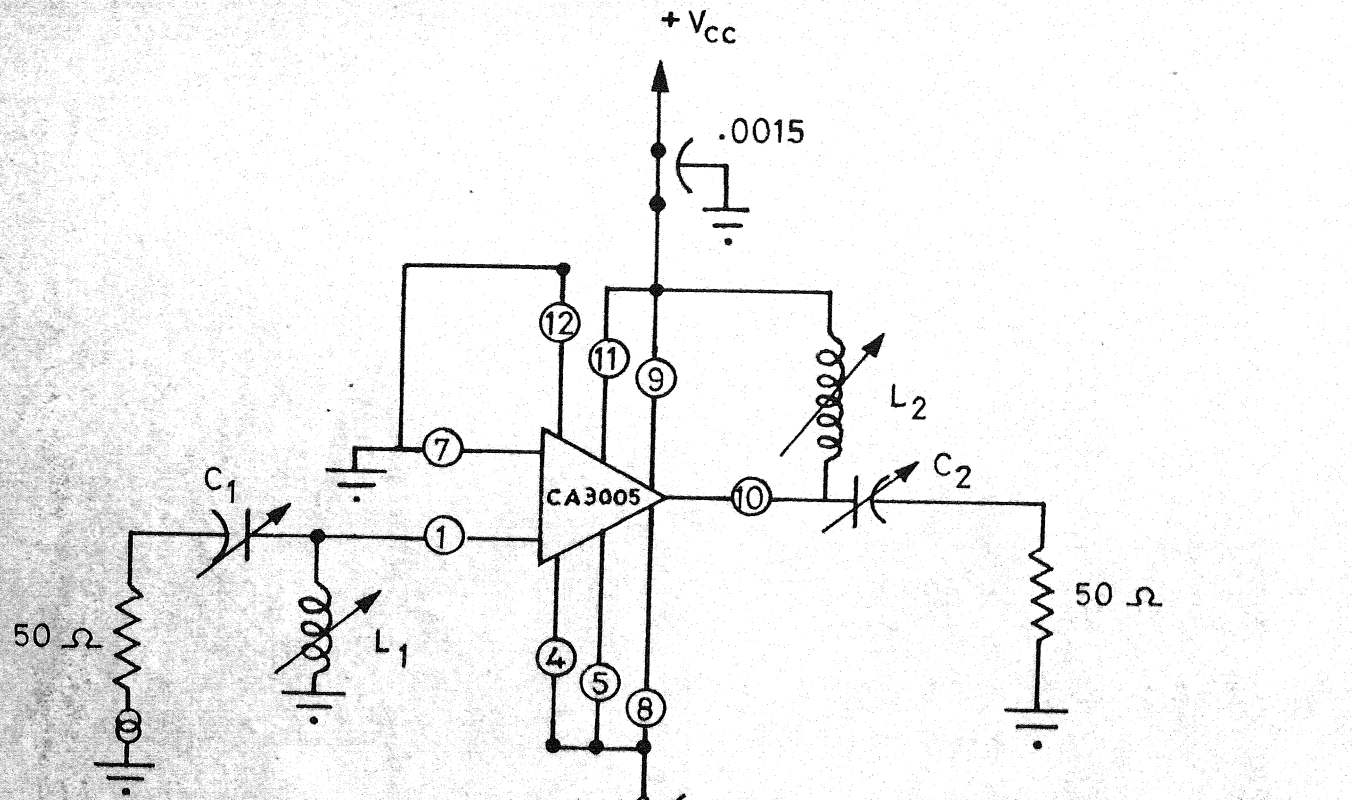

POWER GAIN PERFORMANCE	
DC SUPPLLIES	POWER GAIN (dB)
±6 VOLTS	29

CIRCUIT ELEMENTS

FREQ (MHz)	L_1 (μH)	C_1 (PF)	L_2 (μH)	C_2 (PF)
30	1.2-2	5.40	1.2-2	1.5-20

APPENDIX B

NUMERICAL EVALUATION OF INTEGRALS

NUMERICAL EVALUATION OF INTEGRALS

General Remarks:

This Appendix presents a Fortran IV program written for the numerical evaluation of integrals of type,

$$I(p,n,n') = \int_0^\infty dy \left\{ \left[\left(\int_0^\infty dx \left[g(x) \right]^{\frac{1}{2}} J_{p+\frac{1}{2}}(xy)\, x^{3/2-n} \right) x \right. \right.$$
$$\left. \left. \left(\int_0^\infty dx \left[g(x) \right]^{\frac{1}{2}} J_{p+\frac{1}{2}}(xy)\, x^{3/2-n'} \right) \right] \right\}$$

It is noted that the integrals $I(p,n)$ are evaluated from $I(p,n,n')$ with $n=n'$. The program includes two subroutines; i) A Gauss quadrature ii) A Bessel function routine. In the illustrative program presented here, $\pm$ 32 point densities hav been used. The Bessel function routine contains 2 parts. Fo smaller values of the arguement of $J_{p+\frac{1}{2}}(xy)$ (say $xy < 2$) the following series has been used:

$$J_{\nu}(x) = \left(\frac{x}{2}\right)^{\nu} \sum_{m=0} \frac{(-1)^m}{m!\, \Gamma(\nu + m+1)} \left(\frac{x}{2}\right)^{2m}$$

where $\nu = p+\frac{1}{2}$. For arguments greater than 2, the fractional order Bessel functions (order p) written in terms of elementa Sin and Cosine functions have been used. The Bessel function routines were tested by comparison with standard tables for

many selected values of arguments in all the orders (p) and were found to be accurate. For the values of p,n,n' used in work, convergence in the x integration is generally achieved with an upper limit of x not exceeding 5. The corresponding limit in the y integration is around 30-50. The 'execution' presented in the example program displays the convergence achieved for I(5,6,12) at two different temperatures.

```
$JOB   PHG122, TIME    PAGES    NAME S. RAJAN
$*                      DATE
$IBJOB          MAP
$IBFTC MAIN

PHG122                          FORTRAN SOURCE LIST
     ISN       SOURCE STATEMENT

       0 $IBFTC MAIN
         C       SRI RAMAJAYAM
       1         DIMENSION POINT (32), WEIGHT(32)
       2         COMMON / RAJAN / POINT,WEIGHT
       3         READ 700,(POINT(I),I=1,32)
      10         READ 700,(WEIGHT(I),I=1,32)
      15    700  FORMAT(7F10.5)
      16      5  READ 800,IP,BE,AN,BN,AL
      20    800  FORMAT(I5,4F10.5)
      21         PRINT 900,IP,BE,AN,BN,AL
      22    900  FORMAT(4X,*P=*,I5,4X,*BE=*,F10.5,4X,*N=*,F10.5,4X,*
                                                  *,F10.5,*4X,*L=*,F10.5)
      23         CALL FLUN(    )
      24         CALL GAUSS(BE,AN,BN,AL,IP)
      25         GO TO 5
      26      10 STOP
      27         END
PHG122                          IBMAP ASSEMBLY MAIN

   NO MESSAGES FOR ABOVE ASSEMBLY

PHG122                          FORTRAN SOURCE LIST
     ISN    SOURCE STATEMENT
       0 $IBFTC GAUSS
       1         SUBROUTINE GAUSS(BE,AN,BN,AL,IP)
       2         DIMENSION POINT(32),WEIGHT(32)
       3         COMMON / RAJAN / POINT,WEIGHT
       4         DIMENSION SUMT(1),SUMY(64),SUMZ(64)
       5         XINT=3.0
       6         SUMT(1)=0.0
       7         YL=0.0
      10      25 YL=YL+XINT
      11         DO 35 I=1,64
      12      35 SUMY(I)=0.0
      14         DO 45 I=1,64
      15      45 SUMZ(I)=0.0
      17         XL=0.0
      20         IXL=0
      21      30 XL=XL+XINT
      22         IYY=0
      23         IZZ=0
```

```
          24        SSSUM=0.0
          25        DO 20 IY=1,32
          26        YP=POINT(IY)
          27      5 YP1=YL+(YP-1.0)*XINT/2.0
          30        D1=3.0*AL**2/4.0/YP1**2
          31        D2=EXP(-D1)
          32        SUM1=0.0
          33        SUM2=0.0
          34        DO 15 IX=1,32
          35        XP=POINT(IX)
          36     10 XP1=XL+(XP-1.0)*XINT/2.0
          37        XY1=XP1*YP1
          40        XGPT=XP1**(-6)
          41        XGPT1=XGPT-1.0
          42        GX=2.0*BE*XGPT1*XGPT
          43        IF(GX.LT.60.0) GX=EXP(-GX)
          46        IF(GX.GE.60.0) GX=0.0
          51        T1=GX*BESSEL(XY1,IP)/XP1**(AN-1.5)
          52        T2=GX*BESSEL(XY1,IP)/XP1**(BN-1.5)
          53        SUM1=SUM1+WEIGHT(IX)*T1
          54        SUM2=SUM2+WEIGHT(IX)*T2
          55        XP=-XP
          56        IF(XP.LT.0.0) GO TO 10
          61     15 CONTINUE
          63        IYY=IYY+1
          64        IZZ=IZZ+1
          65        SUMY(IYY)=SUMY(IYY)+XINT/2.0*SUM1
          66        SUMZ(IZZ)=SUMZ(IZZ)+XINT/2.0*SUM2
          67        SSSUM=SSSUM+WEIGHT(IY)*D2*SUMY(IYY)*SUMZ(IZZ)
          70        YP=-YP
          71        IF(YP.LT.0.0) GO TO 5
          74     20 CONTINUE
          76        TERM=SSSUM*XINT/2.0
          77        IXL=IXL+1
         100        SUMT(IXL)=SUMT(IXL)+TERM
         101        PRINT 900, XL,YL,IXL,SUMT(IXL)
         102    900 FORMAT(4X,E15.8,4X,E15.8,4X,I5,4X,E15.8)
PHG122                          FORTRAN SOURCE LIST GAUSS
     ISN  SOURCE STATEMENT
         103        IF(YL.LT.40.0) GO TO 25
         106        RETURN
         107        END
PHG122                          FORTRAN PROGRAM GAUSS
  USER FUNCTION SUBPROGRAM REFERENCES
BESSEL
PHG122                        IBMAP ASSEMBLY GAUSS

  NO MESSAGES FOR ABOVE ASSEMBLY
```

```
PHG122                          FORTRAN SOURCE LIST
     ISN    SOURCE STATEMENT
      0   $IBFTC BESSEL
      1          FUNCTION BESSEL(X,P)
        C        GENERATE BESSEL FUNCTION OF ORDER P+1/2
      2          INTEGER P
      3          PI=3.14159625
      4          IF(X.GT.2.0) GO TO 115
      7          GAM=SQRT(PI)
     10          NP=P+1
     11          DO 5 I=1,NP
     12        5 GAM=GAM*(FLOAT(I)-0.5)
     14          PNU=FLOAT(P)+0.5
     15          SUM=1.0/(2.0**PNU)/GAM
     16          POWER=2.0**PNU
     17          FACT=1.0
     20          PROD=1.0
     21          XM2=1.0
     22          M=1
     23    105   I=M
     24          IF(M.GT.1) GO TO 6
     27          POWER=POWER*4.0
     30          PROD=-PROD
     31          FACT=FACT*FLOAT(M)
     32          GAM=GAM*(PNU+FLOAT(M))
     33          XM2=XM2*X*X
     34          TERM=PROD*XM2/POWER/FACT/GAM
     35          GO TO 7
     36        6 Z=X*X/FLOAT(M)/(PNU+FLOAT(M))/4.0
     37          TERM=-TERM*Z
     40        7 SUM=SUM+TERM
     41          IF(ABS(TERM/SUM).LT.1.0E-10) GO TO 15
     44          M=M+1
     45          GO TO 105
     46       15 BESSEL=SUM*(X**PNU)
     47          RETURN
     50      115 A1=945.0*SIN(X)/X**5
     51          A2=945.0*COS(X)/X**4
     52          A3=420.0*SIN(X)/X**3
     53          A4=105.0*COS(X)/X**2
     54          A5=15.0*SIN(X)/X
     55          A6=COS(X)
     56          BESSEL=A1-A2-A3+A4+A5-A6
     57          BESSEL=SQRT(2.0/(PI*X))*BESSEL
     60          RETURN
     61          END
PHG122                  IBMAP ASSEMBLY BESSEL

  NO MESSAGES FOR ABOVE ASSEMBLY
                        IBLDR--JOB    000000
```

M E M O R Y M A P

SYSTEM, INCLUDING IOCS 00000 THRU 12251

FILE BLOCK ORIGIN 12260

NUMBER OF FILES - 2

1. S. FBIN 12260
2. S. FBOU 12303

OBJECT PROGRAM 12326 THRU 21641

1.	DECK'MAIN ' *	12326
2.	DECK'GAUSS ' *	12616
3.	DECK'BESSEL '	13533
4.	SUBR'INSYFB '	14274
5.	SUBR'OUSYFB '	14333
6.	SUBR'POSTX '	14364
7.	SUBR'CNSTNT '	14736
8.	SUBR'FPR '	14745
9.	SUBR'FRD '	14746
10.	SUBR'IOS '	14747
11.	SUBR'RWD '	15226
12.	SUBR'ECV '	16402
13.	SUBR'FCV '	16650
14.	SUBR'HCV '	16742
15.	SUBR'ICV '	17045
16.	SUBR'XCV '	17065
17.	SUBR'INTJ '	17103
18.	SUBR'FFC '	17417
19.	SUBR'FPT '	20041
20.	SUBR'FLUN '	20455
21.	SUBR'XEM '	20472
22.	SUBR'XP3 '	21037
23.	SUBR'XPN '	21110
24.	SUBR'LOG '	21216
25.	SUBR'SCN '	21363
26.	SUBR'SQR '	21542

(*INSERTIONS OR DELETIONS MADE IN THIS DECK)

INPUT-OUTPUT BUFFERS 76637 THRUE

UNUSED CORE 21642 THRU

***OBJECT PROGRAM IS BEING ENTERED INTO STORAGE AT

EXECUTION

P=	5	BE=	0.29200	N=	6.00000		N1=12.00000	L=0.(
0.30000000E	01		0.30000000E	01		1	0.7513719E-04	
0.30000000E	01		0.60000000E	01		1	0.1073933E-01	
0.30000000E	01		0.90000000E	01		1	0.25978577E-01	
0.30000000E	01		0.12000000E	01		1	0.28388557E-01	
0.30000000E	01		0.15000000E	02		1	0.29102499E-01	
0.30000000E	01		0.18000000E	02		1	0.29520153E-01	
0.30000000E	01		0.21000000E	02		1	0.29775154E-01	
0.30000000E	01		0.24000000E	02		1	0.29903062E-01	
0.30000000E	01		0.27000000E	02		1	0.29954653E-01	
0.30000000E	01		0.30000000E	02		1	0.29973829E-01	
0.30000000E	01		0.33000000E	02		1	0.29983715E-01	
0.30000000E	01		0.36000000E	02		1	0.29991106E-01	
0.30000000E	01		0.39000000E	02		1	0.29996229E-01	
0.30000000E	01		0.42000000E	02		1	0.29998906E-01	

P=	5	BE=	0.35040	N=	6.000000		NI=12.00000	L =
0.30000000E	01		0.30000000E	01		1	0.73610313E-04	
0.30000000E	01		0.60000000E	01		1	0.10247663E-01	
0.30000000E	01		0.90000000E	01		1	0.23716505E-01	
0.30000000E	01		0.12000000E	02		1	0.26060639E-01	
0.30000000E	01		0.15000000E	02		1	0.26726083E-01	
0.30000000E	01		0.18000000E	02		1	0.27075648E 01	
0.30000000E	01		0.21000000E	02		1	0.27289895E-01	
0.30000000E	01		0.24000000E	02		1	0.27405759E-01	
0.30000000E	01		0.27000000E	02		1	0.27457277E-01	
0.30000000E	01		0.30000000E	02		1	0.27476596E-01	
0.30000000E	01		0.33000000E	02		1	0.27484278E-01	
0.30000000E	01		0.36000000E	02		1	0.27488837E-01	
0.30000000E	01		0.39000000E	02		1	0.27491968E-01	
0.30000000E	01		0.42000000E	02		1	0.27494564E-01	